Characterizing Turbulent Magnetic Field, Density and Velocity Fluctuations in Earth-Directed ICMEs

A Thesis

submitted to
Indian Institute of Science Education and Research Pune
in partial fulfilment of the requirements for the ***BS-MS Dual Degree Programme***

by

Deep Prakash Ghuge
20191028

INDIAN INSTITUTE OF SCIENCE EDUCATION AND RESEARCH (IISER), PUNE
Dr. Homi Bhabha Road,
Pashan, Pune 411008, INDIA

April, 2024

Supervisor: Prof. **Prasad Subramanian**

Certificate

This is to certify that this dissertation entitled *"Characterizing Turbulent Magnetic Field, Density and Velocity Fluctuations in Earth-Directed ICMEs"* towards the partial fulfillment of the BS-MS dual degree programme at the Indian Institute of Science Education and Research, Pune represents study/work carried out by **Deep Prakash Ghuge** at IISER Pune under the supervision of **Dr. Prasad Subramanian, Professor, Department of Physics, IISER Pune** during the academic year 2023-2024.

Prof. Prasad Subramanian

Committee:

Prof. Prasad Subramanian

Prof. Bhas Bapat

This thesis is dedicated to

To my late Ajoba, whose faith and wisdom guide and inspire me every day.

Declaration

I hereby declare that the matter embodied in the report entitled *“Characterizing Turbulent Magnetic Field, Density and Velocity Fluctuations in Earth-Directed ICMEs”* are the results of the work carried out by me at the Department of *“Physics”*, *“Indian Institute of Science Education and Research (IISER), Pune’*, under the supervision of **“Prof. Prasad Subramanian”** and the same has not been submitted elsewhere for any other degree.

Deep Prakash Ghuge

Acknowledgements

I would like to express my deepest gratitude to my supervisor, Professor Prasad Subramanian, for his support throughout the thesis. Professor Prasad Subramanian is not merely a distinguished researcher; he embodies the quintessence of an outstanding mentor and educator. I first met him when he taught the fluid dynamics course, and I was instantly captivated by his teaching. He possesses a unique ability to simplify complex concepts in a way that actually feels fun to delve deeper into, and I have come across very few teachers who have such an ability. I had faced some hiccups before starting my thesis, and the first person that came to my mind to seek help was him, and he instantly agreed to accept me as a master's project student.

I enjoyed every bit of my MS thesis journey and it has not only given a direction to my interests in astrophysics but fulfilled my childhood dream of getting a degree in astrophysics. Prof. Prasad Subramanian remains at the forefront of helping me fulfill it. His mentorship has been a beacon of inspiration, and I regard him not just as an academic guide but as a role model. Expressing my gratitude with just a few paragraphs seems insufficient to capture the depth of my appreciation for his unwavering support and guidance.

I'm grateful to Prof. Bhas Bapat, expert member of my Thesis Advisory Committee (TAC), for dedicating his valuable time and effort to examine my work and provide formative feedback. I also wish to extend my thanks to Dr. Debesh Bhattacharjee for his consistent and invaluable assistance throughout my thesis journey.

I cannot conclude without expressing my heartfelt appreciation for the support and love from my parents —Aai, Baba, my cousin sister Manju Didi, and my beloved Aaji. Their faith in me has been my constant source of strength and motivation. A big thank you to all my friends at IISER for making my five-year BS-MS memorable, along with many others who have crossed my path and have influenced me, inspired me, and encouraged me along the way.

Contents

List of Figures

List of Tables

Abstract

Earth-directed solar Coronal Mass Ejections (CMEs) often interact with the magnetosphere, causing geomagnetic storms that disrupt a range of technologies we routinely rely on. A good understanding of the CME-magnetosphere interactions are key to mitigating the consequences of such storms. The extent of CME-magnetosphere interaction is governed substantially by conditions in the CME sheath (which is the leading part of Earth-directed CMEs). It is possible that turbulence in the sheath and magnetic obstacle (MO) of CMEs could show different characteristics compared to background/ambient solar wind. We have attempted to characterize the CME sheath based on a comparison with power present inside the turbulent high-frequency fluctuations in CME sheaths, MO and background solar wind by the help of Power Spectral Density (PSD) calculation where frequencies were around the inertial subrange. This comparison was based of a quantity (modulation index) is a measure of power inside these high-frequency fluctuations to that of low-frequency fluctuation. Previous studies have shown that there is a difference in the geomagnetic impact of sheath and MO based on Dst Index values, we have tried to check for such differences through correlations with the modulation index. The comparison was carried out with data from NASAs WIND spacecraft for proton density (N_p), magnetic field magnitude (B) and velocity magnitude (V). This data was separated into two different set of events one consisted of 130 events with ICME shock and another with 271 events that have mix of events with and without shock along with Dst index values. We found that the modulation index effectively characterizes the sheath as a highly turbulent structure, MO is comparatively less turbulent, and the chosen background solar wind is the least turbulent. Spectral indexes furthermore show that there is a similarity in MO and sheath spectra however, background solar wind spectra is different.

Chapter 1

Introduction

The sun and coronal surface is a place of constant unrest and with the influence of magnetic fields, resulting in phenomena such as sunspots, solar flares, and coronal mass ejections. It sends a steady flow of charged particles called the solar wind, which ultimately travels to distant corners of our solar system and beyond before being obstructed by the interstellar medium. This forms an enclosure around the solar system along with the magnetic field of the sun, known as the Heliosphere. It acts as a shield from galactic cosmic radiation, in a similar way Earth's magnetosphere also acts as a shield, protecting us from the energetic charged particles coming towards it. During a strong influx of such charged particles during solar storms, a strong interaction between the Earth and solar wind can be seen through increased geomagnetic disturbances. [1] This can raise auroral activity in the polar regions where such charged particles collide with the atmospheric contents, energy exchanges of which create glowing effects. Apart from the spectacle they create, these disturbances/storms are a prime source of disruption in satellite operations, they affect GPS navigation, interfere with communication systems, and also cause power outages by overloading power grid infrastructures. Therefore, it is crucial to study the phenomena that lead to geomagnetic storms thoroughly.

Figure 1.1: Image of Aurora (aurora australis) captured from space over the Indian Ocean by astronauts in International Space Station. *Image Credit: Image Science & Analysis Laboratory, NASA Johnson Space Center* (http://eol.jsc.nasa.gov)

Coronal mass ejection (CME) is a phenomenon that is associated with geomagnetic storms. It is a large eruption characterized by the expulsion of plasma and magnetic fields from the Sun's corona.[1] It is worth noting that CMEs that travel well ahead into the heliosphere are called Interplanetary Coronal Mass Ejections or ICMEs.

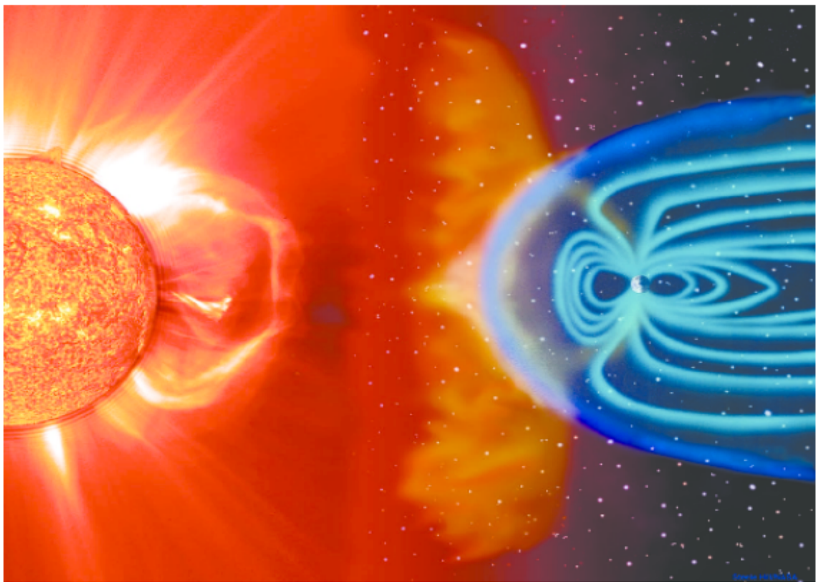

Figure 1.2: An illustration depicting ICME interacting with the outer atmosphere of the Earth. *Image credit: NASA space weather awareness*

ICME speeds often exceed the sound speed and magnetosonic speed in the background solar wind creating a shock or ICME shock and giving a structure to the ICME, which is differentiable based on some specific signatures. To better understand the differences in causes when ICME impacts the Earth, characterization of these structures becomes essential.

1.1 Coronal Mass Ejections

CMEs consist of large-scale plasma fragments entwined with magnetic fields that burst forth from the solar corona into the heliosphere. They possess an average kinetic energy around 10^{25} joules and thus rank among the most energetic eruptive phenomena in the solar system. [2] CMEs that travel deep into the heliosphere is known as interplanetary coronal mass ejection (ICME). It can carry a mass ranging from 10^{11} to 10^{12} kilograms and travels at speeds from 350 to 1000 km/s. [3]

CMEs and solar flares are two types of eruptions that occur in the Sun's atmosphere and are the main phenomena driving storm activity. The occurrence rate of CMEs varies with the solar cycle. It is an 11-year cycle that describes the changes in the Sun's activity and appearance, which includes variations in the number of solar flares, sunspots, CMEs and the Sun's irradiance. For a long time, flares were thought to drive solar and magnetic storms, yet a direct connection between storms and flares was never established: a flare can occur without leading to a magnetic storm, and similarly, a storm can occur without a solar flare.[4] Eventually, it was found that CMEs are the main drivers of magnetic storms. During the solar maximum, solar flare and CME activity usually increase, with up to $\sim$ 4-5 CMEs per day, and decreases to about ≈ 1 during the solar minimum. [5]

1.1.1 CME and ICME Observations

CMEs are studied via remote sensing observations, whereas ICMEs are studied through in-situ measurements. Each can offer a different perspective on the CME. Remote sensing observations provide early observations of CMEs by capturing their initial stages just after sprouting out, which is a less evolved state of a CME, and its trajectory near the Sun. In contrast, in situ measurements give direct insights into the more evolved version of CMEs as they travel through interplanetary space and are typically measured at about 1AU. As CMEs travel they undergo a lot of changes. In situ measurements give insights into changes in their structure, composition, and dynamics. When remote sensing and in-situ observations are used together, they offer a much better viewpoint, from the CME's initiation near the Sun to its more mature form away from the Sun.

Remote Sensing Observations

Remote sensing observations of CMEs primarily rely on the analysis of images captured by coronagraphs. A coronagraph is an instrument designed to simulate an artificial eclipse by using an occulter to block out the Sun's bright disk. This allows for the observation of the Sun's faint outer atmosphere, or corona, and the structure CMEs as they occur. In white-light coronagraph observations, a halo coronal mass ejection appears as an expanding ring that completely surrounds the coronagraph's occulting disk. Since images are 2D and the structure of CME is 3D, taking into account the directionality of the projection of CME can impact the observation.

CMEs that are directed towards or away from the observing coronagraph are interpreted as halo CMEs. The CME is called a partial halo coronal mass ejection when the expanding ring does not surround the occulting disk entirely and has an angular expanse of more than 120 degrees around the circumference of the disk. Partial and full halo CMEs account for about 10% of all CMEs, and among these, full halo CMEs represent about 4%. In remote sensing observations, we have practically limited to observing partial helo CMEs which face the coronagraph. [6]

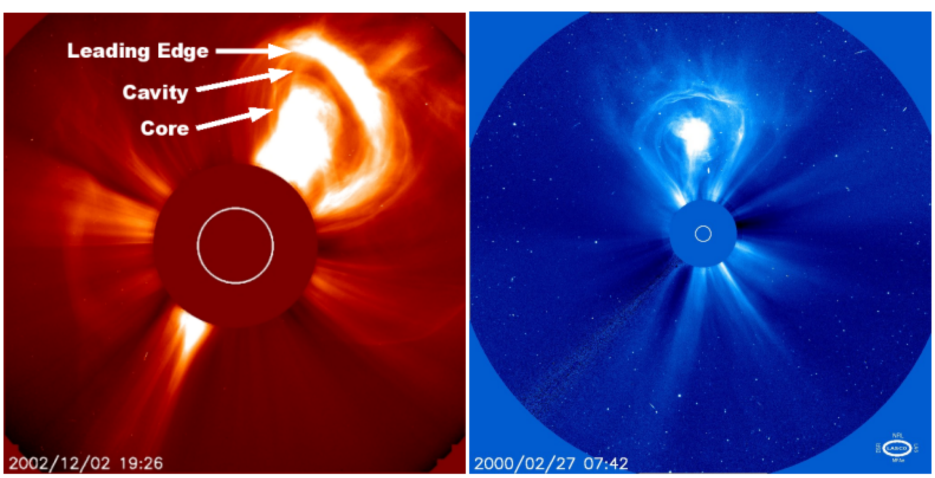

Figure 1.3: Coronagraph images of a CME by SOHO LASCO C2 (left) and SOHO LASCO C3 (right) on December 2, 2002, and December 27, 2002, respectively. The image on the left shows the classic three-part structure of CME (see section 1.1.2). *Image Credit: SOHO (NASA and ESA)*

Ground-based coronagraphs are limited by atmospheric interference and thus have reduced use for CME studies. In contrast, space-based coronagraphs, such as the LASCO on the SOHO spacecraft, offer much clearer observations. LASCO features three coronagraphs—C1, C2, and C3—with varying occulter radii. The combined field of view studied by them ranges from $\approx 1R_{\odot}$ to $32R_{\odot}$.Where C1 and C2 are inner coronagraphs and C3 is an outer coronagraph.Inner coronagraphs are used for observations closer to the solar limb; a smaller occulter radius is used in them, which allows the telescope to capture the inner corona, starting from just above the solar surface. However, a smaller radius can lead to increased stray light and diffraction effects.Outer coronagraphs, on the other hand, have a larger occulter radius which reduces the amount of light from the lower corona reaching the detector, focusing on the fainter, more extended features of the corona and CMEs in the middle to the outer corona.

In-Situ Observations

In-situ observations provide insights into the internal dynamics and composition of ICMEs, something remote sensing observations cannot directly probe into. As an ICME passes through a spacecraft, it captures magnetic and plasma parameters such as the total magnetic field (B), magnetic field components and their rotations (B_x, B_y, B_z), temperature (T), velocity components (V_x, V_y, V_z), plasma beta (β), the number density of particles (n), azimuthal and polar angles of ICME rotation, and more. Since this is time series data, these parameters are recorded by the spacecraft as a function of time during the passage of the ICME. The Solar and Heliospheric Observatory (SOHO), the twin Solar Terrestrial Advanced Composition Explorer (ACE), Relations Observatory (STEREO) spacecraft, and the WIND Spacecraft are known for their significant contributions to our understanding of CMEs through in-situ measurements and excellent working track record. These spacecraft are positioned at the L1 point, close to 1 AU from the Sun.
In situ observatories like the ones mentioned typically contain the following instruments.

- Magnetometers: They measure the magnitude and direction of the magnetic field. A commonly used type is the fluxgate magnetometer, which works by detecting changes in the magnetic field's effect on the magnetic material inside the sensor.

- Solar Wind Ion Composition Spectrometers: Used for finding the composition of charged particles (ions) in the solar wind. They primarily work by first ionizing collected particles and then sorting these ions based on their mass-to-charge ratio using electric and magnetic fields. This process helps find the elemental and isotopic composition of particles.

- Plasma Analyzers: They measure plasma parameters like velocity, density, and temperature inside the plasma. They use electrostatic analyzers (ESAs), which filter particles by energy per charge ratio through which finding the velocity distribution function of solar wind ions.

- Electron Spectrometers: Used to find the energy distribution of electrons. Like ion spectrometers, they can utilize ESAs to differentiate electrons based on their energy.

- Faraday Cups: These devices measure the flux of charged particles by collecting them in a conducting cup where the current produced by their impact is measured.

Wind Spacecraft houses a Plasma analyzer (SWE), Magnetic Field Investigation Magnetometers (MFI), 3D Plasma Analyzer (3DP), Energetic Particles: Acceleration, Composition and Transport (EPACT) WAVES experiment and Gamma-ray instrument.

1.1.2 CME onset and evolution

A lot of questions are still unanswered about the dynamics, origin, onset and evolution; propagation, and structure of CMEs, even when they have been quite extensively studied for the past 70 years. Based on observation, new theories or CME models are constantly constructed and discarded. We still do not have a good understanding of the CME onset process.

The CME plasma expands due to an expansion of the magnetic field, which is shaped like helical field lines with varying pitch angles; it is called a flux rope.[7] CME is thought of as having a three-part structure that consists of a leading front/edge, a dark cavity, and a bright core. The dark cavity follows the leading front, followed by the bright core. It is believed that an erupting flux rope corresponds to the dark cavity, while the accumulation of coronal loops above this erupting flux rope forms the bright frontal loop, and the bright core is identified as an internal filament. Thus, a CME can be described as the expulsion of a magnetic flux-rope structure from the lower corona, appearing as a three-part configuration.[8][9]

CMEs are typically classified as slow and fast CMEs, which is related to the early acceleration and onset phase of the CME evolution. [7] Fast CMEs have high acceleration and originate with a strong explosion like a solar flare. The primary theoretical challenges are about understanding the energy release mechanisms behind fast CMEs. Slow CMEs have slow acceleration and are related to helmet streamers which are formed above regions where the Sun's magnetic field is closed and loops back down to the surface, creating a stable structure that can extend several solar radii into space.

Disrupting the corona's hydrodynamic, magnetic, and gravitational balance should trigger the onset of a CME, leading to an eruption. If the eruption is sufficiently strong and faces minimal obstructions, plasma gets expelled into interplanetary space. The disruption to equilibrium can arise from different processes: It could be a flux rope, from below the solar surface, magnetic reconnection within the coronal field, or minor alterations to the local field.[3] CME onset models are generally divided into two categories based on the presence or absence of magnetic reconnection. Magnetic reconnection is believed to restructure magnetic field lines, lessening stress caused by flux emergence and the Sun's differential rotation. [10] Alternatively, models that do not rely on reconnection encompass methods like flux injection, kink, and torus instability. [11][12][13]

The development of a CME unfolds through distinct phases [14]. Initially, following its emergence from the solar corona, the CME enters a phase of rapid acceleration. Subsequently, it transitions into a phase characterized by movement at a nearly constant velocity, albeit with occasional minor fluctuations in speed throughout its journey. [14] Slower CMEs may pick up speed and accelerate, while faster ones tend to decelerate in regions around the outer corona. [15] This acceleration-deceleration mainly happens near to the Sun, with further movement guided by the obstructions in space through which the CME travels. Past a certain distance from the Sun, the magnetic field's influence weakens, and the hydrodynamics of the plasma become more significant in determining the CME's path.[16] After its projection, the CME continues on its journey through interplanetary space.

1.1.3 ICME Structure

An ICME consists of an ejecta and a sheath. The ejecta of ICME is sometimes referred to as ICME. The sheath describes the space between the shock front and the leading edge of the ejecta when a fast ICME propels an interplanetary shock (slower CMEs also precede with a sheath area). The ejecta might remain connected to the Sun or become disconnected, forming a magnetically enclosed entity, referred to as a “plasmoid” or Magnetic Obstacle (MO). [17]

Despite the acceleration and deceleration of ICMEs (slow and fast ICMEs) and velocity changes, they typically are faster than the surrounding solar wind. When their speeds surpass the local magnetosonic speed, a shock (or ICME shock) is formed, and this shock precedes sheaths.

Shock signatures are identified in in-situ data as a rise in magnetic field, proton density, temperature, plasma speed and other plasma parameters. In the sheath, the solar wind is compressed, which leads to an increased magnetic field along with large amplitude fluctuations. These fluctuations often produce high negative values of the parameters. [19] It is interesting to note that not all ICMEs have shock and even a well-defined MO. Previous studies have shown that around 66% of observed ICMEs have some sort of shock signature present.[20]

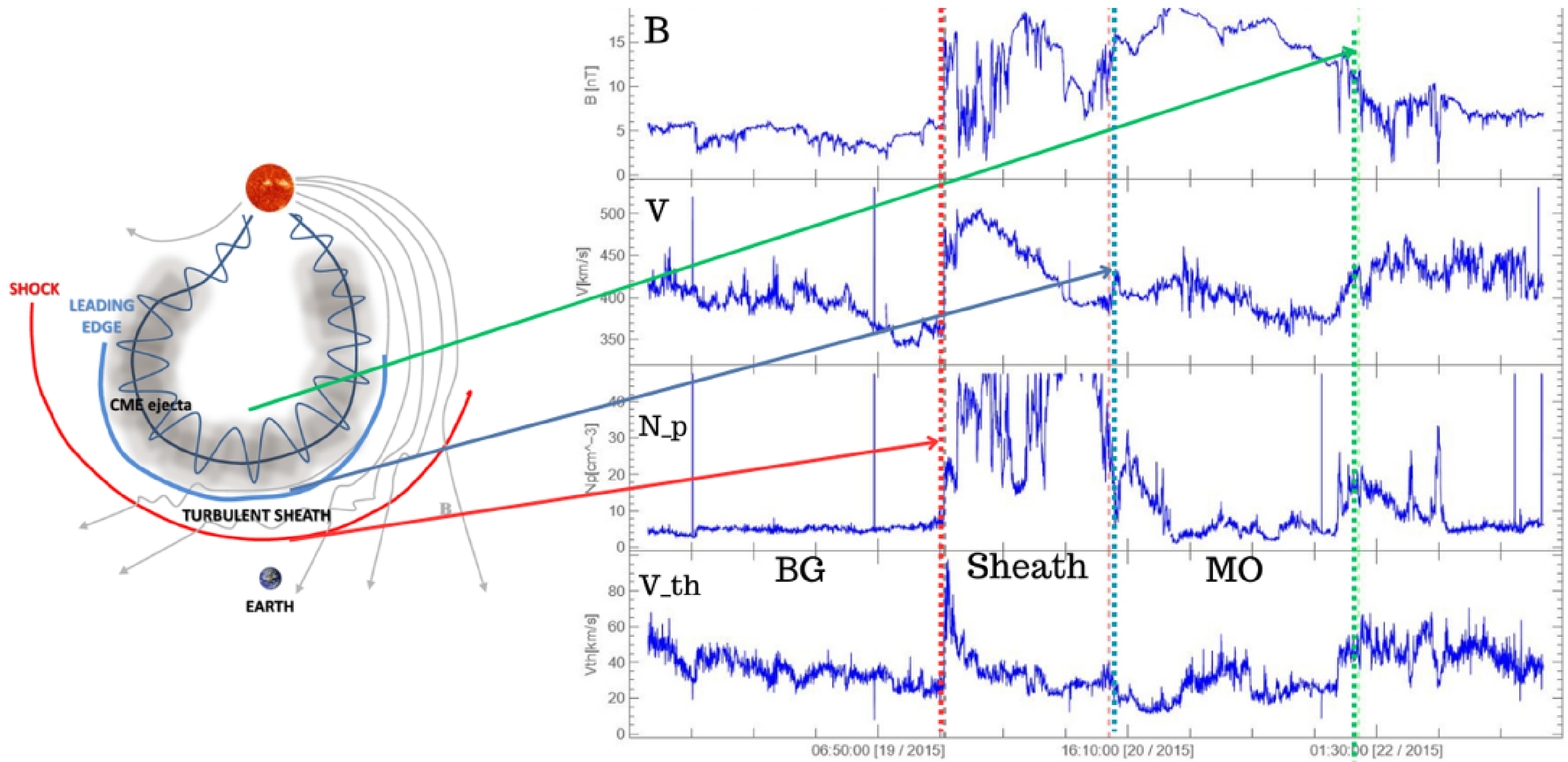

Figure 1.4: The Image on the left shows ICME with sheath, MO/ejecta leading edge, and the image on the right shows in situ parameters observed with time from the WIND spacecraft. Comparison between background (BG), sheath, and MO shows a highly fluctuating nature of sheaths. Image (left) taken from Palmerio et al. (2015) [18]

1.1.4 ICME and Sheath Signatures

The signatures that are used to identify ICME can vary from source to source and It is very evident that every ICME is not the same, yet certain characteristic features in specific parameters help in recognizing it and defining its boundaries. These signatures vary in intensity, shape, and sensitivity based on parameter type. For instance, Kilpua et al. (2017) [21] identified ICMEs by looking for: i) magnetic field strength, ii) magnetic field strength compared to the surrounding solar wind, iii) reduced proton temperature, iv) low plasma beta value, v) reduced proton density, vi) large magnetic field rotation, vii) decreasing velocity, and viii) presence of shock. Now in this study specific to what we are using (velocity, magnetic field and proton density) the observations of ICME events and their average values in the previous known studies are listed below. However, it must be noted that studies ded-

Study	**Time window**	**B [nT]**	**V [km s^{-1}]**	**N_p [cm^{-3}]**
Bothmer and Schwenn (1998)	1974 – 1981	17.7	478	6.47
Liu et al. (2005)	1975 – 2002	7.35	458	6.16
Wang et al. (2005)	1975 – 2003	8.3	456	6.7
Forsyth et al. (2006)	1975 – 1980	10.3	483	7.03
Gopalswamy (2008)	1996 – 2005	18	487	8.5
Mitsakou et al. (2009)	2003 – 2006	9.2	525	6.5
Richardson and Cane (2010)	1996 – 2009	10.1	476	6.9
Mitsakou and Moussas (2014)	1996 – 2008	10.1	467	6.8

Table 1.1: Comparison of ICMEs signatures for at 1 AU from different observational studies as discussed in Mitsakou et al. [20]

icated exclusively to identifying ICME sheaths and their characteristics are uncommon, and the works shown in Table 1.1, might not be consistent in observational data and considered parameters. Moreover, variations in catalog and event selection, as well as the definitions and boundaries employed to distinguish sheaths, contribute to inconsistencies and do not rightfully show a typical sheath signature. Consequently, interpretations of these signatures can vary significantly across different sources.

A statistical study by Mitsakou et al. [20] had shown that in the sheath region, the magnetic field strength, the speed, the proton density and temperature, and the plasma β have higher mean values than in the ICME and are shorter in duration than an ICME, suggesting that sheaths have higher plasma pressure, Alfvén Mach number. Other recent studies have shown that compositional characteristics of sheaths, such as the alpha-to-proton ratio, O^{+7}/O^{+6} ratio, and the iron-to-oxygen (Fe/O) ratio, are helpful in distinguishing plasma of different origins.[22] These studies demonstrate the difference in solar wind properties within ICMEs.

Parameter	**ICME**	**Sheath**
B (nT)	10.1 ± 0.2	11.3 ± 0.3
N_p (cm^{-3})	6.8 ± 0.2	12.1 ± 0.5
T (K)	$(0.76 \pm 0.05) \times 10^5$	$(2.06 \pm 0.01) \times 10^5$
V (km s^{-1})	467 ± 6	504 ± 7
Plasma β	0.84 ± 0.05	2.1 ± 0.2
Duration (hours)	24.8 ± 0.7	9.2 ± 0.4
Width (AU)	0.27 ± 0.01	0.111 ± 0.005

Table 1.2: Statistical properties of ICMEs and Sheaths from 325 events by Mitsakou et al. [20]

Observing CME signatures often presents a lot of difficulties. A CME usually takes several days to travel from the corona to the point where the spacecraft is present, about 1 AU away from the Sun. Its composition can alter considerably throughout this journey due to interactions with the background solar wind, which can make it challenging to figure out its state during ejection. Apart from that, information about the evolution of ICME beyond the typical observation distance of 1AU and its interaction with the heliospheric boundary remains less known. Magnetohydrodynamic (MHD) simulations have shed light on the shape changes ICMEs go through while moving through the heliosphere, revealing a stretching and flattening of ICMEs, described as “pancaking”. Yet, there is a lack of observational evidence to back these results. Thus creating and proving an all-inclusive theoretical model for CME is a challenge.

1.2 Geomagnetic Impact

ICMEs are primary sources of geomagnetic storms on the Earth, which are prolonged disturbances in Earth’s geomagnetic field, lasting from hours to weeks Since ICMEs-magnetosphere interaction poses a significant threat to human health and technology, which includes communication channels. Our dependence on these technologies makes it essential to understand the ICME-magnetosphere interaction in greater depth.

Geomagnetic storms are caused by a complex interplay of ICMEs, ionospheric and magnetospheric activity. The mechanism of magnetic storms revolves around the large-scale advection or convection within the Earth's magnetosphere, a process first proposed by Dungey in 1961. This interaction begins when magnetic reconnection at the subsolar magnetopause allows for the solar wind to transfer magnetic flux into the Earth's magnetotail which gets accumulated in the tail lobes. Over time, this accumulation triggers reconnection in the distant magnetotail, closing the magnetic flux and propelling it back towards the side (with a day) of the magnetosphere. This cyclical process is known as the Dungey cycle. [23] which results in the energization and transport of charged particles into the near-Earth space environment, leading to a strong ring current around Earth. The ring current is primarily composed of drifting electrons and ions in the energy range of a few tens to several hundreds of keVs that can have a large impact on Earth's geomagnetic field.

The intensity of this ring current is found by the hourly Dst index, which is calculated from observations made by low-latitude magnetometers. [24] A Decrease in the Dst index signifies an enhancement of the ring current, which can signify the development of a magnetic storm. This relationship underscores the connection between the dynamic processes in the magnetosphere induced by solar wind-magnetosphere interactions and the observable changes in Earth's geomagnetic field during magnetic storms.

The strength of a magnetic storm is defined by the minimum Dst value. The z component of the IMF is a good indicator of geomagnetic storms.[25] A severe storm will typically have $B_z \leq 10$ nT lasting ≥ 3 hours, with Dst ≤ 100 nT.

It is interesting to note that storm strength varies between sheath region-induced storms and those caused by MO or ejecta, as either can independently trigger a storm due to their distinct structures. A portion of the thesis will look at such differences along with MO-induced storms.

Chapter 2

Solar Wind Turbulence

In his 1975 lectures, Alexander J. Chorin [26] makes a note on turbulent flows which beautifully demonstrates the complexity and intriguing dynamics of turbulence. He noted:

> *"In turbulent flows, the velocity field appears to be random and varies unpredictably; the flow, however, does follow a set of equations that are not random. This contrast is the source of much of what is interesting in turbulence theory."*

Navier stocks are the fundamental equations that describe hydrodynamic turbulence, which are valid for incompressible flows.

$$\nabla \cdot \mathbf{u} = 0, \tag{2.1}$$

$$\frac{\partial \mathbf{u}}{\partial t} + (\mathbf{u} \cdot \nabla)\mathbf{u} = -\nabla P + R_e^{-1} \nabla^2 \mathbf{u} + \mathbf{F}, \tag{2.2}$$

where $\mathbf{u}$ represents the velocity field of the fluid, P represents the pressure field, R_e is the Reynolds number ($R_e = \frac{LU}{\nu}$, with L being the characteristic length and ν is the kinematic viscosity), and $\mathbf{F}$ is the body force per unit mass acting on the fluid.
Hydrodynamic turbulence theory describes that turbulence begins as large-scale motion by excitation of waves of large wavelength eddies and, through a chained effect, produces eddies of smaller wavelengths. Kolmogorov's work on the energy cascade in turbulence attempted to interpret and explain the complex phenomenon of turbulence within the framework provided by the Navier-Stokes equations by creating a phenomenological model that describes the behavior of energy in hydrodynamic turbulent systems with the assumption of isotropy and local k-space interaction. He concluded that energy transports scales as

$$E(k) \propto k^{-5/3} \tag{2.3}$$

where k is the wavenumber and E(k) is energy dependent on the eddy wavelength. This energy scaling law is valid for the inertial subrange, which contains wavenumbers between the forcing scale at small wavenumber and dissipation scale at large wavenumber. Wavenumber (k) value can be written interchangeably with frequency (f) by Taylor's hypothesis.

Plasma turbulence works very similarly to hydrodynamic turbulence and in most of the astrophysical observations, Kolmogorov's scaling law is still valid but it should also involve additional forcing due to electromagnetic effects and charged particle dynamics, which are governed by the magnetohydrodynamics (MHD) equations. This kind of turbulence is present throughout the universe and a wide range of environments, which includes accretion disks, galaxy clusters, interstellar medium, planetary magnetospheres, and stellar/solar winds. While being a fascinating aspect of our universe, it has an essential effect on the large-scale properties of such astrophysical systems. For example, it can be involved in galactic magnetic field amplification [27], can create angular momentum transport in accretion disks [28], it could also determine the dispersal of elements in the interstellar medium. [29] Turbulent plasmas exhibit chaotic, unpredictable, and complex fluctuations. These are typically understood as a scale-invariant cascade of energy from larger scales to smaller scales, that is, from where the energy is injected to where it is dissipated. Yet, numerous questions still exist regarding both the cascade and dissipation of this energy. The solar wind poses to be the best place to understand the physics of plasma turbulence and is also regarded as a laboratory for understanding plasma behavior.

2.1 MHD and Alfvénic Turbulence

Unlike purely hydrodynamic turbulence, MHD turbulence involves the coupling between the kinetic energy of the fluid motions and the magnetic energy associated with the magnetic field. This coupling leads to a complex cascade process, where energy can be transferred not only through the velocity field (similar to hydrodynamic turbulence) but also through the magnetic field, mediated by Alfvén waves. It has been established that the solar wind contains large-scale fluctuations that are Alfvénically polarized and are predominantly moving away from the Sun [30]. Such fluctuations are considered to be Alfvén waves that are produced at or near the Sun's vicinity, and these waves then move into the expanse of interplanetary space, creating a cascade of turbulence. Observational evidences reveal that these large-scale magnetic fluctuations exhibit a frequency spectrum of $1/f$, It has been explained either as the result of disparate, uncorrelated processes occurring on the Sun [31] or as the outcome of a cascade propelled by wave reflections. Our primary interest is in the turbulence at relatively smaller scales that is stimulated by these large forcing scale fluctuations.

Magnetohydrodynamics (MHD) equations govern the dynamics of Alfvénic turbulence with incompressibility assumption, represented in the context of fluctuating Elsasser variables as,

$$\frac{\partial \delta z^{\pm}}{\partial t} \mp v_A \nabla_{\parallel} \delta z^{\pm} + \delta z^{\mp} \cdot \nabla \delta z^{\pm} = -\nabla P, \tag{2.4}$$

$$\nabla \cdot \delta z^{\pm} = 0, \tag{2.5}$$

(without considering forcing and dissipation influences)
wherein $\delta z^{\pm} = \delta v \pm \delta b$ denote the Elsasser variables in their fluctuating states, with v representing the flow velocity, $b = B/\sqrt{\mu_0 \rho}$ shows the magnetic field expressed in Alfvén units, ρ indicating the mass density, and $v_A = B_0/\sqrt{\mu_0 \rho}$ is Alfvén velocity, P shows total pressure (magnetic and thermal), and $\nabla_parallel$ shows the gradient aligned with the mean magnetic field B_0. Iroshnikov (1963) and Kraichnan (1965) proposed an initial model to understand Alfvénic turbulence (also referred to as IK). The nonlinear interaction terms, $(\delta z^{\mp} \cdot \nabla \delta z^{\pm})$, shows the engagement between oppositely moving Alfvén wave packets (δz^{+} and δz^{-}). Assumptions of isotropy in turbulence imply that only weak interactions will happen in a strong magnetic field, so multiple interactions would be required for energy to cascade to smaller scales. If a constant energy flux is considered, based on the cascading time, it provides the inertial range spectrum of energy (total), which is given by,

$$E(k) \propto k^{-3/2}, \tag{2.6}$$

where k is the wavenumber associated with the fluctuations.

2.2 Turbulence in ICME

The structure of ICMEs comprises a highly compressed and turbulent sheath region in which fluctuations are so large that it is hard to get a clear picture of the inherent fields (average values) on top of which fluctuations are riding. It is present following the shock and is succeeded by a colder, quieter magnetic obstacle. In MOs, fluctuations are not as intense as sheath. The differences in the speed, size, geometry, and magnetic configuration of ICMEs and their regions can give diverse dynamical properties, for which statistical observations might help in predicting some sort of "expected" behavior. Their interactions with the inhomogeneous background/ambient solar wind can also play a significant role in determining their expansion and related properties, including magnetospheric coupling.

2.2.1 Significance of turbulence in Sheath Region

The sheath acts as a barrier between shock and the MO. Turbulence within this sheath is not just a mere consequence of the interaction between the ICME/MO and the solar wind; it creates a mechanism for energy transfer and dissipation along with it; this turbulence in the sheath plays a significant role in the ICME's ability to affect the Earth's magnetosphere. Understanding the turbulence characteristics within the sheath can be critical for understanding the geomagnetic impact of ICMEs.

Turbulence in the interplanetary plasma is influenced by encounters with ICMEs, which, in turn, affects the propagation of the ICMEs themselves. The dynamics of how sheaths and solar wind interact show difference in turbulence spectra which currently is uncharted territory. Highly turbulent ICME sheaths significantly influence the magnetosphere of the Earth and are a greater cause of geomagnetic disturbances. Our ability to mitigate the effects of space weather on technological systems and infrastructure on Earth depends on a good understanding of ICME sheaths.[32]

2.3 Motivation and Objectives of the thesis

Previous research on the interactions between turbulence and ICMEs typically views each ICME as a monolithic structure—essentially as one cohesive unit. However, this approach glosses over the internal complexities of ICMEs, particularly the varying turbulence characteristics found within different regions of these space phenomena. Our study seeks to delve into these complexities.

Turbulence within an ICME isn't uniform; it varies widely and has different properties depending on where you look within the ICME. To explore these variations, we are focusing on the role of high-frequency fluctuations, which are essential elements of these turbulent characteristics.

In the analysis of time series data, which captures various signals including those from space phenomena like ICMEs, two primary types of frequency components are observed: lower-frequency components and high-frequency components. Lower-frequency components are stable, forming the foundational or baseline frequencies of the signal. These frequencies are crucial as they define the core characteristics of the signal. In contrast, high-frequency components are more volatile and contribute to the signal's noise. It is these high frequencies that introduce randomness and fluctuations, creating what can be described as a "turbulent" signal.

We aim to examine how these high-frequency fluctuations influence the behavior and properties of space plasma turbulence. We are particularly interested in their impact across different environments such as the sheath (the region between a shock and the front of the ICME), the background solar wind, and the Magnetic Obstacle (MO) — the region within the ICME characterized by enhanced magnetic field strength and distinct from the surrounding solar wind. By analyzing these high frequencies, we hope to gain a deeper understanding of the internal dynamics of ICMEs and their interaction with surrounding space plasma, thus offering a more nuanced view than the prevailing assumption of ICME uniformity.

This approach not only challenges existing models but also aims to refine our understanding of space weather phenomena by acknowledging and characterizing the intricate internal structures and turbulence behaviors within ICMEs.

- We analyze time series data for plasma density (N_p), velocity magnitude (V), and magnetic field magnitude (B). Through Fourier transforms, we decompose this data into its frequency components. Our goal is to isolate and compare the power in high-frequency fluctuations against the power in low-frequency fluctuations, which constitute the baseline signal.

- We also assess the impact of different ICME regions on the Earth's geomagnetic field, specifically using the Dst Index. By correlating changes in the Dst Index with plasma conditions within ICMEs, we aim to understand better how these solar events affect geomagnetic disturbances. This approach is informed by prior studies, such as [21], which highlighted the sheath region as a significant contributor to geomagnetic disturbances. Our analysis will consider correlations between Dst indices and the measured values of density, magnetic field magnitude, and velocity magnitude as ICMEs encounter Earth.

- The tasks outlined will be applied across a broad spectrum of events to discern patterns of large-scale statistical behavior. Additionally, we will explore the influence of shock presence or absence on the outcomes, assessing its significance in the observed results.

Chapter 3

Data and Methodology

3.1 Data

3.1.1 About the Spacecraft

The data used for this study was taken from WIND spacecraft. It was launched by NASA in November 1994 with the aim of making in-situ solar wind measurements and detecting disturbances in interplanetary space. It is currently operating at L1 point and it had earlier spent a few years at the Lagrangian point L1 after the commencement of the mission, but after a while, it acquired an elliptical orbit that took it further away from the Sun-Earth line till it completed L2 operation in 2003. [33]

3.1.2 Data

The data distribution portal for WIND Spacecraft https://wind.nasa.gov/mfi_swe_plot.php is an open-source portal that provides a comprehensive list of plasma and magnetic field parameters that can be used for any investigation. For this study, our analysis is limited to using 1-minute spaced time series data of magnetic field magnitude (B), velocity magnitude (V), and proton Number Density (N_p), readings of which are taken from Magnetic Field Investigation (MFI) and Solar Wind Electron (SWE) instrumentation present onboard WIND Spacecraft. In essence, velocity magnitude is the overall speed at which the bulk of the plasma is moving past the spacecraft, and N_p is the concentration of protons in a given volume of space measured in cm^{-3}.
Magnitudes for magnetic field and velocity are the net resultants produced from the readings in x, y, and z directions in the geocentric solar ecliptic (GSE) coordinate system. Units for which are nT and km/s, respectively.

A catalog of Interplanetary Coronal Mass Ejection (ICME) events is made available online by Nieves-Chinchilla et al. [34] at the NASA Wind mission website. The catalog can be accessed through the following URL: `https://wind.nasa.gov/ICME_catalog/ICME_catalog_viewer.php`. This catalog serves as a central repository from which modified lists of ICME events are derived (discussed in the sections ahead). It consists of ICME events that are not susceptible to other solar wind transients since it is important to consider ICME events that have a definite detectable structure. The strategy involves a two-step process centered around the retrieval and utilization of data. Initially, the task is to identify and gather events devoid of interference from other solar transients from the catalog, also referred to as the central list, based on meeting predetermined criteria for shortlisting. Following this initial selection, the focus shifts to leveraging the time information (start and end times) of these shortlisted events. This time information is then used to retrieve corresponding datasets from the WIND data repository/portal.

The catalog (central list) mentioned here is documented in Table A.3 of the appendix. It contains ICME events from 1995 to 2021 containing an array of parameters like ICME sheath start time, shock, magnetic obstacle (MO) start and end times, MO Type, mean magnetic field magnitude value in the MO interval (B), mean solar wind bulk velocity in the MO interval (V_{sw}), expansion velocity (V_{exp}) and Disturbance storm time (Dst) index. For this study, all MO types (Flux-rope (Fr), Small rotation flux-rope (F-), Large rotation flux-rope (F+), Complex (Cx), or Ejecta (E)) in ICME events were included.

3.2 Event and Region Selection Criteria

We shortlist instances where there is a gap of at least 3 days between successive events from the catalog (Table A.3), so if the gap is smaller than 3 days, the event is rejected. This is to ensure that the ambient/background solar wind is free of any solar transients that could potentially add fluctuations in the background solar wind.
As our aim is to compare the power inside the sheath and MO and the background solar wind, we need concrete criteria to define the background; that is, it should be quiet and in the vicinity of the sheath and MO. Since we exclude events occurring less than 3 days apart to prevent interference from transients, the three-day interval before the detection of a shock or the onset of a sheath serves as the background solar wind.

3.2.1 Defining Sheath and Magnetic Object

As stated earlier, the sheath is defined as the region between shock or sheath start to the leading edge of the MO/ICME. It follows the background solar wind and is immediately followed by the MO. While the sheath-ICME boundary could be very turbulent, it is relatively short-lived, about 1.7-3 hours [35], and because of the broad nature of this study, the boundary layer as a region is ignored. Magnetic obstacle (MO) begins from the sheath-MO/ICME frontal boundary (leading edge) and ends at the rear boundary. Our MO start and end times follow catalog times similar to the sheath.

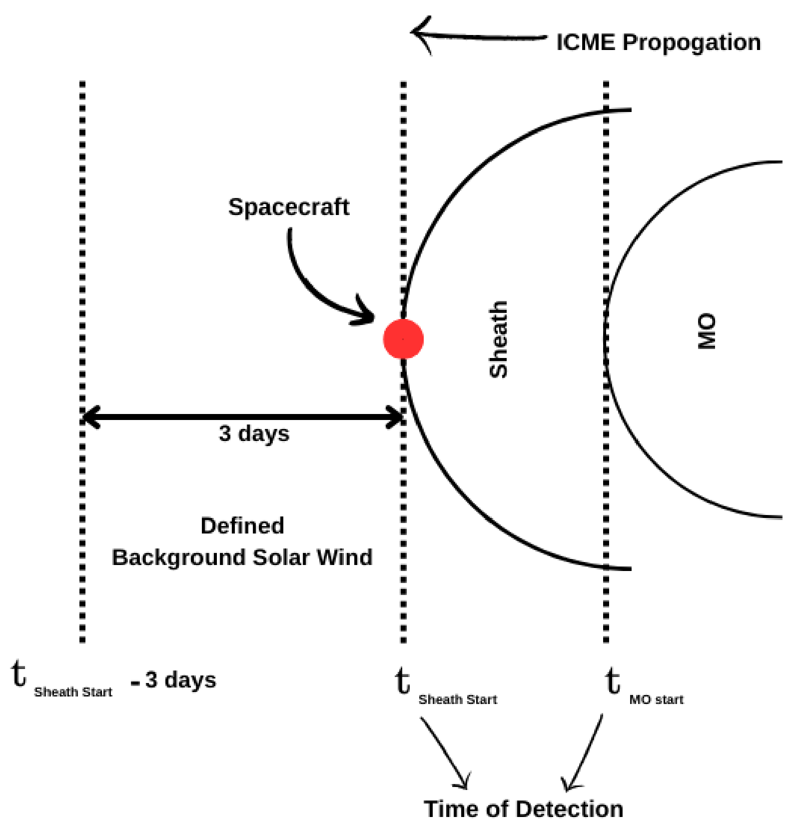

Figure 3.1: A cartoon depiction showing the definition of background solar wind along with sheath and MO start timings of a propagating ICME.

3.2.2 Events with Shock and Mixed Events

Typically, an ICME event that has a clear shock shows a discontinuity at the shock front. However, in many cases, these discontinuities are not vivid in observations; they appear as subtle signatures of shock. In the catalog used, events with a clear shock show a defined discontinuity. The shock signatures are subtle for the other events, and the sheath start boundary acts as a proxy for the shock boundary. Based on this, events are classified into two categories: those accompanied by a defined shock and also meeting the previously mentioned 3-day gap criterion are labeled “shock = Y”. A list of 130 events fitting these criteria is compiled in Table A.1 of the Appendix. These are referred to as ICME events with shock. Additionally, another list, comprising 271 events that include both categories—with and without shock (where the sheath start boundary is taken as the shock)—but also adhering to the 3-day gap criterion, is presented in Table A.2 of the Appendix. These are referred to as mixed ICME events.

This classification is pivotal because ICMEs that feature shocks may exhibit distinct characteristics compared to those ICMEs lacking shocks. For an ICME to drive a shock, its speed in the solar wind frame must exceed the speed of the MHD wave. The presence of shock is marked with a discontinuity, and an encounter with sheath subsequently shows increased values in the magnetic field, velocity, density, and temperature. ICMEs that propagate faster than the preceding solar wind but not fast enough to drive a shock also deflect and compress the plasma flow ahead, creating a sheath. However, there is a possibility that the properties of the sheaths with and without a shock or with shock might differ. Our fundamental assumption rests on defining the sheath as the region between the shock and the leading edge of the MO, which holds true exclusively in the cases where a shock is present. Detecting the sheath in case shock is present is fairly straightforward because of its distinct signatures. The time of detection of shock is calculated using algorithms that detect the discontinuity in solar wind properties that is with the help of the ratio of the downstream density to the up-stream density $\rho 2/\rho 1$ and the ratio of fast-mode Mach numbers in the upstream and downstream regions M_{f1}/M_{f2} [36], where upstream is the region behind the shock and downstream is the region ahead of the shock towards the direction of propagation of the shock front. While shock detection is relatively straightforward, identifying the Sheath-MO boundary is a complex subject.

The detection of event boundaries can vary significantly depending on the chosen catalog.[37] To ensure consistency across this study, the catalog by Nieves-Chinchilla et al.[34] was exclusively used. This approach means that Tables A.1 (events with a shock) and A.2 (a mixed list of events) were derived using the ICME catalog by Nieves-Chinchilla et al. (Table A.3), with a specific focus on selecting only those events that meet the criterion of a minimum 3-day gap between successive events. The catalog (Table A.3 in the appendix) provides detailed timing for the detection of shocks, leading edges, and the end of ICME events.

3.3 Power-Frequency Analysis

We employ Discrete Fourier Transform (DFT) on the magnetic field, density, and velocity data retrieved from the WIND data portal, which essentially operates based on the time information (start and end times) from events. The analysis is applied separately to time series data from three distinct regions: the background solar wind, the sheath, and the MO region. This DFT process is performed for every event in our dataset, including those categorized as having a shock and those in the mixed events list (A.1 and A.2, respectively).

DFT, in general is a mathematical operation that translates a discrete signal from its time or space domain into the frequency domain and vice versa, while Fourier transforms are used where the signal is a continuous time function. In reality, in almost all practical situations, time series signals are discrete, thus making DFT highly useful for analyzing time series data. The use of power-frequency analysis is not only essential here, but it also extends to practical applications across diverse domains such as telecommunications, seismology, audio processing, etc.

3.3.1 Discrete Fourier Transform (DFT) and Short Time Fourier Transform (STFT)

The DFT converts a finite sequence of equally-spaced samples of a function into a sequence of coefficients of a finite combination of complex sinusoids, ordered by their frequencies. For converting to the frequency domain from the time domain, these coefficients are of the form,

$$X(k) = \sum_{t=0}^{N-1} x(t) \cdot e^{-j\frac{2\pi}{N}kt} \tag{3.1}$$

Where $X(k)$ represents the k-th element in the frequency domain coming from the t-th sample $x(t)$ in the time domain, where N denotes the total number of samples. The index k is associated with a specific frequency, denoted as $f_k = \frac{kf_s}{N}$, with f_s being the sampling frequency. These frequencies in the Discrete Fourier Transform (DFT) output are uniformly allocated between 0 and f_s. The sampling frequency f_s is inversely proportional to T_{max}, which is the longest duration within the sample set. Given that our signal data is sampled every 100 seconds, the resolution $\frac{f_s}{N}$ approximates to 1/100 seconds.

This study primarily focuses on identifying the power distribution across various frequencies. However, converting from the time to the frequency domain leads to the loss of time-specific information. To overcome this, one of the effective ways is to involve segmenting the DFT into shorter time frames and applying Fourier transforms individually to these segments. This approach addresses the loss of temporal details to an extent as it navigates the trade-off between time and frequency resolution inherent in Fourier analysis. Specifically, enlarging the time window enhances the transform's accuracy but at the cost of reducing time resolution and vice versa. This is frequency-time uncertainty. An optimal balance between time and frequency resolution is vital for obtaining accurate results from the analysis.

The STFT, particularly, is used to determine the sinusoidal frequency and phase content of local sections of a signal as it changes over time. This can be achieved by multiplying the signal by a window function that isolates a particular section of the signal very similar to fourier transform. The STFT is defined as:

$$STFT\{x(t)\}(f,\tau) = \int_{-\infty}^{\infty} x(t) \cdot w(t-\tau) \cdot e^{-j2\pi ft}\, dt \tag{3.2}$$

where $w(t-\tau)$ is the window function centered around time τ, and f is the frequency. This allows for the analysis of the signal in both time and frequency. Use of STFT will come in our case when slicing the time series data inside ICME events to find out the smallest possible slice time width, which can basically replicate the results for a smaller duration.

The Power Spectral Density (PSD) measures the power of a signal as a function of frequency, which is useful for identifying power distribution across frequencies. For a signal, the PSD can be estimated using the periodogram, which is the square of the magnitude of the Fourier Transform of the signal per unit frequency. The power in a small frequency range *df* can be calculated by:

$$\text{Power} = \int_{f_1}^{f_2} PSD(f)\,df \tag{3.3}$$

where frequencies vary from $f1$ to $f2$, PSD (f) = $|X(f)|^2$, $X(f)$ is the Fourier transform of the signal.

Power Spectral Densities (PSDs) were generated for the background, sheath, and magnetospheric object (MO) regions across all events featuring shocks as well as mixed events, as cataloged in Tables A.1 and A.2. Subsequently, we quantified the aggregate power within the designated "high frequency" spectrum, the parameters for which are elaborated in the next section and chapter 4. Figure 3.2 showcases the PSD of the magnetic field's magnitude plotted on a log-log scale. Although these power estimations on a log-log scale act primarily as approximations rather than exact measures of power, they suffice for our analytical purposes. Our principal objective centers on comparing the power ratios between the high and low-frequency components.

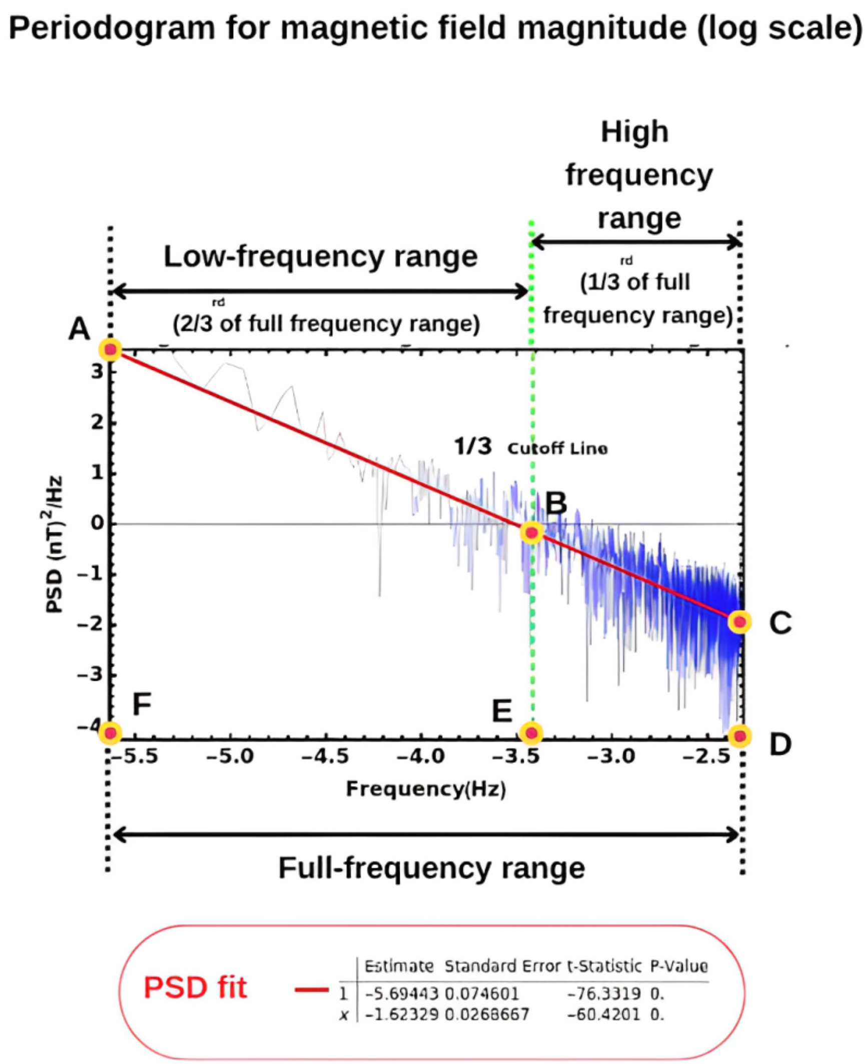

$$\text{Modulation Index} \left(\frac{\delta B}{B}\right) = \frac{\text{Area (BCDE)}}{\text{Area (ABEF)}}$$

Figure 3.2: PSD, displayed on a logarithmic scale, illustrates the spectrum of magnetic field fluctuations in the background solar wind. It includes a spectral index or fitted slope (refer to section 3.3.2) and marks a high-frequency cutoff line (detailed in section 4.1). The Modulation Index is calculated as the ratio of the areas of two trapeziums, BCDA and ABEF, defined by this cutoff line.

PSD in Figure 3.2 and, for the most part, show roughly a frequency range $\approx$ -6 to -1, which takes in part of forcing scale and inertial scale fluctuations.

3.3.2 Spectral and Modulation Index

The Spectral Index is the slope obtained from linear least squares fitting of the Power Spectral Density (PSD) on a log-log scale. It is crucial for understanding energy scaling laws in turbulence, as discussed in earlier sections. A steeper slope indicates more rapid energy dissipation. These scaling laws differ based on the origin and location of the turbulence, leading to variations in turbulence signatures across the Sheath, MO, and background solar wind regions of an ICME.

We look at the following parameters:

- **Power in frequencies**: Earlier discussions highlighted that fluctuations within the solar wind or ICME sheath comprise both high and low-frequency components, contributing to turbulence. Analyzing the power in high-frequency regions is key to understanding this turbulence. However, defining a precise cutoff for high-energy fluctuations is challenging, so we explore multiple cutoff points to compare outcomes (see section 4.1). Based on the linear fits obtained (or the spectral index) in the PSDs and the cutoff used, the PSD produces two trapezoidal regions, for example, in Figure 3.2, trapezium BCDE and trapezium ABEF. Power present inside trapezium BCDE is contributed by "high frequencies" present in the spectrum since the cutoff is defined in such a way that the frequencies above the cutoff are "high" and below it are called "low frequencies". Using this, it can be justified that the power in trapezium ABEF contributed by "low frequencies". We calculate the power by calculating the area of the trapeziums.

$$\text{Power in high frequencies} = \text{Area (BCDE)} \tag{3.4}$$

$$= \frac{(BE+CD)}{2}\,ED \tag{3.5}$$

$$\text{Power in low frequencies} = \text{Area (ABEF)} \tag{3.6}$$
$$= \frac{(AF + BE)}{2}\, EF \tag{3.7}$$

With this, we aim to compare the power of higher frequency components to lower frequency components within the PSD of the background solar wind, the sheath, and the MO, highlighting variations in turbulence among these regions.

- **Modulation index**: The modulation index for the background solar wind, sheath, and MO is calculated using the PSD as exemplified in Figure 3.2. While Figure 3.2 specifically showcases the PSD for the background solar wind using magnetic field data, it's important to note that the PSDs for the sheath and MO, including those derived from velocity and density data, follow a similar pattern. For the sake of understanding, look beyond the specific example of a magnetic field PSD presented in Figure 3.2. Instead, consider this as a general model for PSD applicable to any dataset, whether it be the background solar wind, sheath, or MO, encompassing a range of data types, including density, velocity, or magnetic field.

  Modulation Index is defined as:

$$\left(\frac{\delta A}{A}\right)_{\text{X}} = \frac{\text{Power in high-frequency trapezium}}{\text{Power in low-frequency trapezium}} \tag{3.8}$$
$$\tag{3.9}$$
$$= \frac{\text{Area(BCDE)}}{\text{Area(ABEF)}} \tag{3.10}$$
$$\tag{3.11}$$
$$= \frac{(BE + CD) \cdot ED}{(AF + BE) \cdot EF} \tag{3.12}$$

The variable X in the modulation index $\left(\frac{\delta A}{A}\right)_X$ represents the specific region being analyzed in the PSD. This variable X can refer to one of the following regions:

1. The background solar wind, denoted as BG,
2. The sheath region, denoted as $sheath$,

3. The Magnetic Obstacle, denoted as MO.

Accordingly, we calculate three modulation indices: $\left(\frac{\delta A}{A}\right)_{BG}$, $\left(\frac{\delta A}{A}\right)_{sheath}$, and $\left(\frac{\delta A}{A}\right)_{MO}$, corresponding to each region. These indices are derived for three types of data (or "A" variable) which can be density (N_p), magnetic field (B), and velocity (V), respectively.

The general idea behind the modulation index is that solar wind carries baseline fluctuations or low-frequency signals that make up the basic construct of the signal. High frequencies act as noise. ICMEs introduce these additional fluctuations on top of baseline frequencies, which is noise. This can be considered modulation of the pre-existing baseline solar wind signal. In summary, the modulation index acts as a measure of turbulence.
For each ICME event listed in the tables for events with shocks and mixed events, we perform linear fitting to obtain spectral indices and modulation indices. This analysis covers density, magnetic field, and velocity data across the background solar wind, sheath, and MO regions for every individual event.

3.4 Summary of Procedure and Definitions

- We began by selecting ICME events from catalog A.3, ensuring a minimum gap of 3 days between events to maintain clarity in the analysis. Based on this criterion, we compiled two lists: A.1 and A.2. Events featuring a shock were included in both tables, while those without a shock were cataloged exclusively in table A.2.
- To maintain consistency in background conditions, we designated a fixed duration of 3 days prior to the onset of the shock or sheath start as the background period for each event. The sheath is the region between shock (or sheath start) and MO start. Whereas the region between MO start and MO end is the MO region.
- For all events in A.1 and A.2 spectral index, Modulation index were calculated using PSDs separately for background, sheath, and MO inside that event along with Dst index data.

Chapter 4

Results: ICME Turbulence Profiling

4.1 Organization of Chapter 4 (Results)

This chapter is organized as follows:

- **Histogram for Duration:** This section starts by examining the duration of the sheath and MO in the mixed events. It also investigates any potential correlation between the duration of the sheath and MO with the strength of magnetic storms, as indicated by the Dst index.

- **Modulation Index Cutoff Selection:** Here, we establish the methodology for selecting the cutoff for the modulation index and assess which cutoff is most effective.

- **Histograms for Density:** This part presents histograms of the density modulation index and spectral index for the events listed in Tables A.1 and A.2. It also examines the correlation between these indices and the Dst index.

- **Histograms for Magnetic Field:** In this section, we analyze histograms of the magnetic field magnitude modulation index and spectral index for the events in Tables A.1 and A.2, alongside exploring their correlation with the Dst index.

- **Histograms for Velocity:** Finally, we evaluate histograms of the velocity modulation index and spectral index for the events in Tables A.1 and A.2, investigating their correlation with the Dst index.

Each section dedicated to presenting histogram results begins with a description of the findings, followed by a brief discussion of the results.

4.2 Histogram for Duration

- The duration of the sheath and MO were found using the aforementioned definitions for the mixed events list.

- The results indicate that the sheath is shorter than the MO by ≈ 2.68 times. Where most sheaths lie between 0 to 600 minutes having a mean duration ($\langle t \rangle_{\text{Sheath}}$) of $\approx 566 \pm 24.8$ minutes and MOs have a mean duration ($\langle t \rangle_{\text{MO}}$) of $\approx 1520 \pm 47.6$ minutes.

- The median duration of MOs (1382 minutes) in the histogram is greater than sheaths (482 minutes).

Results are close to what Mitsakou and Moussas [20] found out in their statistical study of ICME sheaths. The comparison between mean and medians can suggest that there is a lot of variability and a wider range of physical conditions and processes that can affect their formation and structure, as opposed to the relatively more uniform conditions under which sheaths are formed.

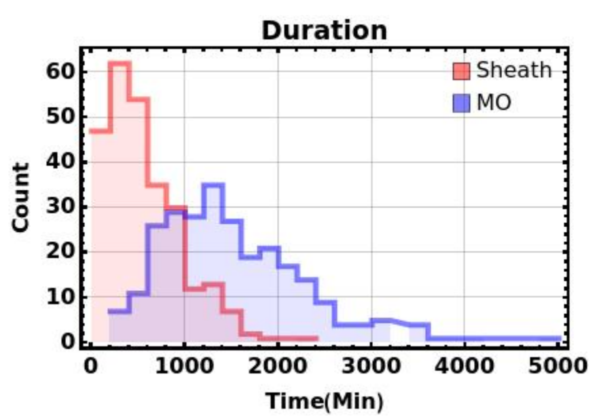

Figure 4.1: Combined histograms showing the duration distribution of sheath and MO for ICME events (mixed events), highlighting the fact that sheaths have a shorter mean duration compared to MOs. $\langle t \rangle_{\text{Sheath}} \approx 566$ minutes and $\langle t \rangle_{\text{MO}} \approx 1520$ minutes

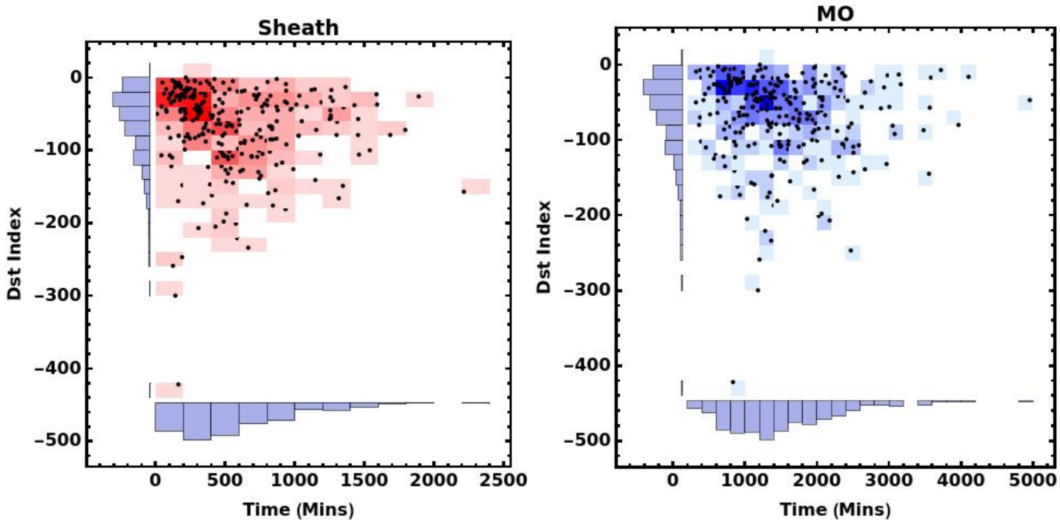

Figure 4.2: Dst index correlations with t_{Sheath} (left) and t_{MO} (right) for events in the mixed events list.

Correlations between the Dst index and the durations of the sheath and MO were investigated, as depicted in the scatter-plots in Figure. 4.2. However there is no definitive pattern emerges that strongly correlates the duration of sheaths and MOs with higher Dst index values in the histograms. One possible interpretation from this can be that the most intense geomagnetic storms (Dst ≤ -100 nT) are predominantly associated with ICMEs that have sheath and MO durations close to their respective average values.

4.3 Modulation Index Cutoff Selection

A cutoff is required to categorize frequencies into high and low frequencies. This cutoff acts as a separator between high and low-frequency fluctuations. Identifying the optimal cutoff that accurately characterizes turbulence within ICME regions poses a challenge, as there is no definitive method to ascertain the best cutoff a priori. So the best possible way is to try the analysis with a variety of cutoffs and look at how they compare at the characterization of turbulence or at separating ICME regions.

For this reason, the analysis was carried out with 1/n cutoff, where 'n' was chosen as (5,4,3,2 and 3/2) here 1/n cutoff implies 1-(1/n) of the total frequencies in the PSD calculated act as low frequencies where they start from the lowest frequency, and the rest 1/n of the remaining are labeled as high-frequency fluctuations.

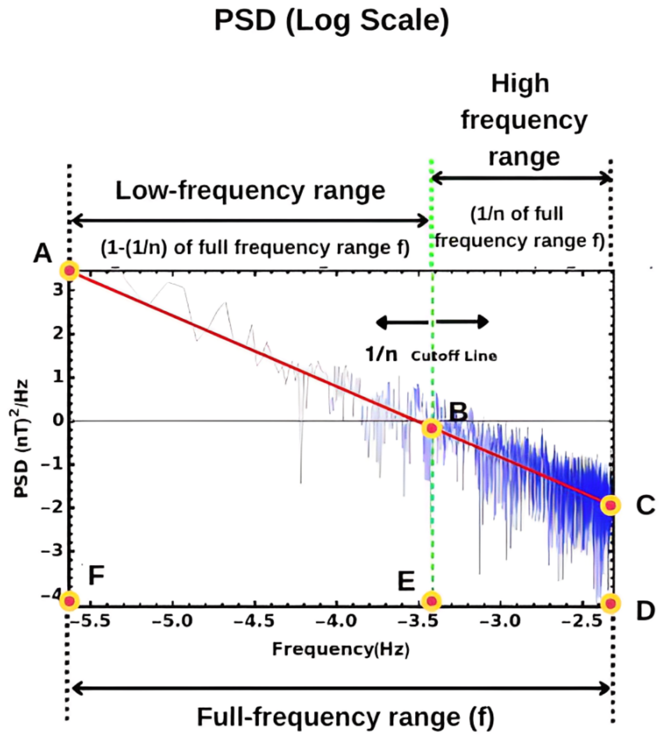

Figure 4.3: A PSD includes a cutoff line defined by $f_{\min} + \left|1 - \frac{1}{n}\right| f$, where f is the entire frequency range ($f_{max} - f_{min}$). As detailed in Chapter 3, this cutoff line delineates two trapezoidal areas: high-frequency (BCDE) and low-frequency (ABEF). We adjust n to values of 5, 4, 3, 2, and $\frac{3}{2}$ to compute the modulation indices.

The characterization of turbulence of ICME regions depends on the separation of sheath, MO, and ambient/background solar wind inside the in the combined histogram distributions (see figure 4.4 - 2/3 cutoff). For which separation ability of the cutoff is calculated by,

$$\text{Separation value} = \frac{|\text{Median}[data1] - \text{Median}[data2]|}{\text{Mean MAD}}$$

$$\text{Mean MAD} = \frac{\text{MAD}[data1] + \text{MAD}[data2]}{2}$$

Separation value takes into account that the separation in distributions is proportional to the difference between the medians of the distributions and inversely proportional to the MAD values, Where MAD is the median absolute for each region within the distribution. The reason for using median and MAD values instead of mean and standard deviation depends on the nature of the distribution, which, most of the time, is skewed. Here data1 and data2 can be (sheath and background) or (sheath and MO), respectively. Thus it gives two separation values for the distribution of the sheath. The separation values can vary from 0 to positive infinity, 0 meaning the distributions are completely identical and are overlapping, whereas values close to 1 (this is true only for the distributions we are dealing with) would imply a good separation between distributions. We are interested in the characterizability of the turbulence, especially the sheath thus, our ideal condition would be to have as high separation values as possible.

- For the above separation values, based on Figures 4.4, 4.5, and 4.6, it can be confirmed that the 2/3 cutoff works best for fluctuations of density (N_p) and velocity (V).
- A similar was true for the magnetic field fluctuations. It has a separation value of $\sim$ 0.622 and 0.473 for sheath-background and sheath-MO histograms, respectively, for mixed events.
- Figure 4.6 shows histograms for events with shock, and they are analogous to the histograms in Figure 4.5. It suggests there is not much difference between events with and without shock (events with shock and mixed events), which was also true for N_p and B histograms.

It can also be visually seen that the 2/3 cutoff works reasonably better in separation from the selected cutoff values however it might be possible that the optimal cutoff lies somewhere between 1/2 and 2/3. One possible reason behind cutoff $\approx$ 2/3 working better than others could be that the frequencies $\approx$ 2/3 cutoff are part of the forcing scale fluctuations, which would be the same for all sheath, MO, and background solar wind, and the difference in the turbulence of the regions comes in the inertial subrange. A large value of this cutoff makes the spectral index more sensitive to high-frequency data. To keep uniformity in the analysis, all of the results discussed below are based on 2/3 cutoff for the modulation index.

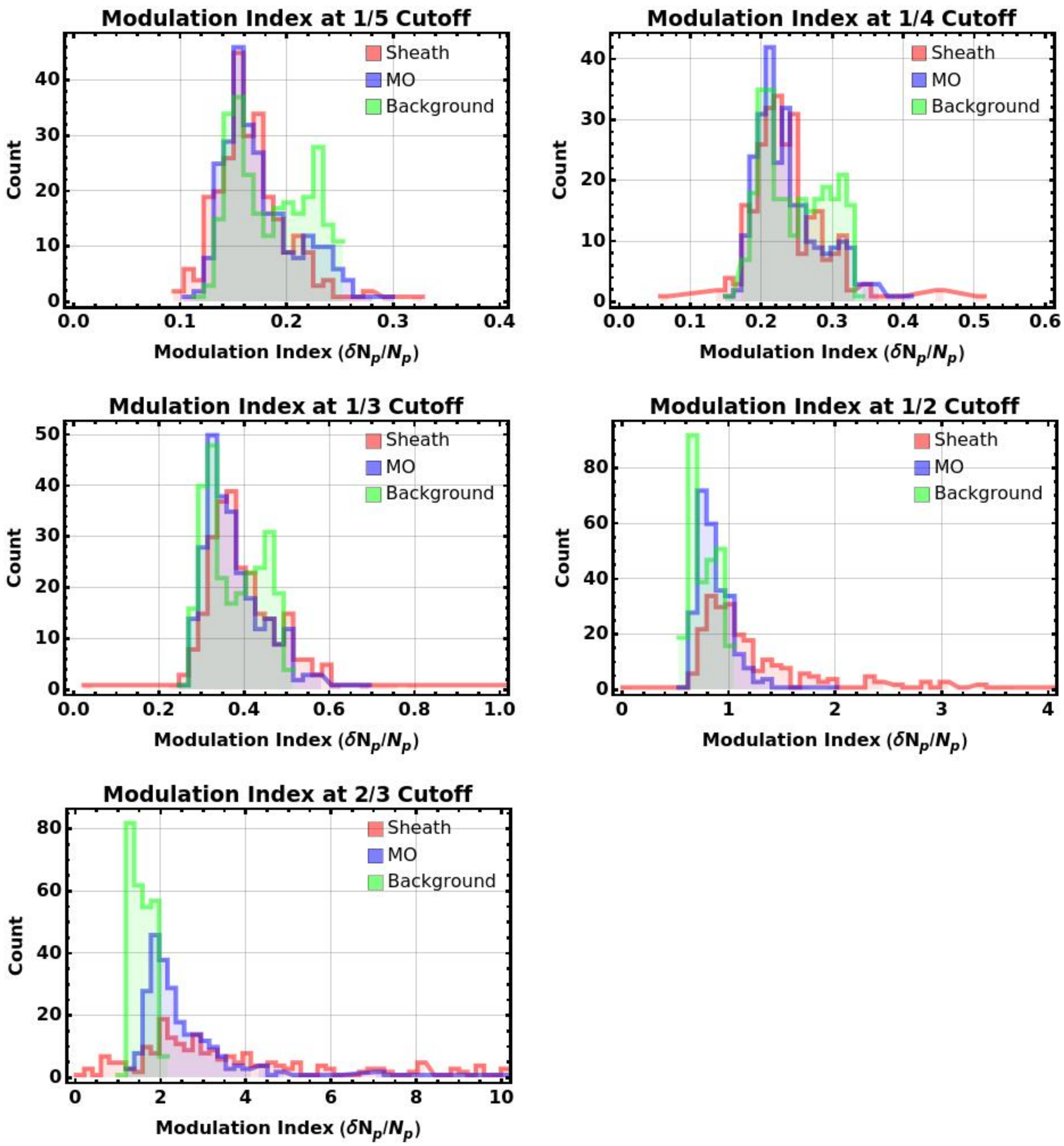

Figure 4.4: Histograms of modulation index ($\delta N_p/N_p$) of proton density N_p data for mixed events gives separation values of (0.190,0.034), (0.113,0.006), (0.048,0.088), (0.455,0.355), (0.538,0.343) for the cutoffs of 1/5, 1/4, 1/3, 1/2 and 2/3 respectively. The bracket structure represents separation values as follows: each pair within the brackets corresponds to the separation values between the sheath and background (first value) and the sheath and MO (second value).

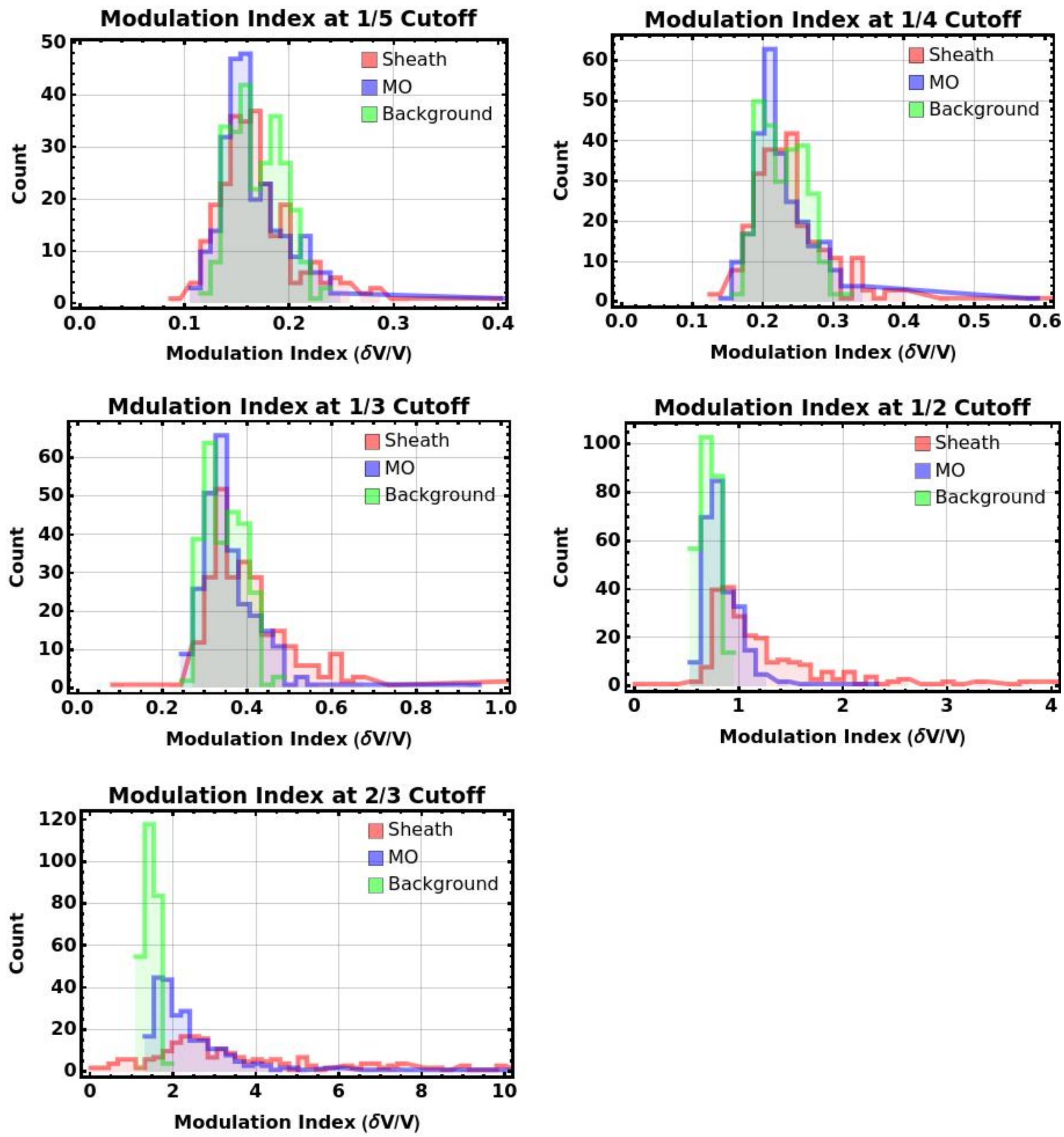

Figure 4.5: Histograms of modulation index ($\delta V/V$) of velocity (V) data for mixed events gives separation values of (0.052,0.063), (0.052,0.125), (0.246,0.236), (0.586,0.450), (0.593,0.371) for the cutoffs of 1/5, 1/4, 1/3, 1/2 and 2/3 respectively. The bracket structure represents separation values as follows: each pair within the brackets corresponds to the separation values between the sheath and background (first value) and the sheath and MO (second value).

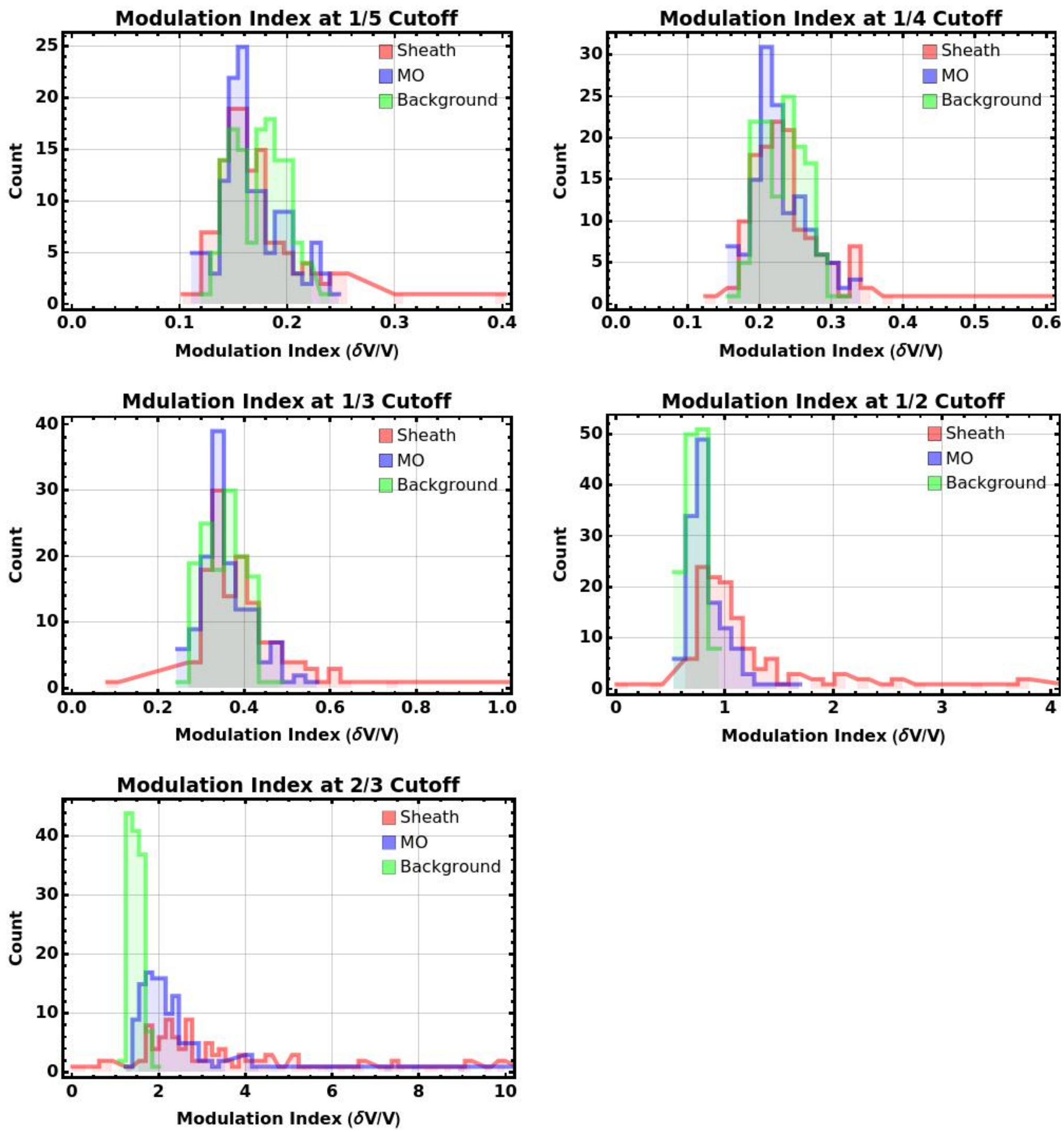

Figure 4.6: Histograms of modulation index ($\delta V/V$) of velocity (V) data for events with shock gives separation values of (0.185,0.009), (0.085,0.078), (0.121,0.179), (0.510,0.386), (0.622,0.423) for the cutoffs of 1/5, 1/4, 1/3, 1/2 and 2/3 respectively. The bracket structure represents separation values as follows: each pair within the brackets corresponds to the separation values between the sheath and background (first value) and the sheath and MO (second value).

4.4 Histograms for Density

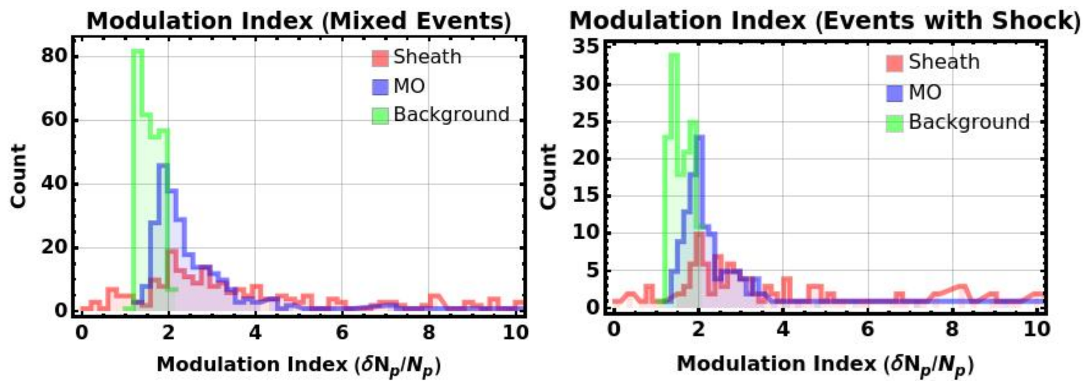

Figure 4.7: Histograms comparing the density modulation index ($\delta N_p/N_p$) for mixed events (left) and events with shocks (right). They show the distribution and variability within background solar wind, sheath, and MO regions.

- For density (N_p) fluctuations (Figure 4.7), the mean value for background fluctuations $\langle \delta N_p/N_p \rangle_{\text{BG}}$ is $\approx 1.55 \pm 0.01$, for sheath fluctuations $\langle \delta N_p/N_p \rangle_{\text{Sheath}}$ is $\approx 8.58 \pm 1.41$ and for MO $\langle \delta N_p/N_p \rangle_{\text{MO}}$ is $\approx 6.69 \pm 3.04$ for mixed events.
- For events with shock the results were similar, with mean values $\langle \delta N_p/N_p \rangle_{\text{BG}}$, $\langle \delta N_p/N_p \rangle_{\text{Sheath}}$ and $\langle \delta N_p/N_p \rangle_{\text{MO}}$ being $\approx 1.58 \pm 0.01$, 7.73 ± 1.00 and 3.78 ± 0.62 respectively.
- The medians of background, sheath, and MO were ≈ 1.51, 3.42, and 2.22, respectively, for mixed events. Events with shock showed medians of 1.58, 3.25, and 2.06 for background, sheath, and MO, respectively.

The spread of the values of the modulation index in background solar wind is comparatively smaller than that of MO and sheath. Since the median values of mixed events and events with shock are fairly similar, except that the modulation index for MO is a little shrunken, it can concluded that for density fluctuations ($\delta N_p/N_p$) having shock makes a small difference.

Previous research by Bhattacharjee et al. [38] [39] discovered that the density modulation index within the solar wind background is lower compared to that within Magnetic Clouds (MCs), a specific type of Magnetic Obstacle MO. However, it's important to note that their approach to calculating the modulation index differed. They employed a moving time window of 40 and 60 minutes to calculate fluctuations (δN_p) from the mean particle density

(N_p) within the window. The modulation index was then determined by the ratio of these fluctuations to the mean. The results shown here also suggest the same thing but additionally generalizing into MOs. The fact that the modulation index in sheaths is very widely spread may also suggest the fact that turbulence in sheaths is stronger than that in the MO. in Figure 4.8 Spectral index is double-peaked. This could be because of the power spectrum that shows a bulge at intermediate frequencies of positive slopes $f^{1/2}$ and $f^{1/3}$.[40]

The spectral index for sheath and MO are very alike, with the mean spectral index of -0.73 $\pm$ 0.03 and -0.72 $\pm$ 0.03, respectively, and median values of $\approx$ -0.69 for both sheath and MO. Background solar wind shows a different mean and median value -0.975 $\pm$ 0.03 and ≈ -1.15, respectively. Dst index correlation suggests that most common value for density modulation index in the geomagnetic storms for MO is $\approx$ 1.80, for the sheath is $\approx$ 3.60, and for the background is $\approx$ 1.35.

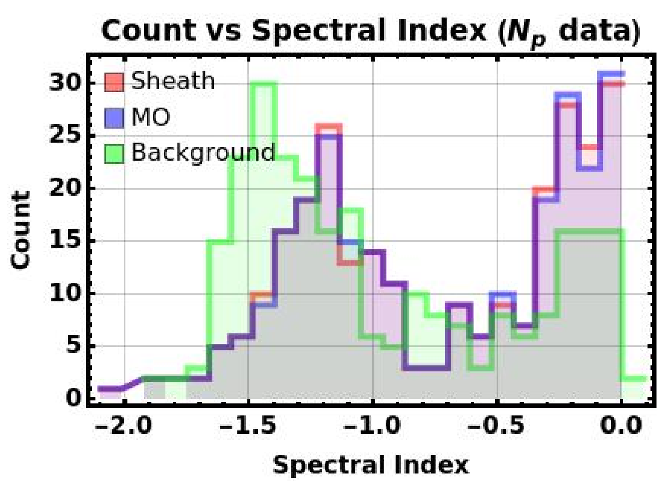

Figure 4.8: Histogram for spectral index of sheath, background, and MO for density spectral index close to inertial range. It shows a double-peaked non-Gaussian spectral index distribution, with the peak on the left close to -5/3

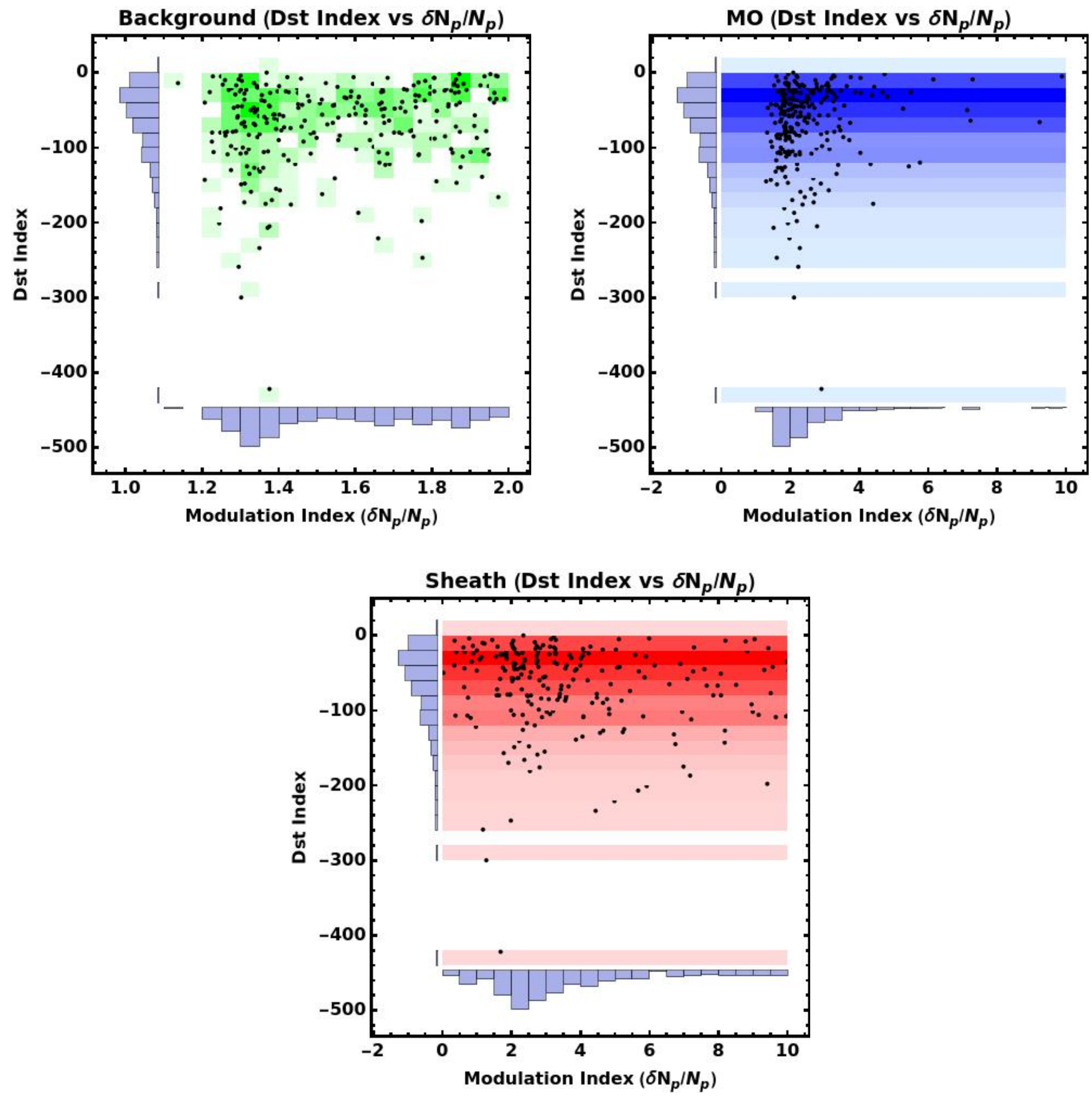

Figure 4.9: Scatter plots showing correlations between density modulation index ($\delta N_p/Np$) for background, MO, sheath, and the Dst index.

4.5 Histograms for Magnetic Field Magnitude

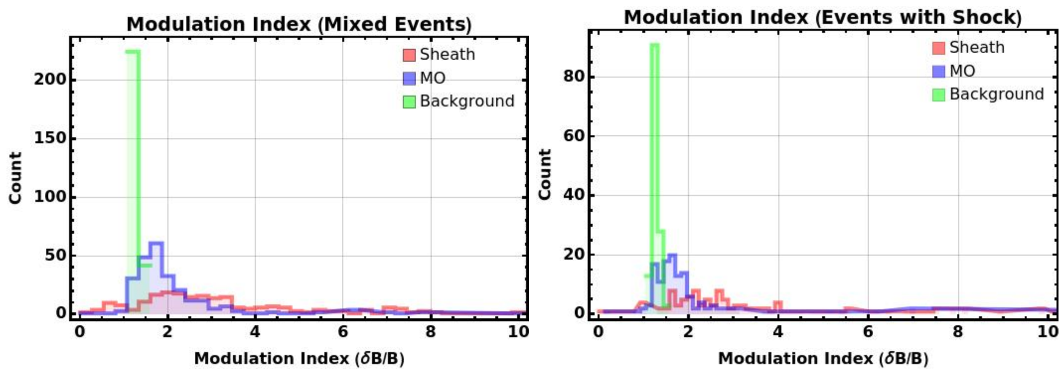

Figure 4.10: Histograms comparing the magnetic filed (magnitude) modulation index ($\delta B/B$) for mixed events (left) and events with shocks (right). They show the distribution and variability within background solar wind, sheath, and MO regions.

- For magnetic field magnitude (B) fluctuations (Figure 4.9) shows that the mean value for background fluctuations $\langle \delta B/B \rangle_{\text{BG}}$ is $\approx 1.25 \pm 0.01$, for sheath fluctuations $\langle \delta B/B \rangle_{\text{Sheath}}$ is $\approx 26.80 \pm 20.35$ and for MO $\langle \delta B/B \rangle_{\text{MO}}$ is $\approx 5.58 \pm 2.53$ for mixed events.
- For events with shock the mean values are $\langle \delta B/B \rangle_{\text{BG}}$, $\langle \delta B/B \rangle_{\text{Sheath}}$ and $\langle \delta B/B \rangle_{\text{MO}}$ being $\approx 1.26 \pm 0.01$, 7.38 ± 1.30 and 7.47 ± 4.17 respectively.
- The medians of background, sheath, and MO were $\approx$ 1.24, 3.13, and 1.79 for mixed events. Events with shock showed medians of 1.25, 2.86, and 1.67 for background, sheath, and MO, respectively.

Median values of mixed events and events with shock are also similar to histograms from the density fluctuation modulation index. It can be inferred that for magnetic field fluctuations ($\delta B/B$), having a shock or not is not a cause for a significant difference.
The spread of the value of the $(\delta B/B)_{BG}$ is remarkably small and most of the events line in this narrow range.
The spectral index for total magnetic field fluctuations in sheath and MO follows IK spectra with mean values of -1.65 $\pm$ 0.01, -1.63 $\pm$ 0.01. Background solar wind has a mean value of -1.81 $\pm$ 0.02. Unlike the density spectral index, the magnetic field spectral index histogram exhibits a single-peaked Gaussian distribution. A possible explanation for this

behavior is that, unlike the density spectral index, the magnetic field spectra manifest a bulge that resembles a flat line, now characterized by scaling of $f^{1/6}$, as suggested by [40]. This difference could explain why fitting a single slope to the magnetic field spectral index results in the observed behavior. Previous studies have shown that dst index is very strongly influenced by B_z component.[21] Figure 4.12 shows a scatter plot to compare correlations with the magnetic field (magnitude) modulation index and dst index, which do not show any strong pattern, which was confirmed in previous studies.

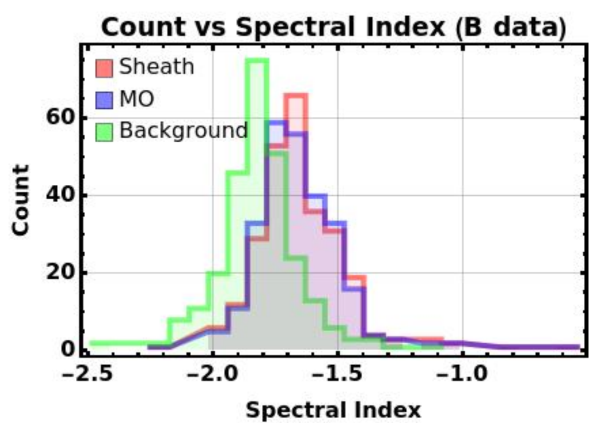

Figure 4.11: Histogram for spectral index of sheath, background, and MO for magnetic field magnitude. It shows a single-peaked Gaussian spectral index distribution, with the peak close to the IK spectral index

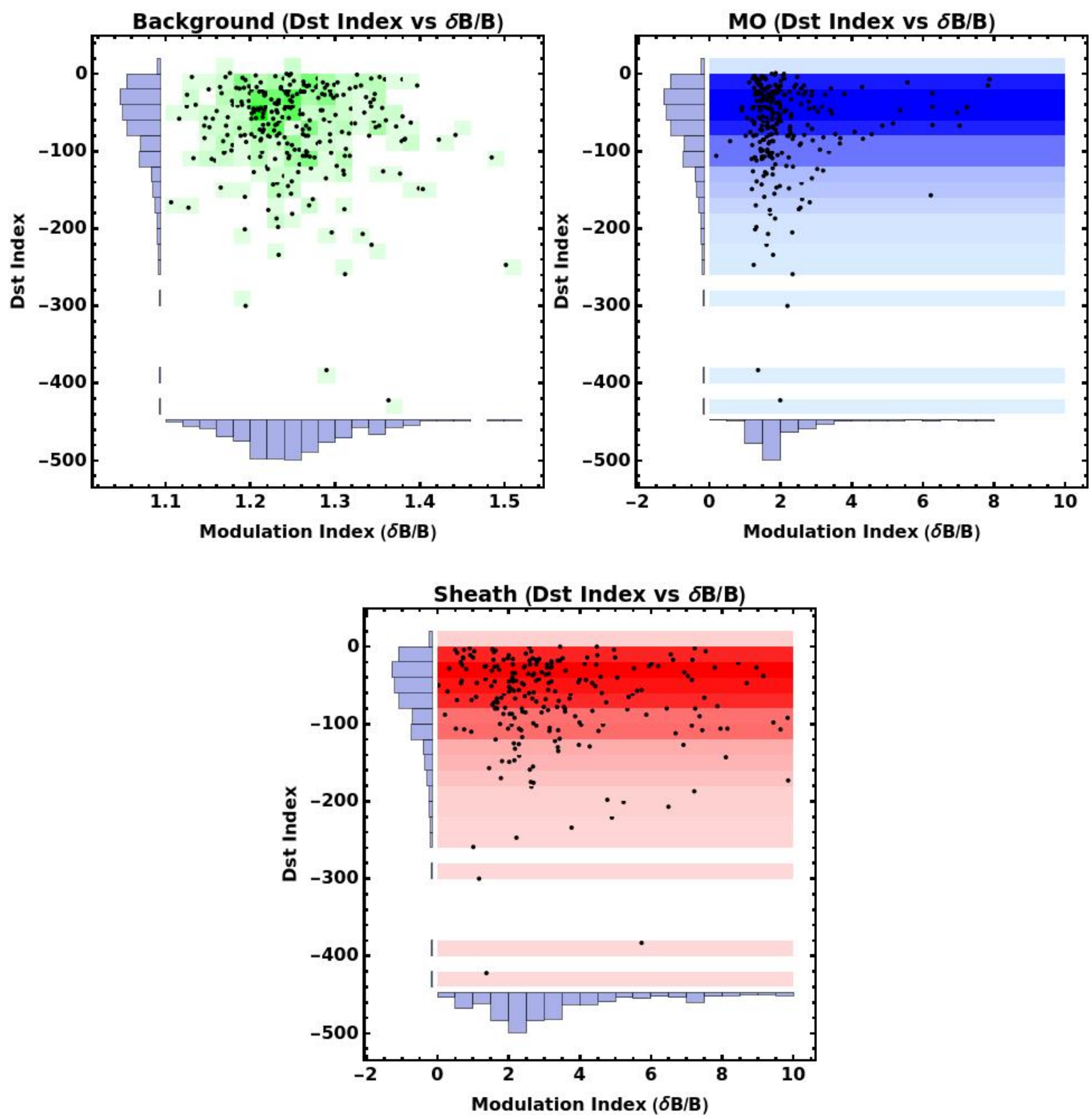

Figure 4.12: Scatter plots showing correlations between magnetic field modulation index ($\delta B/B$) for background, MO, sheath, and the Dst index.

4.6 Histograms for Velocity Magnitude

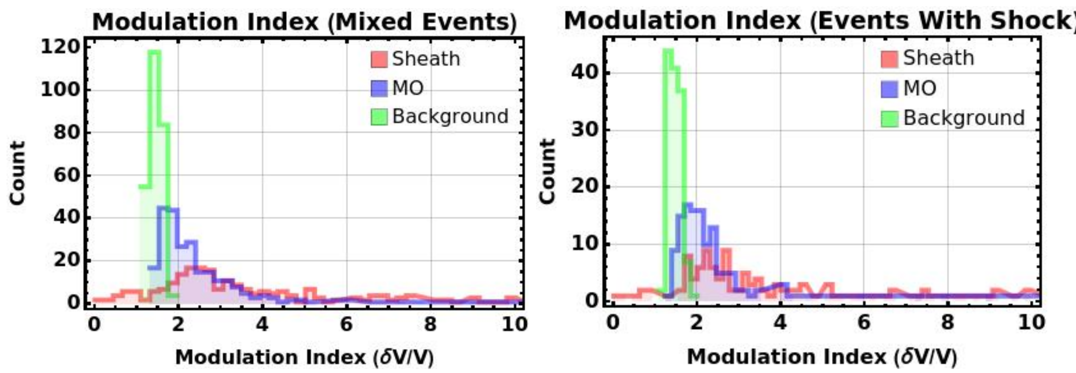

Figure 4.13: Histograms comparing the velocity (magnitude) modulation index ($\delta V/V$) for mixed events (left) and events with shocks (right). They show the distribution and variability within background solar wind, sheath, and MO regions.

- For velocity magnitude (V) fluctuations (Figure 4.12) shows that the mean value for background fluctuations $\langle \delta V/V \rangle_{\text{BG}}$ is $\approx$ 8.68 $\pm$ 0.01, for sheath fluctuations $\langle \delta V/V \rangle_{\text{Sheath}}$ is $\approx$ 1.45 $\pm$ 0.47 and for MO $\langle \delta V/V \rangle_{\text{MO}}$ is $\approx$ 6.42 $\pm$ 2.98 for mixed events.
- For events with shock the mean values are $\langle \delta V/V \rangle_{\text{BG}}$, $\langle \delta V/V \rangle_{\text{Sheath}}$ and $\langle \delta V/V \rangle_{\text{MO}}$ being $\approx$ 1.47 $\pm$ 0.01, 7.86 $\pm$ 1.21 and 3.60 $\pm$ 0.80 respectively.
- The medians of background, sheath, and MO were $\approx$ 1.42, 3.34, and 2.14 for mixed events. Events with shock showed medians of $\approx$ 1.48, 3.32, and 2.06 for background, sheath, and MO, respectively.

In Figure 4.14 spectral index is again double-peaked like the density spectral index. The spectral indices for background, sheath, and MO are also very similar, with a mean spectral index of -1.11 $\pm$ 0.02, -0.92 $\pm$ 0.01, -0.93 $\pm$ 0.03 respectively and median values of $\approx$ -1.28, -0.83, -0.84 respectively. This histogram shows a higher mean than the density and is closer to what was seen in the magnetic field histogram. The modulation index for magnetic field magnitude and density are also very similar this could potentially suggest the presence of alfvénic turbulence.

Given that the mean values of mixed events and events with shocks are similar, as observed in the histograms for density and magnetic field fluctuation modulation indices, it can be deduced that the presence of shocks also does not significantly influence the magnetic field fluctuation ($\delta V/V$) outcomes. Dst index correlation (Figure 4.15) for background shows the two values 0.30 and 0.38 that are most common velocity modulation index across all background solar wind in ICMEs causing a geomagnetic storm. In contrast, correlations for sheath and MO look similar to N_p and B histograms.

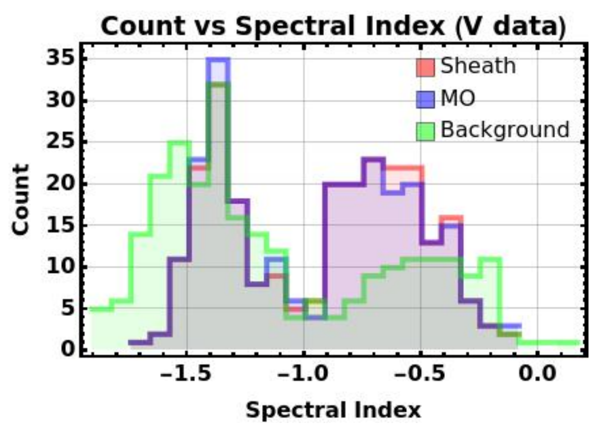

Figure 4.14: Histogram for spectral index of sheath, background, and MO for velocity magnitude. It shows a double-peaked non-Gaussian spectral index distribution.

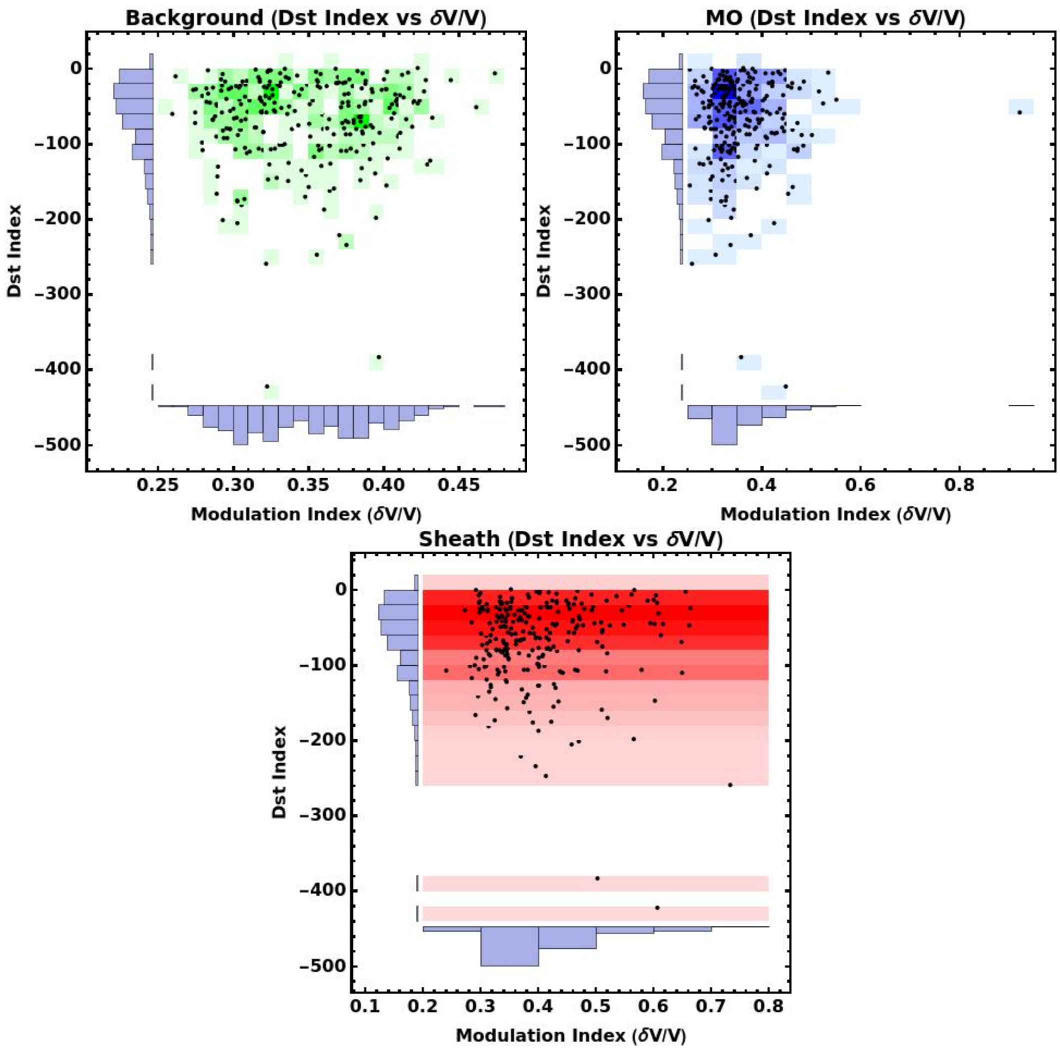

Figure 4.15: Scatter plots showing correlations between velocity modulation index ($\delta V/V$) for background, MO, sheath, and the Dst index.

Chapter 5

Conclusions and Future Work

5.1 Sheath Duration

On average, sheath regions are significantly shorter in duration than MOs, with sheaths lasting approximately 566 $\pm$ 24.8 minutes and MOs extending to about 1520 $\pm$ 47.6 minutes. This result, indicating that sheaths are shorter by a factor of $\approx$ 2.68 times than MOs, highlights the distinct physical processes and structures that define these two components of ICME.

5.2 Modulation Index Cutoff

Based on separation values using a cutoff of 2/3 in the PSD provides a more effective modulation index for distinguishing between sheath, MO, and background solar wind. However, we used only select cutoffs. It might so happen that some other cutoff value which is close to 2/3 is more effective at characterization via the modulation index. It is not very clear why 2/3 cutoff is the best, but it could be related to the fact somewhere close to the cutoff frequency, the energy cascade dynamics change from forcing scale fluctuations to inertial scale fluctuations.

5.3 Modulation and Spectral Indices

We found that for density (N_p) fluctuations the mean value for background fluctuations $\langle \delta N_p/N_p \rangle_{\mathrm{BG}}$ is $\approx 1.55 \pm 0.01$, for sheath fluctuations $\langle \delta N_p/N_p \rangle_{\mathrm{Sheath}}$ is $\approx 8.58 \pm 1.41$ and for MO $\langle \delta N_p/N_p \rangle_{\mathrm{MO}}$ is $\approx 6.69 \pm 3.04$.

Magnetic field magnitude (B) fluctuations show that the mean value for background fluctuations $\langle \delta B/B \rangle_{\mathrm{BG}}$ is $\approx 1.25 \pm 0.01$, for sheath fluctuations $\langle \delta B/B \rangle_{\mathrm{Sheath}}$ is $\approx 26.80 \pm 20.35$ and for MO $\langle \delta B/B \rangle_{\mathrm{MO}}$ is $\approx 5.58 \pm 2.53$.

A previous study by Bhattacharjee et al. (2022) [39] found modulation indices for the selected background and MC (a subset of MO) using a moving time window of 40 and 60 minutes to calculate fluctuations (δN_p and δB) from the mean values within the window. The modulation index was then determined by the ratio of these fluctuations to the mean. The mean and median for $\langle \delta N_p/N_p \rangle_{\rm BG}$ for 40 minutes time window were 0.11,0.1 and $\langle \delta N_p/N_p \rangle_{\rm MC}$ were 0.24, 0.2. For magnetic field fluctuations, mean and median of $\langle \delta B/B \rangle_{\rm BG}$ for a 40-minute window were 0.067, 0.06 and for $\langle \delta B/B \rangle_{\rm MC}$ were 0.044, 0.042 respectively. These results indicate that the modulation index $\langle \delta N_p/N_p \rangle_{\rm BG} < \langle \delta N_p/N_p \rangle_{\rm MC}$ and $\langle \delta B/B \rangle_{\rm BG} > \langle \delta B/B \rangle_{\rm MC}$

Our results indicate that $\langle \delta N_p/N_p \rangle_{\rm BG} < \langle \delta N_p/N_p \rangle_{\rm MO} < \langle \delta N_p/N_p \rangle_{\rm sheath}$ and a similar trend for magnetic field modulation index but a much higher value for sheath compared to background and MO. In essence, the modulation index characterizes the sheath as a highly turbulent structure, MO is comparatively less turbulent, and the chosen background solar wind is the least turbulent. The similarity of ($\delta B/B$) and ($\delta V/V$) histograms could also be indicative of the presence of alfvénic turbulence in both the sheath and MO, but this can be explored further. Characterizing MO and sheath based on the Spectral Index is challenging, whereas the background solar wind exhibits a slightly distinct spectral Index.

5.4 Dst index Correlations

Correlation between the Dst Index and the modulation index, when applied to the background solar wind, MO, and the sheath regions, indicates that the modulation index might not be a reliable metric for evaluating their impact on geomagnetic storms. Moreover, we found no substantial distinctions between ICMEs with shocks and those in mixed events, suggesting that the presence of a shock does not significantly alter the inherent characteristics of ICMEs as measured by the modulation index. Uniformity across different ICME types highlights the complexity of predicting geomagnetic disturbances based solely on the modulation index. We rule out the fact that magnetic field magnitude holds much value here, but since studies have shown that the value of B_z component shows a positive correlation with Dst index [21], a modulation index created with B_z instead of B (magnitude) could improve the correlation results.

5.5 Future work

As this thesis concludes, we present a roadmap for future work into the characterization of ICMEs based on turbulence.

- We are currently limited to using the time series data for the entire sheath, MO, and background wind regions. We plan to find the smallest time slice can be found in which characterization or separation between regions of ICME would be possible. This could be potentially be converted into an algorithm that would demarcate these ICME regions based on the modulation index and the sliding window, which will be of the size of the smallest time slice.
- It is worth looking into the creation of a composite modulation index which would be an amalgamation of two different modulation indices, to check whether the separations of ICME regions based on turbulence can be improved.
- Future studies could explore the potential of developing a modulation index that incorporates directional aspects of velocity and magnetic field. This approach may reveal more nuanced correlations with the Dst index.
- As an extension, an application of power frequency-based modulation index to answer if turbulent fluctuations inside sheaths and MOs can contribute to anomalous resistivity and associated Joule heating inside the plasma similar to Bhattacharjee et al. (2022) [39] but instead treating power inside high-frequency regions in PSDs as turbulent fluctuations.

Appendix A

Data Tables from Chapter 3

A.1 ICME Events with Shock

Sheath start	Shock	MO start	MO type	MO/ICME end	Dst
1995 03 04, 00:36	Y	1995 03 04, 11:23	Fr	1995 03 05, 03:06	-90
1995 08 22, 12:56	Y	1995 08 22, 22:19	Fr	1995 08 23, 18:43	-61
1995 10 18, 10:40	Y	1995 10 18, 19:11	Fr	1995 10 20, 02:23	-127
1997 01 10, 00:52	Y	1997 01 10, 04:47	F+	1997 01 11, 03:06	-78
1997 02 09, 12:50	Y	1997 02 10, 02:52	F-	1997 02 10, 18:28	-68
1997 05 26, 09:09	Y	1997 05 26, 15:35	Fr	1997 05 28, 00:00	-73
1997 09 02, 22:40	Y	1997 09 03, 08:38	Fr	1997 09 03, 20:59	-98 (SA)
1997 11 22, 09:12	Y	1997 11 22, 17:31	F+	1997 11 23, 18:43	-108
1997 12 10, 04:33	Y	1997 12 10, 19:11	Cx	1997 12 12, 00:00	-60
1997 12 30, 01:13	Y	1997 12 30, 09:35	Fr	1997 12 31, 08:51	-77
1998 05 01, 21:21	Y	1998 05 02, 11:31	Fr	1998 05 03, 16:47	-85
1998 08 10, 00:31	Y	1998 08 10, 04:47	E	1998 08 10, 23:30	-27
1998 08 19, 18:40	Y	1998 08 20, 08:38	F+	1998 08 21, 20:09	-67
1998 08 26, 06:40	Y	1998 08 26, 21:07	E	1998 08 28, 00:28	-155
1998 10 23, 12:57	Y	1998 10 23, 19:55	F-	1998 10 24, 19:26	-52
1999 02 18, 02:48	Y	1999 02 18, 09:14	E	1999 02 19, 00:00	-123
1999 07 02, 00:27	Y	1999 07 03, 08:09	Fr	1999 07 05, 13:13	-26
1999 07 06, 14:23	Y	1999 07 06, 19:12	Cx	1999 07 07, 16:46	-4
1999 09 22, 12:09	Y	1999 09 22, 17:59	E	1999 09 23, 09:35	-173
2000 02 11, 23:34	Y	2000 02 12, 12:20	Fr	2000 02 13, 00:35	-135
2000 02 14, 07:11	Y	2000 02 14, 13:11	E	2000 02 15, 15:33	-68
2000 02 20, 21:03	Y	2000 02 21, 14:24	Fr	2000 02 22, 13:16	-25
2000 06 08, 09:07	Y	2000 06 08, 16:47	E	2000 06 10, 01:18	-90
2000 06 23, 12:57	Y	2000 06 24, 09:00	E	2000 06 25, 23:58	-34
2000 07 28, 06:38	Y	2000 07 28, 14:24	F+	2000 07 29, 10:06	-49
2000 08 11, 18:49	Y	2000 08 12, 06:05	F+	2000 08 13, 05:05	-234
2000 09 06, 17:02	Y	2000 09 07, 03:24	Cx	2000 09 08, 14:22	-47 (SA)
2000 10 03, 01:02	Y	2000 10 03, 09:36	F+	2000 10 05, 03:34	-143
2000 10 05, 03:28	Y	2000 10 05, 19:11	Fr	2000 10 06, 19:39	-181
2000 10 12, 22:33	Y	2000 10 13, 18:24	Fr	2000 10 14, 19:12	-106
2000 10 28, 06:38	Y	2000 10 28, 23:18	F-	2000 10 30, 00:16	-126
2000 11 06, 09:30	Y	2000 11 06, 23:05	Fr	2000 11 07, 18:05	-159
2000 11 26, 11:43	Y	2000 11 27, 09:30	Fr	2000 11 28, 09:36	-79
2001 01 23, 10:47	Y	2001 01 24, 08:38	Cx	2001 01 25, 19:12	-61
2001 04 21, 15:29	Y	2001 04 22, 00:28	Fr	2001 04 23, 01:11	-102
2001 04 28, 05:00	Y	2001 04 28, 17:59	Cx	2001 05 02, 04:48	-47
2001 05 27, 14:45	Y	2001 05 28, 07:12	Cx	2001 05 29, 21:34	-42
2001 08 17, 11:01	Y	2001 08 17, 23:59	F-	2001 08 18, 19:12	-105
2001 09 25, 20:16	Y	2001 09 26, 10:04	F-	2001 09 26, 16:47	-102
2001 09 30, 19:14	Y	2001 09 30, 22:33	F-	2001 10 01, 21:34	-148
2001 10 21, 16:39	Y	2001 10 22, 01:17	Fr	2001 10 23, 00:47	-187
2001 10 28, 03:13	Y	2001 10 29, 16:19	E	2001 10 30, 10:47	-157
2001 10 31, 13:46	Y	2001 10 31, 22:04	Fr	2001 11 02, 04:47	-106
2001 11 24, 05:51	Y	2001 11 24, 15:47	Fr	2001 11 25, 13:17	-221

2001 12 30, 20:05	Y	2001 12 30, 23:10	F-	2001 12 31, 07:46	-31
2002 02 28, 05:06	Y	2002 02 28, 19:11	Fr	2002 03 01, 23:15	-71
2002 03 18, 13:14	Y	2002 03 19, 06:14	Fr	2002 03 20, 15:36	-37
2002 03 23, 11:24	Y	2002 03 24, 13:11	Fr	2002 03 25, 21:36	-100
2002 04 14, 12:56	Y	2002 04 14, 15:21	F-	2002 04 15, 04:22	-14
2002 04 17, 11:01	Y	2002 04 17, 21:36	F+	2002 04 19, 08:22	-127
2002 04 19, 08:24	Y	2002 04 20, 06:57	Fr	2002 04 21, 21:36	-149
2002 04 23, 05:00	Y	2002 04 24, 07:11	F-	2002 04 24, 23:59	-57
2002 05 11, 10:30	Y	2002 05 11, 12:37	Fr	2002 05 11, 20:23	-110
2002 05 18, 19:45	Y	2002 05 19, 03:30	Fr	2002 05 20, 03:34	-58
2002 05 20, 03:35	Y	2002 05 20, 16:47	Cx	2002 05 21, 21:35	-36
2002 05 23, 10:44	Y	2002 05 23, 23:02	F-	2002 05 25, 19:12	-109
2002 07 17, 15:56	Y	2002 07 18, 13:26	Fr	2002 07 19, 09:35	-17
2002 08 01, 23:09	Y	2002 08 02, 07:12	Fr	2002 08 02, 21:34	-102
2002 08 18, 18:40	Y	2002 08 19, 19:12	Fr	2002 08 21, 13:25	-106
2002 08 26, 11:16	Y	2002 08 26, 14:23	Fr	2002 08 27, 10:47	-45
2002 09 30, 07:54	Y	2002 09 30, 22:04	F+	2002 10 01, 20:08	-176
2003 11 20, 08:35	Y	2003 11 20, 11:31	Fr	2003 11 21, 01:40	-422
2004 04 03, 09:55	Y	2004 04 04, 01:11	F+	2004 04 05, 19:11	-117
2004 07 22, 09:45	Y	2004 07 22, 13:26	Cx	2004 07 24, 05:45	-99
2004 07 26, 22:25	Y	2004 07 27, 01:12	Cx	2004 07 27, 23:58	-170
2004 08 29, 09:09	Y	2004 08 29, 19:26	Fr	2004 08 30, 21:21	-129 (SA)
2004 09 13, 19:42	Y	2004 09 14, 17:59	E	2004 09 15, 14:23	-45
2004 11 09, 18:25	Y	2004 11 09, 20:38	F+	2004 11 10, 16:47	-259
2004 11 11, 16:47	Y	2004 11 12, 08:35	Fr	2004 11 13, 09:35	-92
2005 01 16, 09:27	Y	2005 01 16, 15:35	F+	2005 01 17, 07:00	-63
2005 01 21, 16:58	Y	2005 01 21, 23:45	F-	2005 01 22, 19:12	-97
2005 02 20, 15:32	Y	2005 02 20, 20:23	Fr	2005 02 22, 07:11	-43
2005 05 15, 02:10	Y	2005 05 15, 05:31	F+	2005 05 16, 22:47	-247
2005 06 12, 06:57	Y	2005 06 12, 15:07	F-	2005 06 13, 17:59	-106
2005 06 14, 17:55	Y	2005 06 15, 05:08	F+	2005 06 16, 08:23	-42
2005 07 10, 02:42	Y	2005 07 10, 10:47	Cx	2005 07 12, 14:23	-92
2006 07 09, 20:40	Y	2006 07 10, 17:45	Cx	2006 07 11, 17:45	-27
2006 08 19, 09:38	Y	2006 08 20, 13:55	Cx	2006 08 21, 17:02	-79
2006 12 14, 13:51	Y	2006 12 14, 22:36	F-	2006 12 15, 13:40	-162
2006 12 16, 17:34	Y	2006 12 17, 00:25	F-	2006 12 17, 19:11	-56
2007 11 19, 17:22	Y	2007 11 20, 00:33	Fr	2007 11 20, 11:31	-2
2009 03 11, 22:04	Y	2009 03 12, 01:12	F+	2009 03 13, 01:40	-28 (SA)
2009 06 27, 11:02	Y	2009 06 27, 17:59	F+	2009 06 28, 20:24	-14
2010 04 05, 07:55	Y	2010 04 05, 11:59	Fr	2010 04 06, 16:48	-81
2010 04 11, 12:20	Y	2010 04 11, 21:36	Fr	2010 04 12, 14:12	-67
2010 05 28, 01:55	Y	2010 05 28, 19:12	Fr	2010 05 29, 17:58	-80
2010 08 03, 17:05	Y	2010 08 04, 02:52	Cx	2010 08 05, 00:56	-74
2010 12 19, 20:35	Y	2010 12 19, 22:33	F+	2010 12 20, 22:04	-35
2011 03 29, 15:12	Y	2011 03 29, 23:59	Fr	2011 04 01, 14:51	-7
2011 06 04, 20:06	Y	2011 06 05, 01:12	Fr	2011 06 05, 18:13	-45
2011 06 17, 02:09	Y	2011 06 17, 05:16	Cx	2011 06 19, 07:11	-14
2011 09 17, 02:57	Y	2011 09 17, 15:35	Fr	2011 09 18, 21:06	-72
2011 10 05, 06:46	Y	2011 10 05, 09:56	Cx	2011 10 07, 02:06	-43
2011 10 24, 17:41	Y	2011 10 25, 00:21	Cx	2011 10 25, 23:31	-147
2011 11 28, 20:59	Y	2011 11 29, 19:40	Cx	2011 11 30, 17:59	-41
2012 01 22, 05:33	Y	2012 01 22, 11:24	F-	2012 01 22, 17:58	-70 (SA)
2012 02 26, 20:59	Y	2012 02 27, 17:59	Cx	2012 03 01, 05:45	-57
2012 03 08, 10:32	Y	2012 03 08, 19:55	Cx	2012 03 11, 07:26	-145
2012 03 12, 08:28	Y	2012 03 12, 16:19	Cx	2012 03 14, 02:52	-64
2012 03 15, 12:35	Y	2012 03 15, 16:04	Fr	2012 03 16, 14:10	-88
2012 04 23, 02:15	Y	2012 04 23, 16:48	F-	2012 04 24, 02:52	-120 (SA)
2012 05 03, 00:59	Y	2012 05 04, 03:36	Fr	2012 05 05, 11:22	-23
2012 06 16, 09:03	Y	2012 06 16, 22:01	F+	2012 06 17, 11:23	-86
2012 07 14, 17:39	Y	2012 07 15, 06:14	Fr	2012 07 17, 03:21	-139
2012 09 30, 10:14	Y	2012 09 30, 12:14	Cx	2012 10 02, 02:53	-122
2012 10 08, 04:12	Y	2012 10 08, 15:50	Fr	2012 10 09, 17:17	-109

2012 10 31, 14:28	Y	2012 10 31, 23:35	F+	2012 11 02, 05:21	-65
2012 11 12, 22:12	Y	2012 11 13, 08:23	F+	2012 11 14, 08:09	-108
2012 11 23, 20:51	Y	2012 11 24, 11:31	F-	2012 11 25, 10:47	-40
2013 01 19, 16:50	Y	2013 01 19, 22:47	F-	2013 01 20, 10:47	-33
2013 03 17, 05:21	Y	2013 03 17, 14:09	Fr	2013 03 19, 16:04	-132
2013 04 13, 22:13	Y	2013 04 14, 17:02	F+	2013 04 17, 05:30	-17
2013 04 30, 08:52	Y	2013 04 30, 12:00	Fr	2013 05 01, 07:12	-47 (SA)
2013 06 27, 13:51	Y	2013 06 28, 02:23	Fr	2013 06 29, 11:59	-101
2013 07 12, 16:43	Y	2013 07 12, 20:24	Cx	2013 07 14, 23:31	-81
2013 12 08, 07:31	Y	2013 12 08, 16:47	F-	2013 12 09, 02:09	-66
2014 02 15, 12:46	Y	2014 02 16, 00:43	Fr	2014 02 16, 14:23	-24
2014 04 20, 10:20	Y	2014 04 21, 07:41	Fr	2014 04 22, 06:12	-32
2014 06 07, 16:30	Y	2014 06 08, 19:12	Cx	2014 06 10, 16:46	-37
2014 07 02, 23:48	Y	2014 07 03, 03:07	F-	2014 07 03, 11:59	-15
2014 08 19, 05:49	Y	2014 08 19, 17:59	F+	2014 08 21, 19:09	-30
2014 09 12, 15:17	Y	2014 09 12, 21:22	F-	2014 09 14, 11:38	-88
2015 03 31, 07:32	Y	2015 03 31, 17:57	F-	2015 04 01, 09:49	-19
2015 04 09, 09:09	Y	2015 04 09, 23:02	Cx	2015 04 11, 09:36	-85
2015 05 06, 00:56	Y	2015 05 06, 16:48	F-	2015 05 07, 14:22	-35
2015 06 22, 18:07	Y	2015 06 23, 02:23	Cx	2015 06 24, 13:03	-198
2015 09 07, 13:05	Y	2015 09 07, 23:31	F+	2015 09 09, 14:52	-105
2015 10 24, 17:59	Y	2015 10 25, 13:11	Fr	2015 10 28, 13:11	-16
2015 11 06, 17:46	Y	2015 11 07, 07:11	Fr	2015 11 08, 16:47	-87
2015 12 19, 15:35	Y	2015 12 20, 13:40	Fr	2015 12 21, 23:02	-166

Table A.1: ICME events consisting of shock, created using the events from Table A.3 that adheres to the criterion of at least a 3-day gap between events

A.2 Mixed ICME Events

Sheath start	Shock	MO start	MO type	MO/ICME end	Dst
1995 02 07, 19:11	-	1995 02 08, 03:21	Cx	1995 02 10, 21:36	-80
1995 03 04, 00:36	Y	1995 03 04, 11:23	Fr	1995 03 05, 03:06	-90
1995 03 06, 02:11	-	1995 03 06, 07:11	F-	1995 03 07, 02:23	-38
1995 04 03, 06:43	-	1995 04 03, 12:45	F+	1995 04 04, 13:25	-21
1995 04 05, 07:11	-	1995 04 05, 17:59	Fr	1995 04 06, 17:15	-18
1995 06 30, 09:21	-	1995 06 30, 14:23	Fr	1995 07 02, 16:47	-56
1995 08 22, 12:56	Y	1995 08 22, 22:19	Fr	1995 08 23, 18:43	-61
1995 09 26, 15:57	-	1995 09 27, 03:36	Fr	1995 09 27, 21:21	-108
1995 10 18, 10:40	Y	1995 10 18, 19:11	Fr	1995 10 20, 02:23	-127
1995 12 15, 14:52	-	1995 12 16, 07:11	F-	1995 12 16, 19:11	-44
1996 05 16, 22:47	-	1996 05 17, 01:36	F+	1996 05 17, 11:58	-26
1996 08 07, 08:23	-	1996 08 07, 11:59	Fr	1996 08 08, 13:12	-23
1996 12 24, 01:26	-	1996 12 24, 03:07	F+	1996 12 25, 11:44	-29
1997 01 10, 00:52	Y	1997 01 10, 04:47	F+	1997 01 11, 03:06	-78
1997 02 09, 12:50	Y	1997 02 10, 02:52	F-	1997 02 10, 18:28	-68
1997 04 10, 17:02	-	1997 04 11, 05:45	Fr	1997 04 11, 19:10	-82
1997 04 21, 10:11	-	1997 04 21, 11:59	F+	1997 04 23, 07:11	-107
1997 05 26, 09:09	Y	1997 05 26, 15:35	Fr	1997 05 28, 00:00	-73
1997 06 08, 15:43	-	1997 06 09, 06:18	Fr	1997 06 09, 23:01	-84
1997 07 15, 03:10	-	1997 07 15, 06:48	F+	1997 07 16, 11:16	-44
1997 08 03, 10:10	-	1997 08 03, 13:55	Fr	1997 08 04, 02:23	-49
1997 08 17, 01:56	-	1997 08 17, 06:33	Fr	1997 08 17, 20:09	-28
1997 09 02, 22:40	Y	1997 09 03, 08:38	Fr	1997 09 03, 20:59	-98 (SA)
1997 09 18, 00:30	-	1997 09 18, 04:07	F+	1997 09 19, 23:59	-56
1997 09 21, 16:42	-	1997 09 21, 22:21	F+	1997 09 22, 17:46	-36
1997 10 01, 11:45	-	1997 10 01, 17:08	Fr	1997 10 02, 23:15	-98
1997 10 10, 03:08	-	1997 10 10, 15:33	F+	1997 10 11, 22:00	-130
1997 11 06, 22:25	-	1997 11 07, 06:00	F+	1997 11 08, 22:46	-110
1997 11 22, 09:12	Y	1997 11 22, 17:31	F+	1997 11 23, 18:43	-108
1997 12 10, 04:33	Y	1997 12 10, 19:11	Cx	1997 12 12, 00:00	-60
1997 12 30, 01:13	Y	1997 12 30, 09:35	Fr	1997 12 31, 08:51	-77
1998 01 28, 16:04	-	1998 01 29, 13:12	F+	1998 01 31, 00:00	-55
1998 02 18, 14:52	-	1998 02 18, 21:35	Fr	1998 02 20, 00:44	-50
1998 03 25, 10:48	-	1998 03 25, 14:23	Fr	1998 03 26, 08:57	-56
1998 05 01, 21:21	Y	1998 05 02, 11:31	Fr	1998 05 03, 16:47	-85
1998 05 04, 02:30	-	1998 05 04, 09:50	F-	1998 05 05, 03:12	-205
1998 06 24, 10:47	-	1998 06 24, 13:26	F+	1998 06 25, 22:33	-25
1998 08 10, 00:31	Y	1998 08 10, 04:47	E	1998 08 10, 23:30	-27
1998 08 19, 18:40	Y	1998 08 20, 08:38	F+	1998 08 21, 20:09	-67
1998 08 26, 06:40	Y	1998 08 26, 21:07	E	1998 08 28, 00:28	-155
1998 09 23, 01:12	-	1998 09 23, 04:19	F-	1998 09 23, 17:31	-25
1998 09 24, 23:18	-	1998 09 25, 04:33	F+	1998 09 26, 17:00	-207
1998 10 18, 19:30	-	1998 10 19, 04:19	F+	1998 10 20, 07:11	-112
1998 10 23, 12:57	Y	1998 10 23, 19:55	F-	1998 10 24, 19:26	-52
1999 02 18, 02:48	Y	1999 02 18, 09:14	E	1999 02 19, 00:00	-123
1999 07 02, 00:27	Y	1999 07 03, 08:09	Fr	1999 07 05, 13:13	-26
1999 07 06, 14:23	Y	1999 07 06, 19:12	Cx	1999 07 07, 16:46	-4
1999 07 30, 19:12	-	1999 07 31, 02:02	E	1999 08 01, 00:00	-53
1999 08 06, 01:55	-	1999 08 06, 14:23	Fr	1999 08 07, 06:18	-23
1999 09 22, 12:09	Y	1999 09 22, 17:59	E	1999 09 23, 09:35	-173
1999 11 13, 12:48	Y	1999 11 14, 14:23	E	1999 11 16, 07:17	-106
1999 12 12, 15:50	Y	1999 12 12, 17:31	Cx	1999 12 13, 18:28	-69
2000 02 11, 23:34	Y	2000 02 12, 12:20	Fr	2000 02 13, 00:35	-135
2000 02 14, 07:11	Y	2000 02 14, 13:11	E	2000 02 15, 15:33	-68

2000 02 20, 21:03	Y	2000 02 21, 14:24	Fr	2000 02 22, 13:16	-25
2000 03 01, 01:58	-	2000 03 01, 03:21	Fr	2000 03 02, 03:07	-44
2000 06 08, 09:07	Y	2000 06 08, 16:47	E	2000 06 10, 01:18	-90
2000 06 23, 12:57	Y	2000 06 24, 09:00	E	2000 06 25, 23:58	-34
2000 07 15, 14:23	-	2000 07 15, 17:31	F+	2000 07 16, 13:28	-300
2000 07 28, 06:38	Y	2000 07 28, 14:24	F+	2000 07 29, 10:06	-49
2000 08 11, 18:49	Y	2000 08 12, 06:05	F+	2000 08 13, 05:05	-234
2000 09 06, 17:02	Y	2000 09 07, 03:24	Cx	2000 09 08, 14:22	-47 (SA)
2000 09 17, 16:04	-	2000 09 18, 01:53	E	2000 09 19, 12:00	-201
2000 10 03, 01:02	Y	2000 10 03, 09:36	F+	2000 10 05, 03:34	-143
2000 10 05, 03:28	Y	2000 10 05, 19:11	Fr	2000 10 06, 19:39	-181
2000 10 12, 22:33	Y	2000 10 13, 18:24	Fr	2000 10 14, 19:12	-106
2000 10 28, 06:38	Y	2000 10 28, 23:18	F-	2000 10 30, 00:16	-126
2000 11 06, 09:30	Y	2000 11 06, 23:05	Fr	2000 11 07, 18:05	-159
2000 11 26, 11:43	Y	2000 11 27, 09:30	Fr	2000 11 28, 09:36	-79
2001 01 23, 10:47	Y	2001 01 24, 08:38	Cx	2001 01 25, 19:12	-61
2001 04 04, 14:39	Y	2001 04 04, 20:54	F-	2001 04 05, 08:22	-50
2001 04 13, 07:26	-	2001 04 13, 13:11	F-	2001 04 14, 01:39	-77
2001 04 21, 15:29	Y	2001 04 22, 00:28	Fr	2001 04 23, 01:11	-102
2001 04 28, 05:00	Y	2001 04 28, 17:59	Cx	2001 05 02, 04:48	-47
2001 05 27, 14:45	Y	2001 05 28, 07:12	Cx	2001 05 29, 21:34	-42
2001 08 05, 12:28	-	2001 08 06, 06:43	E	2001 08 06, 23:59	-40
2001 08 17, 11:01	Y	2001 08 17, 23:59	F-	2001 08 18, 19:12	-105
2001 09 25, 20:16	Y	2001 09 26, 10:04	F-	2001 09 26, 16:47	-102
2001 09 30, 19:14	Y	2001 09 30, 22:33	F-	2001 10 01, 21:34	-148
2001 10 21, 16:39	Y	2001 10 22, 01:17	Fr	2001 10 23, 00:47	-187
2001 10 28, 03:13	Y	2001 10 29, 16:19	E	2001 10 30, 10:47	-157
2001 10 31, 13:46	Y	2001 10 31, 22:04	Fr	2001 11 02, 04:47	-106
2001 11 24, 05:51	Y	2001 11 24, 15:47	Fr	2001 11 25, 13:17	-221
2001 12 30, 20:05	Y	2001 12 30, 23:10	F-	2001 12 31, 07:46	-31
2002 02 28, 05:06	Y	2002 02 28, 19:11	Fr	2002 03 01, 23:15	-71
2002 03 18, 13:14	Y	2002 03 19, 06:14	Fr	2002 03 20, 15:36	-37
2002 03 23, 11:24	Y	2002 03 24, 13:11	Fr	2002 03 25, 21:36	-100
2002 04 14, 12:56	Y	2002 04 14, 15:21	F-	2002 04 15, 04:22	-14
2002 04 17, 11:01	Y	2002 04 17, 21:36	F+	2002 04 19, 08:22	-127
2002 04 19, 08:24	Y	2002 04 20, 06:57	Fr	2002 04 21, 21:36	-149
2002 04 23, 05:00	Y	2002 04 24, 07:11	F-	2002 04 24, 23:59	-57
2002 05 11, 10:30	Y	2002 05 11, 12:37	Fr	2002 05 11, 20:23	-110
2002 05 18, 19:45	Y	2002 05 19, 03:30	Fr	2002 05 20, 03:34	-58
2002 05 20, 03:35	Y	2002 05 20, 16:47	Cx	2002 05 21, 21:35	-36
2002 05 23, 10:44	Y	2002 05 23, 23:02	F-	2002 05 25, 19:12	-109
2002 07 17, 15:56	Y	2002 07 18, 13:26	Fr	2002 07 19, 09:35	-17
2002 08 01, 23:09	Y	2002 08 02, 07:12	Fr	2002 08 02, 21:34	-102
2002 08 18, 18:40	Y	2002 08 19, 19:12	Fr	2002 08 21, 13:25	-106
2002 08 26, 11:16	Y	2002 08 26, 14:23	Fr	2002 08 27, 10:47	-45
2002 09 03, 02:23	-	2002 09 03, 04:47	Cx	2002 09 04, 01:12	-6
2002 09 30, 07:54	Y	2002 09 30, 22:04	F+	2002 10 01, 20:08	-176
2002 11 16, 23:16	-	2002 11 17, 20:24	F-	2002 11 18, 23:58	-52
2002 12 21, 03:21	-	2002 12 21, 10:20	Fr	2002 12 22, 15:36	-75
2003 01 26, 21:43	-	2003 01 27, 01:40	Fr	2003 01 27, 16:04	-18
2003 02 01, 13:06	-	2003 02 02, 19:11	Fr	2003 02 03, 09:35	-72
2003 03 20, 04:30	-	2003 03 20, 11:54	Fr	2003 03 20, 22:22	-64
2003 05 09, 05:16	-	2003 05 09, 09:27	E	2003 05 10, 23:07	-84
2003 06 16, 22:33	-	2003 06 17, 17:48	Fr	2003 06 18, 08:18	-141 (SA)
2003 08 04, 20:23	-	2003 08 05, 01:10	Fr	2003 08 06, 02:23	-58
2003 10 21, 22:00	-	2003 10 22, 02:24	Cx	2003 10 24, 02:24	-61
2003 10 30, 16:12	-	2003 10 31, 02:00	Cx	2003 10 31, 12:00	-383
2003 11 20, 08:35	Y	2003 11 20, 11:31	Fr	2003 11 21, 01:40	-422
2004 01 09, 15:00	-	2004 01 10, 06:01	E	2004 01 11, 05:02	-45
2004 04 03, 09:55	Y	2004 04 04, 01:11	F+	2004 04 05, 19:11	-117
2004 07 22, 09:45	Y	2004 07 22, 13:26	Cx	2004 07 24, 05:45	-99
2004 07 26, 22:25	Y	2004 07 27, 01:12	Cx	2004 07 27, 23:58	-170

2004 08 29, 09:09	Y	2004 08 29, 19:26	Fr	2004 08 30, 21:21	-129 (SA)
2004 09 13, 19:42	Y	2004 09 14, 17:59	E	2004 09 15, 14:23	-45
2004 09 17, 20:52	-	2004 09 18, 12:28	Fr	2004 09 19, 16:58	-33
2004 11 09, 18:25	Y	2004 11 09, 20:38	F+	2004 11 10, 16:47	-259
2004 11 11, 16:47	Y	2004 11 12, 08:35	Fr	2004 11 13, 09:35	-92
2005 01 08, 15:12	-	2005 01 08, 20:51	Fr	2005 01 09, 17:45	-47
2005 01 16, 09:27	Y	2005 01 16, 15:35	F+	2005 01 17, 07:00	-63
2005 01 18, 21:35	-	2005 01 19, 00:28	F-	2005 01 20, 02:23	-80
2005 01 21, 16:58	Y	2005 01 21, 23:45	F-	2005 01 22, 19:12	-97
2005 02 17, 21:35	-	2005 02 18, 14:52	E	2005 02 19, 08:23	-80
2005 02 20, 15:32	Y	2005 02 20, 20:23	Fr	2005 02 22, 07:11	-43
2005 05 15, 02:10	Y	2005 05 15, 05:31	F+	2005 05 16, 22:47	-247
2005 05 20, 04:47	-	2005 05 20, 09:35	F+	2005 05 22, 02:23	-83
2005 06 12, 06:57	Y	2005 06 12, 15:07	F-	2005 06 13, 17:59	-106
2005 06 14, 17:55	Y	2005 06 15, 05:08	F+	2005 06 16, 08:23	-42
2005 07 10, 02:42	Y	2005 07 10, 10:47	Cx	2005 07 12, 14:23	-92
2005 08 10, 04:47	-	2005 08 10, 06:14	F-	2005 08 10, 13:26	-47
2006 02 05, 18:14	-	2006 02 05, 20:23	F+	2006 02 06, 11:59	-20
2006 08 19, 09:38	Y	2006 08 20, 13:55	Cx	2006 08 21, 17:02	-79
2006 09 30, 02:52	-	2006 09 30, 08:23	F+	2006 09 30, 22:03	-21
2006 11 29, 02:58	-	2006 11 29, 05:16	F+	2006 11 30, 09:35	-66
2006 12 14, 13:51	Y	2006 12 14, 22:36	F-	2006 12 15, 13:40	-162
2007 06 08, 05:45	-	2007 06 08, 05:45	Fr	2007 06 09, 05:15	-21
2008 09 03, 16:33	-	2008 09 03, 16:33	F+	2008 09 04, 03:49	-51 (SA)
2008 09 17, 00:43	-	2008 09 17, 03:57	Fr	2008 09 18, 08:09	-23
2008 12 17, 03:35	-	2008 12 17, 03:35	Fr	2008 12 17, 15:35	-15
2009 02 03, 19:21	Y	2009 02 04, 01:12	F+	2009 02 04, 19:40	-42
2009 03 11, 22:04	Y	2009 03 12, 01:12	F+	2009 03 13, 01:40	-28 (SA)
2009 04 05, 16:04	-	2009 04 05, 17:02	F-	2009 04 06, 04:48	-7
2009 04 22, 11:16	-	2009 04 22, 14:09	Fr	2009 04 22, 20:37	-7
2009 06 03, 13:40	-	2009 06 03, 20:52	Fr	2009 06 05, 05:31	-19
2009 06 27, 11:02	Y	2009 06 27, 17:59	F+	2009 06 28, 20:24	-14
2009 09 10, 10:19	-	2009 09 10, 10:19	Fr	2009 09 10, 19:26	1
2009 11 14, 10:47	-	2009 11 14, 10:47	Fr	2009 11 15, 11:45	-17
2009 12 12, 04:47	-	2009 12 12, 19:26	Fr	2009 12 14, 04:47	-2
2010 01 01, 22:04	-	2010 01 02, 00:14	Fr	2010 01 03, 09:06	-4
2010 03 23, 22:29	Y	2010 03 23, 22:33	Fr	2010 03 24, 15:36	-1
2010 04 05, 07:55	Y	2010 04 05, 11:59	Fr	2010 04 06, 16:48	-81
2010 05 18, 02:23	-	2010 05 18, 04:04	Fr	2010 05 19, 07:26	-34
2010 05 28, 01:55	Y	2010 05 28, 19:12	Fr	2010 05 29, 17:58	-80
2010 06 21, 03:35	-	2010 06 21, 06:28	Fr	2010 06 22, 12:43	-11
2010 09 15, 02:24	-	2010 09 15, 02:24	Fr	2010 09 16, 11:58	-24
2010 10 11, 05:45	-	2010 10 11, 05:45	F-	2010 10 11, 18:28	-75 (SA)
2010 10 31, 02:09	-	2010 10 31, 05:16	Fr	2010 11 01, 20:38	-11
2010 12 19, 20:35	Y	2010 12 19, 22:33	F+	2010 12 20, 22:04	-35
2011 02 18, 19:50	Y	2011 02 18, 19:55	F-	2011 02 20, 21:35	-27
2011 04 23, 00:01	-	2011 04 23, 00:01	F-	2011 04 24, 13:11	-14
2011 04 29, 09:07	-	2011 04 29, 13:55	E	2011 04 29, 20:52	-17
2011 05 28, 00:14	-	2011 05 28, 05:31	F+	2011 05 28, 22:47	-80
2011 06 04, 20:06	Y	2011 06 05, 01:12	Fr	2011 06 05, 18:13	-45
2011 06 17, 02:09	Y	2011 06 17, 05:16	Cx	2011 06 19, 07:11	-14
2011 07 03, 19:12	-	2011 07 03, 19:12	Fr	2011 07 04, 19:12	-59 (SA)
2011 09 17, 02:57	Y	2011 09 17, 15:35	Fr	2011 09 18, 21:06	-72
2011 10 05, 06:46	Y	2011 10 05, 09:56	Cx	2011 10 07, 02:06	-43
2011 10 24, 17:41	Y	2011 10 25, 00:21	Cx	2011 10 25, 23:31	-147
2011 11 02, 00:21	-	2011 11 02, 03:35	Fr	2011 11 03, 04:33	-58
2011 11 04, 20:27	Y	2011 11 04, 21:17	Cx	2011 11 05, 20:09	-40
2011 11 11, 03:01	Y	2011 11 11, 03:01	Cx	2011 11 12, 05:02	-11
2011 11 28, 20:59	Y	2011 11 29, 19:40	Cx	2011 11 30, 17:59	-41
2012 01 22, 05:33	Y	2012 01 22, 11:24	F-	2012 01 22, 17:58	-70 (SA)
2012 02 14, 07:11	-	2012 02 14, 20:52	Fr	2012 02 16, 04:47	-67
2012 02 26, 20:59	Y	2012 02 27, 17:59	Cx	2012 03 01, 05:45	-57
2012 03 08, 10:32	Y	2012 03 08, 19:55	Cx	2012 03 11, 07:26	-145

2012 03 12, 08:28	Y	2012 03 12, 16:19	Cx	2012 03 14, 02:52	-64
2012 03 15, 12:35	Y	2012 03 15, 16:04	Fr	2012 03 16, 14:10	-88
2012 04 11, 06:28	-	2012 04 11, 06:28	Cx	2012 04 12, 03:35	-6
2012 04 23, 02:15	Y	2012 04 23, 16:48	F-	2012 04 24, 02:52	-120 (SA)
2012 05 03, 00:59	Y	2012 05 04, 03:36	Fr	2012 05 05, 11:22	-23
2012 05 16, 12:28	-	2012 05 16, 16:04	Fr	2012 05 18, 02:11	-43
2012 06 11, 02:52	-	2012 06 11, 11:31	Fr	2012 06 12, 05:16	-67
2012 06 16, 09:03	Y	2012 06 16, 22:01	F+	2012 06 17, 11:23	-86
2012 07 08, 02:10	-	2012 07 08, 07:58	Cx	2012 07 10, 01:41	-78
2012 07 14, 17:39	Y	2012 07 15, 06:14	Fr	2012 07 17, 03:21	-139
2012 08 12, 12:37	-	2012 08 12, 19:12	Fr	2012 08 13, 05:01	-9
2012 09 01, 07:12	-	2012 09 01, 07:12	Fr	2012 09 03, 11:22	-69
2012 09 12, 19:55	Y	2012 09 12, 19:55	F-	2012 09 13, 15:20	-4
2012 09 30, 10:14	Y	2012 09 30, 12:14	Cx	2012 10 02, 02:53	-122
2012 10 08, 04:12	Y	2012 10 08, 15:50	Fr	2012 10 09, 17:17	-109
2012 10 12, 08:09	-	2012 10 12, 18:29	Fr	2012 10 13, 09:14	-90
2012 10 31, 14:28	Y	2012 10 31, 23:35	F+	2012 11 02, 05:21	-65
2012 11 12, 22:12	Y	2012 11 13, 08:23	F+	2012 11 14, 08:09	-108
2012 11 23, 20:51	Y	2012 11 24, 11:31	F-	2012 11 25, 10:47	-40
2013 01 19, 16:50	Y	2013 01 19, 22:47	F-	2013 01 20, 10:47	-33
2013 03 17, 05:21	Y	2013 03 17, 14:09	Fr	2013 03 19, 16:04	-132
2013 04 13, 22:13	Y	2013 04 14, 17:02	F+	2013 04 17, 05:30	-17
2013 04 30, 08:52	Y	2013 04 30, 12:00	Fr	2013 05 01, 07:12	-47 (SA)
2013 05 14, 02:23	-	2013 05 14, 06:00	Fr	2013 05 15, 06:28	-18
2013 06 06, 02:09	-	2013 06 06, 14:23	F+	2013 06 08, 00:00	-78
2013 06 27, 13:51	Y	2013 06 28, 02:23	Fr	2013 06 29, 11:59	-101
2013 07 04, 17:17	-	2013 07 05, 04:05	Cx	2013 07 07, 14:24	-87
2013 07 12, 16:43	Y	2013 07 12, 20:24	Cx	2013 07 14, 23:31	-81
2013 10 30, 18:14	Y	2013 10 30, 18:14	Fr	2013 10 31, 05:30	-47
2013 11 08, 21:07	-	2013 11 08, 23:59	Fr	2013 11 09, 06:14	-80 (SA)
2013 11 23, 00:14	-	2013 11 23, 04:47	Fr	2013 11 23, 15:35	-27
2013 11 30, 20:23	-	2013 12 01, 04:48	Cx	2013 12 03, 03:21	-22
2013 12 08, 07:31	Y	2013 12 08, 16:47	F-	2013 12 09, 02:09	-66
2013 12 14, 16:47	-	2013 12 15, 16:47	Fr	2013 12 16, 05:30	-38
2013 12 24, 20:36	-	2013 12 25, 04:47	F+	2013 12 25, 17:59	-35
2014 02 05, 12:50	-	2014 02 06, 02:23	E	2014 02 07, 16:03	-31
2014 02 19, 03:09	Y	2014 02 19, 03:09	Cx	2014 02 20, 02:37	-119
2014 04 11, 06:57	-	2014 04 11, 06:57	F+	2014 04 12, 20:52	-87
2014 04 29, 19:11	-	2014 04 29, 19:11	Fr	2014 04 30, 16:33	-67
2014 06 22, 18:28	-	2014 06 22, 18:28	F-	2014 06 23, 22:04	-15
2014 06 29, 16:47	-	2014 06 29, 20:53	Fr	2014 06 30, 11:15	-5
2014 07 02, 23:48	Y	2014 07 03, 03:07	F-	2014 07 03, 11:59	-15
2014 08 19, 05:49	Y	2014 08 19, 17:59	F+	2014 08 21, 19:09	-30
2014 08 26, 02:40	-	2014 08 27, 03:07	Fr	2014 08 27, 21:49	-79
2014 09 12, 15:17	Y	2014 09 12, 21:22	F-	2014 09 14, 11:38	-88
2015 01 07, 05:38	Y	2015 01 07, 06:28	F+	2015 01 07, 21:07	-107
2015 03 28, 03:36	-	2015 03 28, 11:45	Fr	2015 03 29, 14:24	-46
2015 03 31, 07:32	Y	2015 03 31, 17:57	F-	2015 04 01, 09:49	-19
2015 04 09, 09:09	Y	2015 04 09, 23:02	Cx	2015 04 11, 09:36	-85
2015 05 06, 00:56	Y	2015 05 06, 16:48	F-	2015 05 07, 14:22	-35
2015 05 08, 02:52	-	2015 05 08, 07:11	F-	2015 05 09, 10:33	-15
2015 05 10, 08:23	-	2015 05 10, 11:59	F+	2015 05 11, 04:47	-57
2015 06 22, 18:07	Y	2015 06 23, 02:23	Cx	2015 06 24, 13:03	-198
2015 10 06, 21:35	-	2015 10 06, 21:35	Fr	2015 10 07, 10:03	-101
2015 10 24, 17:59	Y	2015 10 25, 13:11	Fr	2015 10 28, 13:11	-16
2015 11 06, 17:46	Y	2015 11 07, 07:11	Fr	2015 11 08, 16:47	-87
2015 12 19, 15:35	Y	2015 12 20, 13:40	Fr	2015 12 21, 23:02	-166
2016 01 19, 03:31	-	2016 01 19, 11:23	Fr	2016 01 20, 14:19	-101 (SA)
2016 01 24, 15:16	-	2016 01 25, 01:11	F-	2016 01 26, 03:09	-19
2016 03 05, 06:08	-	2016 03 05, 19:41	F-	2016 03 06, 14:44	-6
2016 03 20, 09:07	-	2016 03 20, 14:38	Fr	2016 03 21, 04:11	-42
2016 04 13, 15:48	-	2016 04 14, 09:35	Fr	2016 04 15, 10:08	-60
2016 04 16, 20:54	-	2016 04 17, 07:08	Fr	2016 04 18, 05:57	-58

2016 07 20, 02:53	-	2016 07 20, 15:10	Fr	2016 07 22, 15:31	-26
2016 08 02, 07:52	-	2016 08 02, 07:43	F-	2016 08 03, 06:23	-17
2016 11 04, 09:23	-	2016 11 04, 09:23	F-	2016 11 05, 18:27	-27
2017 04 09, 10:38	-	2017 04 09, 10:38	Fr	2017 04 10, 09:09	-21 (P)
2017 04 13, 12:39	-	2017 04 14, 02:31	Fr	2017 04 15, 11:07	-25 (P)
2017 05 27, 13:45	-	2017 05 27, 22:50	F+	2017 05 29, 11:05	-125 (P)
2017 07 16, 05:30	-	2017 07 17, 00:53	F-	2017 07 17, 13:00	-72 (P)
2017 08 21, 20:46	-	2017 08 22, 06:42	F-	2017 08 23, 14:02	-48 (P)
2017 12 25, 14:57	-	2017 12 25, 14:57	F-	2017 12 26, 06:32	-27 (P)
2018 03 09, 16:32	-	2018 03 09, 23:47	F+	2018 03 11, 02:05	-39 (P)
2018 05 13, 02:35	-	2018 05 13, 07:18	F-	2018 05 13, 14:51	-21 (P)
2018 07 10, 12:45	-	2018 07 10, 12:45	Fr	2018 07 11, 08:45	0 (P)
2018 08 25, 01:02	-	2018 08 25, 12:04	F+	2018 08 26, 12:19	-175 (P)
2018 09 23, 08:20	-	2018 09 23, 11:58	F-	2018 09 23, 22:59	-27 (P)
2019 05 07, 21:00	-	2019 05 07, 21:00	E	2019 05 08, 15:16	-2 (P)
2019 05 10, 11:42	-	2019 05 10, 17:04	E	2019 05 12, 21:58	-51 (P)
2019 05 13, 22:54	-	2019 05 14, 09:08	E	2019 05 15, 15:41	-65 (P)
2019 05 16, 22:54	-	2019 05 17, 01:25	F-	2019 05 18, 08:35	-10 (P)
2019 05 26, 22:50	-	2019 05 27, 07:49	Fr	2019 05 28, 00:11	-16 (P)
2019 06 07, 06:36	-	2019 06 07, 10:22	E	2019 06 08, 07:19	0 (P)
2019 11 02, 21:10	-	2019 11 02, 21:10	F-	2019 11 03, 06:46	-3 (P)
2019 11 11, 06:24	-	2019 11 11, 09:42	F-	2019 11 12, 09:48	-23 (P)
2020 01 04, 09:48	-	2020 01 04, 14:22	Fr	2020 01 05, 06:07	-25 (P)
2020 01 14, 02:50	-	2020 01 14, 08:21	E	2020 01 15, 05:08	-8 (P)
2020 03 04, 12:02	-	2020 03 04, 13:55	F-	2020 03 06, 03:52	-22 (P)
2020 12 06, 19:00	-	2020 12 06, 19:00	F-	2020 12 07, 08:31	-2 (P)
2020 12 10, 05:34	-	2020 12 11, 04:34	E	2020 12 13, 09:57	-13 (P)
2021 02 24, 02:39	-	2021 02 24, 04:33	F+	2021 02 24, 17:46	-24 (Q)
2021 03 11, 21:37	-	2021 03 11, 21:37	F-	2021 03 12, 23:17	-17 (Q)

Table A.2: ICME events consisting of both events with shock and without one, created using the events from Table A.3 that adheres to the criterion of at least a 3-day gap between events

A.3 ICME Catalog

Sheath start	Shock	MO start	MO type	MO/ICME end	B	Vsw	Vexp	Dst
1995 02/07 19:11	-	1995 02/08 03:21	Cx	1995 02/10 21:36	8.32	377	53	-80
1995 03/04 00:36	Y	1995 03/04 11:23	Fr	1995 03/05 03:06	10.81	444	11	-90
1995 03/06 02:11	-	1995 03/06 07:11	F-	1995 03/07 02:23	8.24	458	0	-38
1995 04/03 06:43	-	1995 04/03 12:45	F+	1995 04/04 13:25	8.92	295	4	-21
1995 04/05 07:11	-	1995 04/05 17:59	Fr	1995 04/06 17:15	7.3	332	-2	-18
1995 05/13 10:19	-	1995 05/13 10:19	E	1995 05/13 15:59	10.87	329	8	-8
1995 06/30 09:21	-	1995 06/30 14:23	Fr	1995 07/02 16:47	8.58	398	83	-56
1995 08/22 12:56	Y	1995 08/22 22:19	Fr	1995 08/23 18:43	9.71	359	16	-61
1995 09/26 15:57	-	1995 09/27 03:36	Fr	1995 09/27 21:21	9.78	375	-34	-108
1995 10/18 10:40	Y	1995 10/18 19:11	Fr	1995 10/20 02:23	21.15	408	5	-127
1995 12/15 14:52	-	1995 12/16 07:11	F-	1995 12/16 19:11	11.03	396	5	-44
1996 02/15 15:07	-	1996 02/15 15:07	F+	1996 02/16 08:59	6.89	387	24	-23
1996 04/04 11:59	-	1996 04/04 11:59	Fr	1996 04/04 21:36	7.29	389	6	-28
1996 05/16 22:47	-	1996 05/17 01:36	F+	1996 05/17 11:58	7.08	420	8	-26
1996 05/27 14:45	-	1996 05/27 14:45	Fr	1996 05/29 02:22	9.71	368	29	-33
1996 07/01 13:05	-	1996 07/01 17:16	Fr	1996 07/02 10:17	10.98	354	13	-20
1996 07/02 16:04	-	1996 07/02 16:04	F-	1996 07/02 22:47	10.68	395	-24	-2
1996 08/07 08:23	-	1996 08/07 11:59	Fr	1996 08/08 13:12	6.65	345	3	-23
1996 12/24 01:26	-	1996 12/24 03:07	F+	1996 12/25 11:44	10.39	348	38	-29
1997 01/10 00:52	Y	1997 01/10 04:47	F+	1997 01/11 03:06	14.63	437	29	-78
1997 02/09 12:50	Y	1997 02/10 02:52	F-	1997 02/10 18:28	7.87	459	17	-68
1997 04/10 17:02	-	1997 04/11 05:45	Fr	1997 04/11 19:10	18.49	463	4	-82
1997 04/21 10:11	-	1997 04/21 11:59	F+	1997 04/23 07:11	11.31	363	42	-107
1997 05/15 01:15	Y	1997 05/15 10:00	F+	1997 05/16 02:37	18.84	469	-38	-115
1997 05/16 06:01	-	1997 05/16 06:01	Fr	1997 05/16 13:26	7.85	491	17	-40
1997 05/26 09:09	Y	1997 05/26 15:35	Fr	1997 05/28 00:00	9.5	331	17	-73
1997 06/08 15:43	-	1997 06/09 06:18	Fr	1997 06/09 23:01	11.93	374	9	-84
1997 06/19 00:00	-	1997 06/19 05:31	Fr	1997 06/20 22:29	7.32	333	37	-36
1997 07/15 03:10	-	1997 07/15 06:48	F+	1997 07/16 11:16	9.62	359	13	-44
1997 08/03 10:10	-	1997 08/03 13:55	Fr	1997 08/04 02:23	15.12	436	42	-49
1997 08/17 01:56	-	1997 08/17 06:33	Fr	1997 08/17 20:09	6.79	396	14	-28
1997 09/02 22:40	Y	1997 09/03 08:38	Fr	1997 09/03 20:59	13.66	409	-5	-98 (SA)
1997 09/18 00:30	-	1997 09/18 04:07	F+	1997 09/19 23:59	11.73	320	35	-56
1997 09/21 16:42	-	1997 09/21 22:21	F+	1997 09/22 17:46	15	424	56	-36
1997 10/01 11:45	-	1997 10/01 17:08	Fr	1997 10/02 23:15	9.62	450	31	-98
1997 10/10 03:08	-	1997 10/10 15:33	F+	1997 10/11 22:00	12.02	410	36	-130
1997 11/06 22:25	-	1997 11/07 06:00	F+	1997 11/08 22:46	12.97	413	48	-110
1997 11/22 09:12	Y	1997 11/22 17:31	F+	1997 11/23 18:43	15.99	498	16	-108
1997 12/10 04:33	Y	1997 12/10 19:11	Cx	1997 12/12 00:00	11.7	352	19	-60
1997 12/30 01:13	Y	1997 12/30 09:35	Fr	1997 12/31 08:51	11.57	367	-10	-77
1998 01/06 13:29	Y	1998 01/07 02:23	F+	1998 01/08 07:54	16.09	383	33	-77
1998 01/08 15:35	-	1998 01/08 15:35	F-	1998 01/08 22:47	10	369	-27	-22
1998 01/09 08:23	-	1998 01/09 08:23	Fr	1998 01/09 20:38	6.76	476	14	-22
1998 01/21 04:47	-	1998 01/21 04:47	F-	1998 01/22 13:26	13.03	411	36	-11
1998 01/28 16:04	-	1998 01/29 13:12	F+	1998 01/31 00:00	7.9	377	19	-55
1998 02/02 10:27	-	1998 02/02 10:27	F+	1998 02/04 02:22	7.76	335	16	-29
1998 02/04 04:48	-	1998 02/04 04:48	F+	1998 02/06 08:04	9.68	321	32	-34
1998 02/17 06:28	-	1998 02/17 10:48	Fr	1998 02/18 14:22	14.95	397	8	-100
1998 02/18 14:52	-	1998 02/18 21:35	Fr	1998 02/20 00:44	8.7	435	-21	-50
1998 03/04 11:02	Y	1998 03/04 10:48	F+	1998 03/06 07:10	10.03	348	36	-36
1998 03/06 11:59	-	1998 03/06 11:59	Cx	1998 03/07 16:48	5.55	325	13	-16
1998 03/25 10:48	-	1998 03/25 14:23	Fr	1998 03/26 08:57	10.35	407	5	-56
1998 03/31 07:11	-	1998 03/31 11:59	Fr	1998 04/01 16:18	6.23	389	35	-35
1998 04/01 21:07	-	1998 04/01 21:07	E	1998 04/02 19:55	6.21	325	11	-5
1998 05/01 21:21	Y	1998 05/02 11:31	Fr	1998 05/03 16:47	9.38	520	25	-85

1998 05/04 02:30	-	1998 05/04 09:50	F-	1998 05/05 03:12	15.62	653	46	-205
1998 06/02 10:28	Y	1998 06/02 10:28	Fr	1998 06/02 19:16	9.68	398	17	-1
1998 06/24 10:47	-	1998 06/24 13:26	F+	1998 06/25 22:33	12.69	468	50	-25
1998 07/10 22:36	-	1998 07/10 22:36	F+	1998 07/12 21:34	10.67	386	-43	-35
1998 08/10 00:31	Y	1998 08/10 04:47	E	1998 08/10 23:30	7.75	450	18	-27
1998 08/19 18:40	Y	1998 08/20 08:38	F+	1998 08/21 20:09	12.9	317	28	-67
1998 08/26 06:40	Y	1998 08/26 21:07	E	1998 08/28 00:28	13.84	659	169	-155
1998 09/23 01:12	-	1998 09/23 04:19	F-	1998 09/23 17:31	6.47	413	75	-25
1998 09/24 23:18	-	1998 09/25 04:33	F+	1998 09/26 17:00	13.23	663	136	-207
1998 10/02 07:10	Y	1998 10/02 07:10	E	1998 10/02 22:47	7.03	656	32	-56
1998 10/18 19:30	-	1998 10/19 04:19	F+	1998 10/20 07:11	17.15	396	15	-112
1998 10/23 12:57	Y	1998 10/23 19:55	F-	1998 10/24 19:26	6	495	36	-52
1998 11/08 04:41	Y	1998 11/08 04:41	Cx	1998 11/08 23:30	26.66	565	75	-149
1998 11/09 00:44	-	1998 11/09 00:44	F+	1998 11/10 03:47	14.6	456	47	-142
1999 01/22 20:21	Y	1999 01/22 20:21	E	1999 01/23 14:58	16.09	614	36	-49
1999 02/11 17:41	-	1999 02/11 17:41	Fr	1999 02/12 03:35	19.16	443	-9	-17
1999 02/18 02:48	Y	1999 02/18 09:14	E	1999 02/19 00:00	15.2	660	7	-123
1999 04/16 11:14	Y	1999 04/16 19:11	Fr	1999 04/17 19:48	17.56	418	40	-91
1999 04/21 12:37	Y	1999 04/21 12:37	E	1999 04/23 14:23	20.66	396	-6	-29
1999 05/28 21:50	-	1999 05/28 21:50	Cx	1999 05/30 10:47	6.73	397	15	-10
1999 06/26 02:31	Y	1999 06/26 02:31	Fr	1999 06/27 04:47	15.2	384	-80	-15
1999 07/02 00:27	Y	1999 07/03 08:09	Fr	1999 07/05 13:13	4.42	458	87	-26
1999 07/06 14:23	Y	1999 07/06 19:12	Cx	1999 07/07 16:46	7.2	463	-9	-4
1999 07/30 19:12	-	1999 07/31 02:02	E	1999 08/01 00:00	7.77	575	-20	-53
1999 08/06 01:55	-	1999 08/06 14:23	Fr	1999 08/07 06:18	9.59	426	-22	-23
1999 08/09 10:12	-	1999 08/09 10:12	Fr	1999 08/10 16:04	9.9	343	27	-47
1999 09/15 07:43	Y	1999 09/15 07:43	E	1999 09/15 17:44	12.1	609	37	-51
1999 09/21 18:57	-	1999 09/21 18:57	Fr	1999 09/22 11:31	11.2	358	2	-41
1999 09/22 12:09	Y	1999 09/22 17:59	E	1999 09/23 09:35	17.85	560	26	-173
1999 10/21 02:19	Y	1999 10/21 02:19	E	1999 10/22 06:32	21.73	466	-54	-237 (SA)
1999 11/13 12:48	Y	1999 11/14 14:23	E	1999 11/16 07:17	22.79	717	-103	-106
1999 12/12 15:50	Y	1999 12/12 17:31	Cx	1999 12/13 18:28	11.76	592	79	-69
2000 02/11 23:34	Y	2000 02/12 12:20	Fr	2000 02/13 00:35	12.06	549	14	-135
2000 02/14 07:11	Y	2000 02/14 13:11	E	2000 02/15 15:33	6.35	564	77	-68
2000 02/20 21:03	Y	2000 02/21 14:24	Fr	2000 02/22 13:16	14.78	379	32	-25
2000 03/01 01:58	-	2000 03/01 03:21	Fr	2000 03/02 03:07	7.87	473	52	-44
2000 03/28 02:52	-	2000 03/28 02:52	E	2000 03/29 22:47	8.33	405	-92	-16
2000 05/07 03:53	-	2000 05/07 03:53	Cx	2000 05/08 11:59	10.08	385	26	-6
2000 06/08 09:07	Y	2000 06/08 16:47	E	2000 06/10 01:18	11.15	648	132	-90
2000 06/23 12:57	Y	2000 06/24 09:00	E	2000 06/25 23:58	7.17	494	74	-34
2000 07/01 07:12	-	2000 07/01 07:12	Fr	2000 07/02 03:34	7.87	413	-11	3
2000 07/11 22:35	-	2000 07/11 22:35	Fr	2000 07/13 04:33	9.7	508	35	-25
2000 07/13 09:59	Y	2000 07/13 15:35	Fr	2000 07/14 15:35	6.47	621	21	-43
2000 07/15 02:23	-	2000 07/15 06:47	F-	2000 07/15 14:18	8.89	-	-	-57
2000 07/15 14:23	-	2000 07/15 17:31	F+	2000 07/16 13:28	35.8	-	-	-300
2000 07/19 15:30	Y	2000 07/19 15:30	Cx	2000 07/21 05:31	8.71	542	75	-92
2000 07/28 06:38	Y	2000 07/28 14:24	F+	2000 07/29 10:06	14.26	463	-6	-49
2000 07/31 23:28	-	2000 07/31 23:28	Fr	2000 08/01 13:11	11.28	457	2	-32
2000 08/10 05:13	Y	2000 08/10 20:52	F+	2000 08/11 18:43	12.2	422	4	-105
2000 08/11 18:49	Y	2000 08/12 06:05	F+	2000 08/13 05:05	24.63	579	37	-234
2000 09/02 23:16	-	2000 09/02 23:16	Fr	2000 09/03 22:32	6.78	408	35	-19
2000 09/04 13:13	Y	2000 09/04 13:13	Cx	2000 09/06 16:47	8.78	392	63	-36
2000 09/06 17:02	Y	2000 09/07 03:24	Cx	2000 09/08 14:22	8.93	444	14	-47 (SA)
2000 09/17 16:04	-	2000 09/18 01:53	E	2000 09/19 12:00	13.43	726	30	-201
2000 10/03 01:02	Y	2000 10/03 09:36	F+	2000 10/05 03:34	13.67	408	28	-143
2000 10/05 03:28	Y	2000 10/05 19:11	Fr	2000 10/06 19:39	5.15	476	77	-181
2000 10/12 22:33	Y	2000 10/13 18:24	Fr	2000 10/14 19:12	11.84	401	7	-106
2000 10/28 06:38	Y	2000 10/28 23:18	F-	2000 10/30 00:16	13.79	383	28	-126
2000 11/06 09:30	Y	2000 11/06 23:05	Fr	2000 11/07 18:05	20.33	536	60	-159
2000 11/10 06:20	Y	2000 11/10 11:02	E	2000 11/11 04:18	7.64	852	77	-95
2000 11/11 04:11	Y	2000 11/11 04:11	E	2000 11/11 23:59	7.58	826	113	-52
2000 11/26 11:43	Y	2000 11/27 09:30	Fr	2000 11/28 09:36	9.04	574	49	-79
2000 12/03 03:59	Y	2000 12/03 03:59	Cx	2000 12/05 03:06	8.59	394	79	-33

2001 01/23 10:47	Y	2001 01/24 08:38	Cx	2001 01/25 19:12	4.49	412	14	-61
2001 03/04 05:45	-	2001 03/04 05:45	Cx	2001 03/05 23:04	9.38	465	-41	-73
2001 03/19 11:33	Y	2001 03/19 19:55	Fr	2001 03/20 18:17	17.16	419	3	-149
2001 03/20 18:17	-	2001 03/20 18:17	Fr	2001 03/22 00:00	13.06	340	48	-134
2001 03/27 01:59	Y	2001 03/27 01:59	Cx	2001 03/28 14:23	13.75	516	-147	-56
2001 04/04 14:39	Y	2001 04/04 20:54	F-	2001 04/05 08:22	10.3	740	53	-50
2001 04/11 14:09	Y	2001 04/11 22:48	F-	2001 04/12 17:58	18.73	664	51	-271
2001 04/13 07:26	-	2001 04/13 13:11	F-	2001 04/14 01:39	8.15	764	78	-77
2001 04/21 15:29	Y	2001 04/22 00:28	Fr	2001 04/23 01:11	12.05	358	30	-102
2001 04/28 05:00	Y	2001 04/28 17:59	Cx	2001 05/02 04:48	6.31	505	168	-47
2001 05/27 14:45	Y	2001 05/28 07:12	Cx	2001 05/29 21:34	8.33	452	65	-42
2001 06/27 05:59	-	2001 06/27 05:59	Cx	2001 06/29 02:23	3.05	404	28	-16
2001 08/05 12:28	-	2001 08/06 06:43	E	2001 08/06 23:59	8.17	440	-5	-40
2001 08/17 11:01	Y	2001 08/17 23:59	F-	2001 08/18 19:12	14.15	533	65	-105
2001 09/25 20:16	Y	2001 09/26 10:04	F-	2001 09/26 16:47	14.12	639	-6	-102
2001 09/29 09:28	Y	2001 09/29 14:23	Cx	2001 09/30 19:14	11.13	568	125	-55
2001 09/30 19:14	Y	2001 09/30 22:33	F-	2001 10/01 21:34	11.58	506	15	-148
2001 10/21 16:39	Y	2001 10/22 01:17	Fr	2001 10/23 00:47	14.78	578	89	-187
2001 10/28 03:13	Y	2001 10/29 16:19	E	2001 10/30 10:47	6.14	382	13	-157
2001 10/31 13:46	Y	2001 10/31 22:04	Fr	2001 11/02 04:47	11.2	341	42	-106
2001 11/24 05:51	Y	2001 11/24 15:47	Fr	2001 11/25 13:17	16.29	746	152	-221
2001 12/29 05:16	Y	2001 12/30 03:24	Fr	2001 12/30 19:10	17.08	401	-25	-58
2001 12/30 20:05	Y	2001 12/30 23:10	F-	2001 12/31 07:46	12.83	629	150	-31
2002 02/28 05:06	Y	2002 02/28 19:11	Fr	2002 03/01 23:15	10.14	383	7	-71
2002 03/18 13:14	Y	2002 03/19 06:14	Fr	2002 03/20 15:36	14.91	384	-21	-37
2002 03/23 11:24	Y	2002 03/24 13:11	Fr	2002 03/25 21:36	15.35	437	10	-100
2002 04/14 12:56	Y	2002 04/14 15:21	F-	2002 04/15 04:22	9.98	396	13	-14
2002 04/17 11:01	Y	2002 04/17 21:36	F+	2002 04/19 08:22	11.75	490	73	-127
2002 04/19 08:24	Y	2002 04/20 06:57	Fr	2002 04/21 21:36	6.88	506	93	-149
2002 04/23 05:00	Y	2002 04/24 07:11	F-	2002 04/24 23:59	7.18	490	3	-57
2002 05/10 11:09	Y	2002 05/10 22:20	Fr	2002 05/11 10:36	6.84	353	23	-14
2002 05/11 10:30	Y	2002 05/11 12:37	Fr	2002 05/11 20:23	17.42	437	12	-110
2002 05/18 19:45	Y	2002 05/19 03:30	Fr	2002 05/20 03:34	11.2	455	36	-58
2002 05/20 03:35	Y	2002 05/20 16:47	Cx	2002 05/21 21:35	6.13	421	45	-36
2002 05/23 10:44	Y	2002 05/23 23:02	F-	2002 05/25 19:12	10.15	582	244	-109
2002 07/17 15:56	Y	2002 07/18 13:26	Fr	2002 07/19 09:35	9.58	436	36	-17
2002 08/01 05:12	Y	2002 08/01 12:14	Fr	2002 08/01 23:15	12.01	454	15	-51
2002 08/01 23:09	Y	2002 08/02 07:12	Fr	2002 08/02 21:34	11.83	492	30	-102
2002 08/18 18:40	Y	2002 08/19 19:12	Fr	2002 08/21 13:25	7.76	471	44	-106
2002 08/26 11:16	Y	2002 08/26 14:23	Fr	2002 08/27 10:47	11.95	397	3	-45
2002 09/03 02:23	-	2002 09/03 04:47	Cx	2002 09/04 01:12	14.13	358	-16	-6
2002 09/30 07:54	Y	2002 09/30 22:04	F+	2002 10/01 20:08	20.4	381	-15	-176
2002 11/16 23:16	-	2002 11/17 20:24	F-	2002 11/18 23:58	9.36	383	6	-52
2002 12/21 03:21	-	2002 12/21 10:20	Fr	2002 12/22 15:36	9.85	429	4	-75
2003 01/26 21:43	-	2003 01/27 01:40	Fr	2003 01/27 16:04	10.41	520	48	-18
2003 02/01 13:06	-	2003 02/02 19:11	Fr	2003 02/03 09:35	10.18	483	-1	-72
2003 03/20 04:30	-	2003 03/20 11:54	Fr	2003 03/20 22:22	11.14	672	16	-64
2003 05/09 05:16	-	2003 05/09 09:27	E	2003 05/10 23:07	7.38	674	53	-84
2003 06/16 22:33	-	2003 06/17 17:48	Fr	2003 06/18 08:18	12.46	481	-19	-141 (SA)
2003 08/04 20:23	-	2003 08/05 01:10	Fr	2003 08/06 02:23	9.57	443	17	-58
2003 10/21 22:00	-	2003 10/22 02:24	Cx	2003 10/24 02:24	7.97	464	13	-61
2003 10/29 06:00	-	2003 10/29 11:16	Cx	2003 10/30 01:55	25.41	840	-22	-353
2003 10/30 16:12	-	2003 10/31 02:00	Cx	2003 10/31 12:00	14.98	1626	-712	-383
2003 11/20 08:35	Y	2003 11/20 11:31	Fr	2003 11/21 01:40	33.24	594	103	-422
2004 01/09 15:00	-	2004 01/10 06:01	E	2004 01/11 05:02	7.98	531	4	-45
2004 04/03 09:55	Y	2004 04/04 01:11	F+	2004 04/05 19:11	15.86	431	65	-117
2004 07/22 09:45	Y	2004 07/22 13:26	Cx	2004 07/24 05:45	11.52	561	63	-99
2004 07/24 05:32	Y	2004 07/24 07:12	Fr	2004 07/25 14:37	20.45	565	32	-136 (SA)
2004 07/25 17:45	-	2004 07/25 17:45	Fr	2004 07/26 03:34	9.34	669	-5	-130
2004 07/26 22:25	Y	2004 07/27 01:12	Cx	2004 07/27 23:58	16.98	1019	457	-170
2004 08/29 09:09	Y	2004 08/29 19:26	Fr	2004 08/30 21:21	12.16	393	8	-129 (SA)
2004 09/13 19:42	Y	2004 09/14 17:59	E	2004 09/15 14:23	6.35	557	28	-45
2004 09/17 20:52	-	2004 09/18 12:28	Fr	2004 09/19 16:58	6.03	402	33	-33

2004 11/07 17:58	Y	2004 11/07 22:46	Fr	2004 11/09 09:20	16.27	641	60	-374
2004 11/09 18:25	Y	2004 11/09 20:38	F+	2004 11/10 16:47	24.98	732	115	-259
2004 11/11 16:47	Y	2004 11/12 08:35	Fr	2004 11/13 09:35	6.96	553	66	-92
2004 12/10 04:47	-	2004 12/10 04:47	F-	2004 12/10 21:35	8.33	416	12	-27
2005 01/07 08:44	-	2005 01/07 14:23	F+	2005 01/08 07:12	17.35	536	-3	-93
2005 01/08 15:12	-	2005 01/08 20:51	Fr	2005 01/09 17:45	8.65	462	14	-47
2005 01/16 09:27	Y	2005 01/16 15:35	F+	2005 01/17 07:00	8.25	530	32	-63
2005 01/18 21:35	-	2005 01/19 00:28	F-	2005 01/20 02:23	11.83	822	168	-80
2005 01/21 16:58	Y	2005 01/21 23:45	F-	2005 01/22 19:12	14.57	727	43	-97
2005 02/16 10:33	-	2005 02/16 12:14	F-	2005 02/16 23:30	12.4	390	20	-42
2005 02/17 21:35	-	2005 02/18 14:52	E	2005 02/19 08:23	5.94	539	54	-80
2005 02/20 15:32	Y	2005 02/20 20:23	Fr	2005 02/22 07:11	5.4	409	41	-43
2005 05/15 02:10	Y	2005 05/15 05:31	F+	2005 05/16 22:47	23.34	747	238	-247
2005 05/20 04:47	-	2005 05/20 09:35	F+	2005 05/22 02:23	8.93	428	53	-83
2005 06/12 06:57	Y	2005 06/12 15:07	F-	2005 06/13 17:59	12.37	480	20	-106
2005 06/14 17:55	Y	2005 06/15 05:08	F+	2005 06/16 08:23	9.06	484	34	-42
2005 07/10 02:42	Y	2005 07/10 10:47	Cx	2005 07/12 14:23	11.95	438	-1	-92
2005 07/17 14:52	-	2005 07/17 14:52	Fr	2005 07/18 05:59	11.16	427	24	-67 (SA)
2005 08/10 04:47	-	2005 08/10 06:14	F-	2005 08/10 13:26	8.11	447	27	-47
2005 10/31 02:23	-	2005 10/31 02:23	Fr	2005 10/31 18:42	10.72	374	20	-74 (SA)
2006 02/05 18:14	-	2006 02/05 20:23	F+	2006 02/06 11:59	10.25	341	16	-20
2006 04/13 13:26	-	2006 04/13 15:07	F+	2006 04/14 11:02	16.82	521	4	-98
2006 04/14 13:11	-	2006 04/14 13:11	F-	2006 04/14 23:15	8.74	513	7	-81
2006 06/14 08:09	-	2006 06/14 08:09	F-	2006 06/14 16:25	8.29	386	-17	-1
2006 07/09 20:40	Y	2006 07/10 17:45	Cx	2006 07/11 17:45	9	368	-12	-27
2006 08/19 09:38	Y	2006 08/20 13:55	Cx	2006 08/21 17:02	8.08	406	-10	-79
2006 08/30 20:38	-	2006 08/30 20:38	Cx	2006 09/01 07:12	7.76	397	34	-35
2006 09/30 02:52	-	2006 09/30 08:23	F+	2006 09/30 22:03	15.76	394	27	-21
2006 11/01 21:21	-	2006 11/01 21:21	F-	2006 11/02 14:22	5.2	373	25	-28
2006 11/18 07:11	-	2006 11/18 07:11	Fr	2006 11/20 04:47	8.44	400	-7	-20
2006 11/29 02:58	-	2006 11/29 05:16	F+	2006 11/30 09:35	11.81	410	8	-66
2006 12/14 13:51	Y	2006 12/14 22:36	F-	2006 12/15 13:40	12.55	758	21	-162
2006 12/16 17:34	Y	2006 12/17 00:25	F-	2006 12/17 19:11	3.86	584	91	-56
2007 01/14 11:31	-	2007 01/14 11:44	Fr	2007 01/15 07:45	11.42	364	7	-18
2007 01/15 20:49	-	2007 01/15 20:49	F-	2007 01/16 04:44	8	531	-34	-23
2007 03/29 15:04	-	2007 03/29 15:04	Cx	2007 03/30 00:02	4.64	396	3	-11
2007 05/21 22:40	-	2007 05/21 22:45	Fr	2007 05/22 13:25	10.67	454	7	-2
2007 06/08 05:45	-	2007 06/08 05:45	Fr	2007 06/09 05:15	7.82	362	-7	-21
2007 11/19 17:22	Y	2007 11/20 00:33	Fr	2007 11/20 11:31	18.26	465	3	-2
2007 12/25 16:19	-	2007 12/25 16:19	F-	2007 12/26 09:35	4.31	350	15	-8
2008 05/23 01:12	-	2008 05/23 01:12	F+	2008 05/23 10:46	5.15	499	23	-11
2008 09/03 16:33	-	2008 09/03 16:33	F+	2008 09/04 03:49	11.45	467	-22	-51 (SA)
2008 09/17 00:43	-	2008 09/17 03:57	Fr	2008 09/18 08:09	5.67	408	45	-23
2008 12/04 11:59	-	2008 12/04 16:47	Fr	2008 12/05 10:47	7.04	390	6	-26
2008 12/17 03:35	-	2008 12/17 03:35	Fr	2008 12/17 15:35	7.99	338	10	-15
2009 01/02 02:49	-	2009 01/02 04:48	F-	2009 01/02 17:16	6.1	411	-12	-12
2009 01/26 05:02	-	2009 01/26 05:02	E	2009 01/26 15:21	9.9	347	24	-29
2009 02/03 19:21	Y	2009 02/04 01:12	F+	2009 02/04 19:40	9.59	356	17	-42
2009 03/11 22:04	Y	2009 03/12 01:12	F+	2009 03/13 01:40	11.69	361	-18	-28 (SA)
2009 04/05 16:04	-	2009 04/05 17:02	F-	2009 04/06 04:48	4.74	404	-12	-7
2009 04/22 11:16	-	2009 04/22 14:09	Fr	2009 04/22 20:37	3.71	387	16	-7
2009 06/03 13:40	-	2009 06/03 20:52	Fr	2009 06/05 05:31	5.24	316	5	-19
2009 06/27 11:02	Y	2009 06/27 17:59	F+	2009 06/28 20:24	7.61	389	25	-14
2009 07/21 02:53	-	2009 07/21 04:48	Fr	2009 07/22 03:36	7.94	317	17	-83 (SA)
2009 09/10 10:19	-	2009 09/10 10:19	Fr	2009 09/10 19:26	4.73	305	2	1
2009 09/30 00:44	-	2009 09/30 06:59	Fr	2009 09/30 19:11	7.95	346	12	-5
2009 10/29 01:26	-	2009 10/29 01:26	F+	2009 10/29 23:45	8.86	364	-13	-6
2009 11/01 10:04	-	2009 11/01 10:04	F-	2009 11/02 08:20	5.92	347	20	-6
2009 11/14 10:47	-	2009 11/14 10:47	Fr	2009 11/15 11:45	6.71	335	-15	-17
2009 12/12 04:47	-	2009 12/12 19:26	Fr	2009 12/14 04:47	6.11	271	16	-2
2010 01/01 22:04	-	2010 01/02 00:14	Fr	2010 01/03 09:06	6.62	286	13	-4
2010 02/07 18:04	-	2010 02/07 19:11	Fr	2010 02/09 05:42	8.34	362	36	-22
2010 03/23 22:29	Y	2010 03/23 22:33	Fr	2010 03/24 15:36	4.56	292	-17	-1

2010 04/05 07:55	Y	2010 04/05 11:59	Fr	2010 04/06 16:48	9.02	634	131	-81
2010 04/11 12:20	Y	2010 04/11 21:36	Fr	2010 04/12 14:12	10.56	411	19	-67
2010 05/18 02:23	-	2010 05/18 04:04	Fr	2010 05/19 07:26	7.8	355	4	-34
2010 05/28 01:55	Y	2010 05/28 19:12	Fr	2010 05/29 17:58	13.31	354	18	-80
2010 06/21 03:35	-	2010 06/21 06:28	Fr	2010 06/22 12:43	6.08	361	27	-11
2010 08/03 17:05	Y	2010 08/04 02:52	Cx	2010 08/05 00:56	10.57	548	44	-74
2010 09/15 02:24	-	2010 09/15 02:24	Fr	2010 09/16 11:58	7.33	371	-14	-24
2010 09/25 11:45	-	2010 09/25 13:11	F-	2010 09/26 08:09	2.92	473	69	-16
2010 10/11 05:45	-	2010 10/11 05:45	F-	2010 10/11 18:28	10.94	354	6	-75 (SA)
2010 10/31 02:09	-	2010 10/31 05:16	Fr	2010 11/01 20:38	8.67	342	31	-11
2010 12/19 20:35	Y	2010 12/19 22:33	F+	2010 12/20 22:04	7.29	385	-2	-35
2011 01/24 06:43	-	2011 01/24 10:33	F+	2011 01/25 22:04	6.18	344	16	-14
2011 02/18 19:50	Y	2011 02/18 19:55	F-	2011 02/20 21:35	8.7	462	72	-27
2011 03/29 15:12	Y	2011 03/29 23:59	Fr	2011 04/01 14:51	11.27	344	10	-7
2011 04/23 00:01	-	2011 04/23 00:01	F-	2011 04/24 13:11	7	398	-13	-14
2011 04/29 09:07	-	2011 04/29 13:55	E	2011 04/29 20:52	10.52	403	-61	-17
2011 05/28 00:14	-	2011 05/28 05:31	F+	2011 05/28 22:47	11.4	519	-33	-80
2011 06/04 20:06	Y	2011 06/05 01:12	Fr	2011 06/05 18:13	11.48	513	29	-45
2011 06/17 02:09	Y	2011 06/17 05:16	Cx	2011 06/19 07:11	5.84	429	47	-14
2011 06/30 13:26	-	2011 06/30 18:43	F-	2011 07/01 05:16	8.26	329	-18	-48 (SA)
2011 07/03 19:12	-	2011 07/03 19:12	Fr	2011 07/04 19:12	8.9	392	7	-59 (SA)
2011 09/17 02:57	Y	2011 09/17 15:35	Fr	2011 09/18 21:06	8.19	443	2	-72
2011 10/05 06:46	Y	2011 10/05 09:56	Cx	2011 10/07 02:06	10.55	399	51	-43
2011 10/24 17:41	Y	2011 10/25 00:21	Cx	2011 10/25 23:31	16.48	483	-25	-147
2011 11/01 08:09	Y	2011 11/01 08:09	F-	2011 11/01 22:04	10.26	412	16	-66
2011 11/02 00:21	-	2011 11/02 03:35	Fr	2011 11/03 04:33	5.61	371	-22	-58
2011 11/04 20:27	Y	2011 11/04 21:17	Cx	2011 11/05 20:09	5.83	303	30	-40
2011 11/07 06:57	-	2011 11/07 16:19	Fr	2011 11/08 00:43	9.38	349	-1	-5
2011 11/11 03:01	Y	2011 11/11 03:01	Cx	2011 11/12 05:02	5.26	380	14	-11
2011 11/28 20:59	Y	2011 11/29 19:40	Cx	2011 11/30 17:59	8.33	432	10	-41
2012 01/21 04:02	Y	2012 01/21 04:04	Fr	2012 01/22 06:56	10.34	327	-14	-10
2012 01/22 05:33	Y	2012 01/22 11:24	F-	2012 01/22 17:58	20.35	413	17	-70 (SA)
2012 02/14 07:11	-	2012 02/14 20:52	Fr	2012 02/16 04:47	8.37	378	19	-67
2012 02/26 20:59	Y	2012 02/27 17:59	Cx	2012 03/01 05:45	9.28	443	-7	-57
2012 03/08 10:32	Y	2012 03/08 19:55	Cx	2012 03/11 07:26	8.53	576	159	-145
2012 03/12 08:28	Y	2012 03/12 16:19	Cx	2012 03/14 02:52	6.63	627	106	-64
2012 03/15 12:35	Y	2012 03/15 16:04	Fr	2012 03/16 14:10	9.1	697	75	-88
2012 04/05 14:23	-	2012 04/05 19:41	Fr	2012 04/06 21:36	9.66	342	21	-40
2012 04/11 06:28	-	2012 04/11 06:28	Cx	2012 04/12 03:35	7.38	329	8	-6
2012 04/23 02:15	Y	2012 04/23 16:48	F-	2012 04/24 02:52	14.49	373	10	-120 (SA)
2012 05/03 00:59	Y	2012 05/04 03:36	Fr	2012 05/05 11:22	6.47	310	16	-23
2012 05/16 12:28	-	2012 05/16 16:04	Fr	2012 05/18 02:11	9.59	374	-8	-43
2012 06/11 02:52	-	2012 06/11 11:31	Fr	2012 06/12 05:16	8.71	408	-9	-67
2012 06/16 09:03	Y	2012 06/16 22:01	F+	2012 06/17 11:23	30.36	450	58	-86
2012 07/08 02:10	-	2012 07/08 07:58	Cx	2012 07/10 01:41	10.67	417	23	-78
2012 07/14 17:39	Y	2012 07/15 06:14	Fr	2012 07/17 03:21	16.61	491	106	-139
2012 08/12 12:37	-	2012 08/12 19:12	Fr	2012 08/13 05:01	10.61	382	2	-9
2012 08/18 03:25	-	2012 08/18 19:12	Fr	2012 08/19 08:22	11.07	387	13	-18
2012 08/30 15:35	-	2012 08/30 15:35	F-	2012 08/31 05:30	2.77	406	36	-4
2012 09/01 07:12	-	2012 09/01 07:12	Fr	2012 09/03 11:22	7.41	317	13	-69
2012 09/04 22:02	Y	2012 09/05 05:52	Fr	2012 09/05 17:44	11.06	507	12	-64
2012 09/06 00:00	-	2012 09/06 02:23	F-	2012 09/06 15:50	9.72	425	31	-32
2012 09/12 19:55	Y	2012 09/12 19:55	F-	2012 09/13 15:20	9.01	365	-4	-4
2012 09/30 10:14	Y	2012 09/30 12:14	Cx	2012 10/02 02:53	11.77	354	-8	-122
2012 10/08 04:12	Y	2012 10/08 15:50	Fr	2012 10/09 17:17	15.16	398	-10	-109
2012 10/12 08:09	-	2012 10/12 18:29	Fr	2012 10/13 09:14	10.43	480	9	-90
2012 10/31 14:28	Y	2012 10/31 23:35	F+	2012 11/02 05:21	10.93	341	33	-65
2012 11/12 22:12	Y	2012 11/13 08:23	F+	2012 11/14 08:09	20.11	381	2	-108
2012 11/23 20:51	Y	2012 11/24 11:31	F-	2012 11/25 10:47	11.62	381	12	-40
2013 01/16 23:31	-	2013 01/17 14:52	Fr	2013 01/18 12:14	12.52	388	-10	-52
2013 01/18 22:47	-	2013 01/19 00:14	Fr	2013 01/19 16:47	4.8	427	12	-25
2013 01/19 16:50	Y	2013 01/19 22:47	F-	2013 01/20 10:47	6.61	428	-4	-33
2013 03/17 05:21	Y	2013 03/17 14:09	Fr	2013 03/19 16:04	9.28	529	108	-132

2013 04/13 22:13	Y	2013 04/14 17:02	F+	2013 04/17 05:30	6.86	390	52	-17
2013 04/30 08:52	Y	2013 04/30 12:00	Fr	2013 05/01 07:12	10.02	393	15	-47 (SA)
2013 05/14 02:23	-	2013 05/14 06:00	Fr	2013 05/15 06:28	7.59	356	30	-18
2013 06/06 02:09	-	2013 06/06 14:23	F+	2013 06/08 00:00	10.43	428	47	-78
2013 06/27 13:51	Y	2013 06/28 02:23	Fr	2013 06/29 11:59	11.23	391	8	-101
2013 07/04 17:17	-	2013 07/05 04:05	Cx	2013 07/07 14:24	9.46	339	31	-87
2013 07/12 16:43	Y	2013 07/12 20:24	Cx	2013 07/14 23:31	11.89	421	69	-81
2013 09/01 06:14	-	2013 09/01 13:55	Fr	2013 09/02 01:56	3.86	487	55	-30
2013 10/02 01:15	Y	2013 10/02 15:35	E	2013 10/02 21:35	5.76	594	12	-72
2013 10/03 00:00	-	2013 10/03 00:00	Fr	2013 10/03 14:52	8.01	488	51	-53
2013 10/30 18:14	Y	2013 10/30 18:14	Fr	2013 10/31 05:30	8.88	341	10	-47
2013 11/08 21:07	-	2013 11/08 23:59	Fr	2013 11/09 06:14	12.72	411	-7	-80 (SA)
2013 11/23 00:14	-	2013 11/23 04:47	Fr	2013 11/23 15:35	8.6	356	-4	-27
2013 11/30 20:23	-	2013 12/01 04:48	Cx	2013 12/03 03:21	8.74	442	68	-22
2013 12/08 07:31	Y	2013 12/08 16:47	F-	2013 12/09 02:09	5.02	553	27	-66
2013 12/14 16:47	-	2013 12/15 16:47	Fr	2013 12/16 05:30	7.27	460	6	-38
2013 12/24 20:36	-	2013 12/25 04:47	F+	2013 12/25 17:59	10.56	300	24	-35
2014 02/05 12:50	-	2014 02/06 02:23	E	2014 02/07 16:03	6.25	369	39	-31
2014 02/15 12:46	Y	2014 02/16 00:43	Fr	2014 02/16 14:23	14.51	389	23	-24
2014 02/18 05:59	-	2014 02/18 15:07	Fr	2014 02/19 09:35	11.22	421	-36	-119
2014 02/19 03:09	Y	2014 02/19 03:09	Cx	2014 02/20 02:37	11.91	496	-38	-119
2014 04/05 09:58	-	2014 04/05 22:18	Fr	2014 04/07 14:24	11.92	370	34	-15
2014 04/11 06:57	-	2014 04/11 06:57	F+	2014 04/12 20:52	9.11	351	25	-87
2014 04/20 10:20	Y	2014 04/21 07:41	Fr	2014 04/22 06:12	5.69	552	43	-32
2014 04/29 19:11	-	2014 04/29 19:11	Fr	2014 04/30 16:33	8.81	303	-6	-67
2014 06/07 16:30	Y	2014 06/08 19:12	Cx	2014 06/10 16:46	4.42	489	105	-37
2014 06/22 18:28	-	2014 06/22 18:28	F-	2014 06/23 22:04	2.9	358	28	-15
2014 06/29 16:47	-	2014 06/29 20:53	Fr	2014 06/30 11:15	8.55	347	23	-5
2014 07/02 23:48	Y	2014 07/03 03:07	F-	2014 07/03 11:59	6.36	333	18	-15
2014 08/19 05:49	Y	2014 08/19 17:59	F+	2014 08/21 19:09	13.92	349	39	-30
2014 08/26 02:40	-	2014 08/27 03:07	Fr	2014 08/27 21:49	13.17	308	-16	-79
2014 09/12 15:17	Y	2014 09/12 21:22	F-	2014 09/14 11:38	17.57	594	139	-88
2015 01/07 05:38	Y	2015 01/07 06:28	F+	2015 01/07 21:07	17.57	451	15	-107
2015 03/28 03:36	-	2015 03/28 11:45	Fr	2015 03/29 14:24	12.04	392	42	-46
2015 03/31 07:32	Y	2015 03/31 17:57	F-	2015 04/01 09:49	12.34	404	-3	-19
2015 04/09 09:09	Y	2015 04/09 23:02	Cx	2015 04/11 09:36	15.24	392	40	-85
2015 05/06 00:56	Y	2015 05/06 16:48	F-	2015 05/07 14:22	12.89	421	18	-35
2015 05/08 02:52	-	2015 05/08 07:11	F-	2015 05/09 10:33	6.52	383	-9	-15
2015 05/10 08:23	-	2015 05/10 11:59	F+	2015 05/11 04:47	11.03	359	20	-57
2015 06/22 18:07	Y	2015 06/23 02:23	Cx	2015 06/24 13:03	10.68	598	68	-198
2015 09/07 13:05	Y	2015 09/07 23:31	F+	2015 09/09 14:52	14.74	468	84	-105
2015 10/06 21:35	-	2015 10/06 21:35	Fr	2015 10/07 10:03	14.51	425	-41	-101
2015 10/24 17:59	Y	2015 10/25 13:11	Fr	2015 10/28 13:11	5.62	392	84	-16
2015 11/06 17:46	Y	2015 11/07 07:11	Fr	2015 11/08 16:47	15.69	530	66	-87
2015 12/19 15:35	Y	2015 12/20 13:40	Fr	2015 12/21 23:02	15.67	398	15	-166
2016 01/19 03:31	-	2016 01/19 11:23	Fr	2016 01/20 14:19	14.11	362	8	-101 (SA)
2016 01/24 15:16	-	2016 01/25 01:11	F-	2016 01/26 03:09	6	416	49	-19
2016 03/05 06:08	-	2016 03/05 19:41	F-	2016 03/06 14:44	11.72	366	-10	-6
2016 03/20 09:07	-	2016 03/20 14:38	Fr	2016 03/21 04:11	6.84	405	10	-42
2016 04/13 15:48	-	2016 04/14 09:35	Fr	2016 04/15 10:08	7.31	405	62	-60
2016 04/16 20:54	-	2016 04/17 07:08	Fr	2016 04/18 05:57	8.12	400	15	-58
2016 07/20 02:53	-	2016 07/20 15:10	Fr	2016 07/22 15:31	9.71	438	66	-26
2016 07/24 13:51	-	2016 07/25 03:23	E	2016 07/25 13:08	6.33	440	-4	-38
2016 08/02 07:52	-	2016 08/02 07:43	F-	2016 08/03 06:23	15.63	401	-45	-17
2016 10/12 21:37	-	2016 10/13 06:27	F+	2016 10/14 16:19	19.34	384	37	-109
2016 11/04 09:23	-	2016 11/04 09:23	F-	2016 11/05 18:27	4.59	360	10	-27
2016 11/09 09:45	-	2016 11/10 01:30	F-	2016 11/10 10:09	11.13	362	-11	-9
2017 04/04 04:46	-	2017 04/04 04:46	Fr	2017 04/04 14:50	13.47	416	-2	-44 (P)
2017 04/09 10:38	-	2017 04/09 10:38	Fr	2017 04/10 09:09	7.61	453	25	-21 (P)
2017 04/13 12:39	-	2017 04/14 02:31	Fr	2017 04/15 11:07	6.16	369	50	-25 (P)
2017 05/27 13:45	-	2017 05/27 22:50	F+	2017 05/29 11:05	3.08	318	26	-125 (P)
2017 07/16 05:30	-	2017 07/17 00:53	F-	2017 07/17 13:00	11.57	540	53	-72 (P)

2017 08/21 20:46	-	2017 08/22 06:42	F-	2017 08/23 14:02	4.55	506	74	-48 (P)
2017 09/06 22:21	-	2017 09/07 09:13	E	2017 09/08 06:35	3.79	502	44	-122 (P)
2017 09/07 16:17	-	2017 09/08 00:19	E	2017 09/09 16:57	8.65	683	127	-122 (P)
2017 12/25 14:57	-	2017 12/25 14:57	F-	2017 12/26 06:32	7.37	448	6	-27 (P)
2018 03/09 16:32	-	2018 03/09 23:47	F+	2018 03/11 02:05	13.71	401	34	-39 (P)
2018 05/13 02:35	-	2018 05/13 07:18	F-	2018 05/13 14:51	9.13	433	7	-21 (P)
2018 06/06 11:23	-	2018 06/06 17:32	Fr	2018 06/07 08:29	10.03	404	34	-25 (P)
2018 06/25 08:02	-	2018 06/25 08:02	Fr	2018 06/26 03:33	6.84	412	-3	-48 (P)
2018 07/10 12:45	-	2018 07/10 12:45	Fr	2018 07/11 08:45	9.39	338	20	0 (P)
2018 08/25 01:02	-	2018 08/25 12:04	F+	2018 08/26 12:19	15.65	406	14	-175 (P)
2018 09/23 08:20	-	2018 09/23 11:58	F-	2018 09/23 22:59	8.17	441	8	-27 (P)
2019 03/16 12:20	-	2019 03/17 01:15	Fr	2019 03/17 19:12	7.64	397	24	-40 (P)
2019 04/17 21:15	-	2019 04/17 21:15	F-	2019 04/18 19:37	4.48	309	25	-9 (P)
2019 05/07 21:00	-	2019 05/07 21:00	E	2019 05/08 15:16	2.79	333	12	-2 (P)
2019 05/10 11:42	-	2019 05/10 17:04	E	2019 05/12 21:58	8.34	348	16	-51 (P)
2019 05/13 22:54	-	2019 05/14 09:08	E	2019 05/15 15:41	8.13	475	70	-65 (P)
2019 05/16 22:54	-	2019 05/17 01:25	F-	2019 05/18 08:35	5.34	440	41	-10 (P)
2019 05/26 22:50	-	2019 05/27 07:49	Fr	2019 05/28 00:11	10.52	338	27	-16 (P)
2019 06/07 06:36	-	2019 06/07 10:22	E	2019 06/08 07:19	5.45	290	25	0 (P)
2019 10/13 04:55	-	2019 10/13 09:48	Fr	2019 10/14 06:07	2.95	335	16	-5 (P)
2019 10/29 05:30	-	2019 10/29 05:30	F-	2019 10/30 23:52	8.11	388	26	-22 (P)
2020 04/20 03:52	-	2020 04/20 08:26	Fr	2020 04/21 05:03	14.69	345	18	-59 (P)
2020 12/06 19:00	-	2020 12/06 19:00	F-	2020 12/07 08:31	6.05	365	12	-2 (P)
2020 12/10 05:34	-	2020 12/11 04:34	E	2020 12/13 09:57	4.72	426	65	-13 (P)
2021 02/24 02:39	-	2021 02/24 04:33	F+	2021 02/24 17:46	7.42	479	0	-24 (Q)
2021 03/11 21:37	-	2021 03/11 21:37	F-	2021 03/12 23:17	6.86	351	10	-17 (Q)
2021 04/05 00:28	-	2021 04/05 10:23	F-	2021 04/06 09:32	7.99	327	1	-2 (Q)

Table A.3: A catalog of Interplanetary Coronal Mass Ejection (ICME) events by Nieves-Chinchilla et al. [34]. The dst Index column (SA) denotes index values from Slightly After the MO end time if the storm seems to be generated by the trailing region of the ICME, (P) shows Provisional Dst values, and (Q) are Quicklook Dst values

Bibliography

[1] D. F. Webb et al. “Relationship of halo coronal mass ejections, magnetic clouds, and magnetic storms”. In: *Journal of Geophysical Research: Space Physics* 105.A4 (2000), pp. 7491–7508. DOI: 10.1029/1999JA000275.

[2] H. Hudson, J.-L. Bougeret, and J. Burkepile. “Coronal mass ejections: Overview of observations”. In: *Coronal Mass Ejections*. Springer, 2006, pp. 13–30.

[3] T. Howard. *Coronal mass ejections: An introduction*. Vol. 376. Springer, 2011.

[4] J. T. Gosling. “The solar flare myth”. In: *Journal of Geophysical Research: Space Physics* 98.11 (Nov. 1993), pp. 18937–18950.

[5] S. Yashiro et al. “A catalog of white light coronal mass ejections observed by the SOHO spacecraft”. In: *Journal of Geophysical Research: Space Physics* 109.A7 (2004). DOI: https://doi.org/10.1029/2003JA010282.

[6] D. F. Webb and T. A. Howard. “Coronal mass ejections: Observations”. In: *Living Reviews in Solar Physics* 9 (2012), pp. 3–83.

[7] N. Sheeley et al. “Continuous tracking of coronal outflows: Two kinds of coronal mass ejections”. In: *Journal of Geophysical Research: Space Physics* 104.A11 (1999), pp. 24739–24767.

[8] A. Hundhausen. “Coronal Mass Ejections”. In: *The Many Faces of the Sun: A Summary of the Results from NASA’s Solar Maximum Mission*. Ed. by Keith T. Strong et al. New York, NY: Springer New York, 1999, pp. 143–200. ISBN: 978-1-4612-1442-7. DOI: 10.1007/978-1-4612-1442-7_5.

[9] B.C. Low. “Solar activity and the corona”. In: *Solar Physics* 167 (1996), pp. 217–265. DOI: 10.1007/BF00146338.

[10] M. J. Aschwanden. *Physics of the Solar Corona. An Introduction with Problems and Solutions*. 2nd ed. 2005.

[11] J. Chen. “Theory of prominence eruption and propagation: Interplanetary consequences”. In: *Journal of Geophysical Research* 101.A12 (Dec. 1996), pp. 27499–27520. DOI: 10.1029/96JA02644.

[12] T. Török and B. Kliem. “The evolution of twisting coronal magnetic flux tubes”. In: *Astronomy Astrophysics* 406 (Aug. 2003), pp. 1043–1059. DOI: 10.1051/0004-6361:20030692.

[13] B. Kliem and T. Török. “Torus Instability”. In: *Physical Review Letters* 96.25 (June 2006), p. 255002. DOI: 10.1103/PhysRevLett.96.255002.

[14] J. Zhang et al. “On the temporal relationship between coronal mass ejections and flares”. In: *The Astrophysical Journal* 559.1 (2001), p. 452.

[15] R. Schwenn et al. “Coronal observations of CMEs”. In: *Space Science Reviews* 123.1-3 (2006), pp. 127–176.

[16] Timothy Howard. *Coronal Mass Ejections: An Introduction*. Vol. 376. Springer, 2011.

[17] J. Gosling and D. McComas. “Field line draping about fast coronal mass ejecta: A source of strong out-of-the-ecliptic interplanetary magnetic fields”. In: *Geophysical Research Letters* 14.4 (1987), pp. 355–358.

[18] Erika Palmerio, Emilia KJ Kilpua, and Neel P. Savani. “Planar magnetic structures in coronal mass ejection-driven sheath regions”. In: *Annales Geophysicae*. Vol. 34. 2. Copernicus Publications. Göttingen, Germany, 2016, pp. 313–322.

[19] R. J. Forsyth et al. “ICMEs in the Inner Heliosphere: Origin, Evolution and Propagation Effects. Report of Working Group G”. In: *Space Science Reviews* 123.1-3 (Mar. 2006), pp. 383–416. DOI: 10.1007/s11214-006-9022-0.

[20] E. Mitsakou and X. Moussas. “Statistical Study of ICMEs and Their Sheaths During Solar Cycle 23 (1996 – 2008)”. In: *Coronal Magnetometry*. Ed. by Steven Tomczyk, Jie Zhang, and Timothy Bastian. New York, NY: Springer New York, 2014, pp. 515–535. ISBN: 978-1-4939-2038-9. DOI: 10.1007/978-1-4939-2038-9_30.

[21] E. Kilpua, H.E.J. Koskinen, and T.I. Pulkkinen. “Coronal mass ejections and their sheath regions in interplanetary space”. In: *Living Reviews in Solar Physics* 14 (2017), p. 5. DOI: 10.1007/s41116-017-0009-6.

[22] E. K. J. Kilpua et al. “Unraveling the drivers of the storm time radiation belt response”. English. In: *Geophysical Research Letters* 42.9 (May 2015), pp. 3076–3084. ISSN: 0094-8276. DOI: 10.1002/2015GL063542.

[23] J. W. Dungey. “Interplanetary Magnetic Field and the Auroral Zones”. In: *Phys. Rev. Lett.* 6 (2 Jan. 1961), pp. 47–48. DOI: 10.1103/PhysRevLett.6.47.

[24] P. N. Mayaud. "Derivation, Meaning, and Use of Geomagnetic Indices". In: *Geophysical Monograph Series* 22 (Jan. 1980), p. 607. DOI: 10.1029/GM022.

[25] I. G. Richardson et al. "Major geomagnetic storms (Dst 100 nT) generated by corotating interaction regions". In: *Journal of Geophysical Research: Space Physics* 111.A7 (2006). DOI: https://doi.org/10.1029/2005JA011476.

[26] Alexandre Chorin. "Lecture II Theories of turbulence". In: *Turbulence Seminar*. Ed. by Peter Bernard and Tudor Ratiu. Berlin, Heidelberg: Springer Berlin Heidelberg, 1977, pp. 36–47. ISBN: 978-3-540-37074-1.

[27] Russell M. Kulsrud and Ellen G. Zweibel. "On the origin of cosmic magnetic fields". In: *Reports on Progress in Physics* 71.4, 046901 (Apr. 2008), p. 046901. DOI: 10.1088/0034-4885/71/4/046901. arXiv: 0707.2783 [astro-ph].

[28] Steven Balbus and John Hawley. "Instability, Turbulence, and Enhanced Transport in Accretion Disks". In: *Reviews of Modern Physics* 121 (Jan. 1998), p. 90. DOI: 10.1103/RevModPhys.70.1.

[29] Bruce G. Elmegreen and John Scalo. "Interstellar Turbulence I: Observations and Processes". In: *Annual Review of Astronomy and Astrophysics* 42.1 (Sept. 2004), pp. 211–273. ISSN: 1545-4282. DOI: 10.1146/annurev.astro.41.011802.094859. URL: http://dx.doi.org/10.1146/annurev.astro.41.011802.094859.

[30] J. W. Belcher and Leverett Davis Jr. "Large-amplitude Alfvén waves in the interplanetary medium, 2". In: *Journal of Geophysical Research (1896-1977)* 76.16 (1971), pp. 3534–3563. DOI: https://doi.org/10.1029/JA076i016p03534.

[31] W. H. Matthaeus, M. L. Goldstein, and J. H. King. "An interplanetary magnetic field ensemble at 1 AU". In: *Journal of Geophysical Research: Space Physics* 91.A1 (), pp. 59–69. DOI: https://doi.org/10.1029/JA091iA01p00059.

[32] Luca Sorriso-Valvo et al. "Turbulent Cascade and Energy Transfer Rate in a Solar Coronal Mass Ejection". In: *The Astrophysical Journal Letters* 919.2 (Oct. 2021), p. L30. DOI: 10.3847/2041-8213/ac26c5. URL: https://doi.org/10.3847/2041-8213/ac26c5.

[33] A. Szabo and L. I. Wilson. *Wind 2013 Senior Review Proposal*. Executive Summary. 2013.

[34] T. Nieves-Chinchilla, A. Vourlidas, et al. "Understanding the internal magnetic field configurations of ICMEs using more than 20 years of wind observations". In: *Solar Physics* 293.2 (2018), p. 25. DOI: 10.1007/s11207-018-1247-z.

[35] Fengsi Wei et al. "Identification of the magnetic cloud boundary layers". In: *Journal of Geophysical Research (Space Physics)* 108 (June 2003), pp. 1263–. DOI: 10.1029/2002JA009511.

[36] Y.-M. Wang. "ON THE RELATIVE CONSTANCY OF THE SOLAR WIND MASS FLUX AT 1 AU". In: *The Astrophysical Journal Letters* 715.2 (May 2010), p. L121. DOI: 10.1088/2041-8205/715/2/L121.

[37] I. G. Richardson and H. V. Cane. "Near-Earth Interplanetary Coronal Mass Ejections During Solar Cycle 23 (1996 - 2009): Catalog and Summary of Properties". In: 264.1 (June 2010), pp. 189–237. DOI: 10.1007/s11207-010-9568-6.

[38] B. Bavassano, R. Bruno, and L. W. Klein. "Density-temperature correlation in solar wind magnetohydrodynamic fluctuations: A test for nearly incompressible models". In: *Journal of Geophysical Research* 100.A4 (Apr. 1995), pp. 5871–5875. DOI: 10.1029/94JA02571.

[39] Debesh Bhattacharjee et al. "Turbulence and anomalous resistivity inside near-Earth magnetic clouds". In: *Monthly Notices of the Royal Astronomical Society* 518.1 (Nov. 2022), pp. 1185–1194. ISSN: 1365-2966. DOI: 10.1093/mnras/stac3186. URL: http://dx.doi.org/10.1093/mnras/stac3186.

[40] R. A. Treumann, W. Baumjohann, and Y. Narita. "On the ion-inertial-range density-power spectra in solar wind turbulence". In: *Annales Geophysicae* 37.2 (2019), pp. 183–199. DOI: 10.5194/angeo-37-183-2019. URL: https://angeo.copernicus.org/articles/37/183/2019/.